2015-06-01

Studies on the Roles of Translationally Recoded Proteins from Cyclooxygenase-1 and Nucleobindin Genes in Autophagy

Jonathan J. Lee
Brigham Young University

Studies on the Roles of Translationally Recoded Proteins from Cyclooxygenase-1 and Nucleobindin Genes in Autophagy

Jonathan J. Lee

A dissertation submitted to the faculty of
Brigham Young University
in partial fulfillment of the requirements for the degree of

Doctor of Philosophy

Daniel L. Simmons, Chair
Richard K. Watt
Joshua L. Andersen
Barry M. Willardson
Jeffery Barrow

Department of Chemistry and Biochemistry

Brigham Young University

June 2015

ABSTRACT

Studies on the Roles of Translationally Recoded Proteins from
Cyclooxygenase-1 and Nucleobindin Genes in Autophagy

Jonathan J. Lee
Department of Chemistry and Biochemistry, BYU
Doctor of Philosophy

Advances in next-generation sequencing and ribosomal profiling methods highlight that the proteome is likely orders of magnitude larger than previously thought. This expansion potentially occurs through translational recoding, a process that results in the expression of multiple variations of a protein from a single messenger RNA. Our laboratory demonstrated that cyclooxygenase-3/1b (COX-3/1b), a frameshifted, intron-1-retaining, alternative splice variant from the COX-1 gene, is multiply recoded, which results in the translation of at least seven different COX-3 proteins.

Two of the recoded COX-3 proteins that we identified are active prostaglandin synthases and are inhibited by non-steroidal anti-inflammatory drugs (NSAIDs). Here we show that the other non-prostaglandin-generating recoded COX-3 proteins perform new roles in innate immunity, a process in which COX are known to generally function. Our analyses determined that these recoded COX-3 proteins bind at or near the amino-terminal region of ATG9a, a critical regulator of both canonical (i.e. digestive autophagy associated with mTORc inhibition and nutrient deprivation) and non-canonical (i.e. xenophagy involved in the innate immune response to invading organisms) autophagy. We further show that this process requires mTORc signaling activity, which opposes the digestive pathway. As a final confirmation of the biological relevance of these recoded COX-3 proteins and their central role in xenophagy, we demonstrate that expression of these COX-3 proteins in an encephalomyocarditis virus infection model system differentially affects infectious virion production.

These COX-3 proteins also associate with recoded cytosolic nucleobindin around large, innate immune-related, **l**arge **L**C3-II **p**ositive **s**tructures (LLPSs). Through mutagenizing catalytic residues of recoded COX-3 proteins and drug assays, we determine LLPS formation is dependent on oxylipin generation.

Keywords: Cyclooxygenase, COX-3, Oxylipin, Autophagy, Xenophagy, Non-canonical autophagy, Nucleobindin

ACKNOWLEDGEMENTS

I must share my most heartfelt appreciation to Dr. Simmons for his support, patience, friendship, and direction as his graduate student. His foresight and knowledge have aided me in my experimental design and analysis of data. Dr. Simmons' sound advice has led me to better understand the process of science and discovery. His energy has been a boon in my graduate career and I hope to emulate his excitement in science in future projects. I would also like to thank both Dr. Simmons, Dr. Bradshaw, and Jacob Cuttler for editing this dissertation.

I am also appreciative of the advice and counsel given me by my committee members Dr. Willardson, Dr. Andersen, Dr. Barrow, and Dr. Watt. Their expression of support and guidance has helped me solve difficult questions which enabled me to move forward in my projects. I must give special thanks to Dr. Andersen for loaning me material for my projects and giving me counsel in the area of autophagy.

I am extremely grateful for the work provided by the undergraduate students Stephen Hill, Tim Visser, Matthew Lelegren, and especially Gideon Logan. Gideon has provided almost all of the confocal images in this dissertation and has given me insights that have propelled my work forward. I must also express gratitude to Dr. John Hunter who has given me advice on techniques and writing. It has been a great pleasure working with everyone involved in the work and writing of this dissertation.

Finally, I must express my deepest love for my wife, Melissa, who has been patient and supportive of my endeavors in the Biochemistry Ph.D. program. Her care and love has sustained me through the many difficulties I faced as a graduate student. I must also say thanks to all those not listed here who have also shown kindness to me and given me support.

TABLE OF CONTENTS

Abstract..... ii

Acknowledgments..... iii

List of Tables..... vii

List of Figures..... viii

Abbreviations..... xi

Chapter 1: **Autophagy, recoded cyclooxygenase and oxylipins**.....1
- Abstract.....1
- Background.....2
  - Macroautophagy.....2
  - Non-canonical autophagy and innate immunity.....4
  - Cargo selection and lipid's role in autophagy..... 6
- References..... 9

Chapter 2: Recoded COXs complex with ATG9a, a vital component of autophagy.....12
- Abstract.....12
- Background.....12
  - ATG9a is a transmembrane protein that shuttles between Golgi and autophagic structures.....12
  - Regulation of ATG9a is dependent on both protein binding and post-translational modifications.....13
  - ATG9a is involved in innate immunity 14
- Materials and Methods.....16
  - Materials..... 16
  - Cell Culture..... 16
  - Plasmid DNA purification..... 16
  - DC protein assay..... 17
  - Transient transfection..... 17
  - Site-directed mutagenesis.....18
  - Co-immunoprecipitation of ectopic ATG9a and rc57.....19
  - Immunoblot analysis.....20
  - Collagenizing glass slides..... 20
  - Confocal microscopy..... 21
  - Acceptor photobleach FRET analysis..... 21
  - EMCV infection.....22
  - Plaque forming assay.....22

Results……23
Confocal microscopy of rcCOXs identifies a role in autophagy……23
rcCOXs do not localize to amphisomes but rc50 associates with autolysosomes……25
Permeabilization of cells shows rcCOXs are not intraluminal autophagosomal cargo……25
rcCOXs co-localize with ATG9a vesicles……29
rcCOXs binds near or at the N-terminus of ATG9a……31
rcCOXs do not co-localize with macroautophagic omegasomes……34
The rcCOX/ATG9a complex does not require COX catalytic residues……36
mTOR inhibitor blocks rcCOX/ATG9a complex……38
rcCOXs differential effect on EMCV replication……39
Discussion……40
References……44

Chapter 3: Recoded COXs and nucleobindin induce large LC3-II positive structures (LLPSs)……48
Abstract……48
Background……48
Nucleobindin is a multi-domain protein with many physiological roles and two subcellular locations……49
Cytosolic nucleobindin occurs through translational recoding……50
Materials and Methods……51
Sample preparation for p62 immunoblot analysis……51
Results……51
Site-directed mutagenesis demonstrates that cNuc is a recoded form of Nuc……51
Recoded COXs translocate with cNuc to LLPSs and act synergistically to drive their formation……54
Co-transfection of cNuc abolishes interaction between rcCOX and ATG9a……56
cNuc blocks autophagic flux before amphisome formation……57
Discussion……60
References……63

Chapter 4: Large LC3-II positive structure (LLPS) formation is affected by rcCOX redox activity and requires oxylipin metabolism……68
Abstract……68
Background……69
Materials and Methods……72
Prostaglandin synthesis activity assay……73

Cellular drug assay…….. 74
Results……74
Evolutionary evaluation of methionines responsible for rcCOX recoding and their roles in cyclooxygenase catalysis……74
Structural comparison of CLPs and rcCOXs reveals evolutionary similarities……75
Site-directed mutagenesis of catalytic residues of rcCOXs Influence rcCOX localization…….. 79
Site-directed mutagenesis of important catalytic COX residues influence LLPS formation……84
Analysis of rcCOX oxygenase activity through $cPLA_2$ inhibition……84
Lipid specific oxygenase inhibitors against LOX and other drugs affect LLPS formation…….. 86
Discussion……87
References……95

Appendix A: Table of Primers…… 103

Appendix B: Antibodies used for this research………… 105

Appendix C: Publications…… 106

LIST OF TABLES

Table 1: Table of both PDB templates for rcCOX construction and PDB templates with similar structure……..80

Table 2: List of p-values comparing LLPS formation between cNuc against cNuc and mutated rcCOX constructs…… 86

Table 3: Appendix A……..103

Table 4: Appendix B……..105

LIST OF FIGURES

Figure 1: Pathway and critical components of macroautoaphagy..... 3

Figure 2: *Salmonella* evokes lipid remodeling in xenophagy.....5

Figure 3: Diagram of recoded enzymes/proteins from COX-3 mRNA..... 8

Figure 4: Sub-cellular localization of rc57, rc50, and rc44..... 24

Figure 5: Recoded 57 and 50 do not localize to amphisomes while only rc50 localizes to autolysosomes.....26

Figure 6: Cellular permeabilization shows rc57 and rc50 reside mainly on cytosolic surface of Golgi, autophagosomes, and autolysosomes.....28

Figure 7: Digitonin treatment removes rc50 from autolysosomes.....28

Figure 8: rcCOXs co-localize with ATG9a.....30

Figure 9: Digitonin treatment does not remove rcCOX from ATG9a.....31

Figure 10: Recoded 57 co-immunoprecipitates with ATG9a..... 32

Figure 11: Recoded 57 co-immunoprecipitates with C-terminally truncated ATG9a.....33

Figure 12: Recoded COXs protect cytosolic N-terminal mRFP tagged ATG9a from trypsin digestion..... 34

Figure 13: Photobleach FRET analysis reveals rcCOXs form a complex with ATG9a at or near the N terminus..... 35

Figure 14: rcCOXs do not co-localize with DFCP1..... 36

Figure 15: Recoded COX/ATG9a complex is independent of rcCOX activity..... 37

Figure 16: mTOR activity is important for rcCOX/ATG9a association..... 39

Figure 17: EMCV replication is affected rcCOXs overexpression..... 40

Figure 18: Mutagenesis reveals Nuc is recoded near the N-terminus.....52

Figure 19: Localization pattern of cNuc and wtNuc……53

Figure 20: Recoded Nuc drives LLPS production……54

Figure 21: Recoded COXs translocate from Golgi to co-localize with cNuc at LLPSs……55

Figure 22: rcCOXs and cNuc co-localize with LC3-II at LLPSs……56

Figure 23: ATG9a does not co-localize with cNuc or rcCOX/cNuc formed LLPSs……57

Figure 24: Cytosolic Nuc causes accumulation of p62……58

Figure 25: Autophagic flux is blocked before autolysosome formation……59

Figure 26: Autophagic flux is blocked before amphisome formation……60

Figure 27: Endocytosed beads not found within LLPSs……62

Figure 28: Evolutionary conservation of initiating Met of rc57, rc50, and rc44……75

Figure 29: Initiating Met of rc57 is important for COX-1 activity……76

Figure 30: Co-expressing rc57 with M57A-COX-1 does not rescue loss activity……77

Figure 31: I-TASSER predicted structure of rc57, rc50, and rc44……78

Figure 32: H388Q- and H207Q-rcCOXs continue co-localizing with cNuc……82

Figure 33: H388/207Q-rcCOX and Y385F-rcCOX cease co-localizing with cNuc……83

Figure 34: Mutation of catalytic residues of rcCOX affects LLPS formation……85

Figure 35: cPLA$_2$ inhibitor blocks LLPS formation……87

Figure 36: Recoded 57/cNuc-induced LLPSs are sensitive to acetaminophen, LOX5, and LOX15 inhibitors……89

Figure 37: Only the LOX15 inhibitor PD146176 inhibited cNuc-induced LLPSs……90

Figure 38: Model of LLPS formation in CHO cells……..93

Abbreviations

COX	Cyclooxygenase
rcCOX	recoded Cyclooxygenase
ATP	Adenosine triphosphate
ATG9a	Autophagic-related protein 9a
Nuc	Nucleobindin
cNuc	Cytosolic Nucleobindin
LLPS	Large LC3-II positive structures
mTOR	Target of rapamycin
ULK1	Unc-51 like autophagy activating kinase 1
RNA	Ribonucleic acid
mRNA	Messenger ribonucleic acid
siRNA	Small interfering ribonucleic acid
PGHS	Prostaglandin H synthase
AA	Arachidonic acid
PGH_2	Prostaglandin H_2
NSAID	Non-steroidal anti-inflammatory drug
ER	Endoplasmic reticulum
PGG_2	Prostaglandin G_2
DNA	Deoxyribonucleic acid
cDNA	Reverse transcribed DNA copy of mRNA
dsDNA	double-stranded DNA
kD	Kilodalton
bp	Base pairs
ATCC	American type culture collection
DMEM	Dulbecco's Modified Eagle Medium
FBS	Fetal bovine serum
P/S	Penicillin/streptomycin
RT	Reverse transcription
PCR	Polymerase chain reaction
BSA	Bovine serum albumin
IP	Immunoprecipitation
PBS	Phosphate buffered saline
PBST	Phosphate buffered saline with 1% Tween 20
LSB	Low salt buffer
PNK	Polynucleotide kinase
DTT	Dithiothreitol
dNTPs	Free deoxyribonucleic acids – triphosphate form
BYU	Brigham Young University
UTR	Untranslated region of mRNA
CDS	Coding region of mRNA
eGFP	Enhanced Green fluorescent protein
His	Histidine

RIA	Radioimmunoassay
PGE_2	Prostaglandin E_2
SDS	Sodium dodecyl sulfate
PI	Protease inhibitor
GAPDH	Glyceraldehyde 3-phosphate dehydrogenase
FITC	Fluorescein isothiocyanate
NCBI	National Center for Biotechnology Information
ORF	Open reading frame
IRES	Internal ribosomal entry site
PI3KIII	Phosphatidylinositol-3 kinase class 3
PI(3)P	Phosphatidylinositol-3 phosphate
FYVE	Fab 1, YOTB, Vac 1, and EEA1
DFCP1	Double FYVE-domain containing protein 1
PE	Phosphatidylethanolamine
PAMPs	Pathogen-associated molecular patterns
IFNγ	Interferon-γ
NFκB	Nuclear factor kappa-light-chain-enhancer of activated B cells
CVB3	Coxsackievirus B3
EMCV	Encephalomyocarditis virus
p62	Sequestrosome-1
PI3KI	class I PI3K
Akt	Activated protein kinase B
PLD	Phospholipase D
PAP	Phosphatidic acid phosphatase
DAG	Diacyglycerol
PKCδ	Protein kinase C isoform δ
JNK	c-Jun N-terminal kinases
NADPH	Nicotinamide adenine dinucleotide phosphate
$cPLA_2$	Cytosolic phospholipase A_2
LTD4	Leukotriene D_4
LTE4	Leukotriene E_4
PGD_2	Prostaglandin D_2
FRET	Förster resonance energy transfer
N-BAR	N-terminal Bin-Amphiphysin-Rvs
p38IP	p38-interacting protein
MAPK	Mitogen-activated protein kinase
AMP	Adenosine monophosphate
AMPK	AMP-activated protein kinase
STING	stimulator of IFN genes
TBK1	TANK-binding kinase 1
MEFs	Mouse embryonic fibroblasts
SCVs	*Salmonella*-containing vacuoles
MTT	3-(4,5-dimethylthiazol-2-yl)-2,5-diphenyltetrazolium bromide
mRFP	Monomeric red fluorescent protein

HA	hemagglutinin
GST	Glutathione S transferase
EDTA	Ethylenediaminetetraacetic acid
CHO	Chinese hamster ovary
SOC	Super optimal broth with catabolite repression
MQ	Milli-Q water
ADRP	Adipose differentiation-related protein
TGN46	Trans-Golgi network protein 46
LAMP-1	Lysosomal-associated membrane protein 1
IRGM	Immunity-related GTPase family M
SNARE	Soluble NSF attachment protein receptor
SLE	Systemic lupus erythematosus
SDS	Sodium dodecyl sulfate
wtNuc	wild type Nuc
ATF6	Activating transcription factor 6
UPR	Unfolded protein response
S1P	Site-1-protease
NPC1	Niemann-Pick type C1
NLS	Nuclear localization signal
FGF2	Fibroblast growth factor 2
Ata-Diox	α-dioxygenase
EGF	Epithelial growth factor
PIOX	Pathogen-inducible oxygenase
CLP	Cyclooxygenase-like peroxidase
ROS	Reactive oxygen species
LOX	Lipoxygenase
7,8-LDS	7,8-linoleate diol synthase
HPETE	hydroperoxy eicosatetraenoic acid
HETE	hydroxyl eicosatetraenoic acid

Chapter 1

Autophagy, recoded cyclooxygenases, and oxylipins

Abstract

Autophagy is a catabolic process by which large amounts of cellular biomass are engulfed in specialized double-membrane structures, denoted autophagosomes, which then fuse with lysosomes to digest cargo for energy and building material.[1] Macroautophagy, or canonical autophagy, is stimulated by nutrient deprivation and provides a means for cellular survival. However, cells may also utilize autophagic machinery for other purposes in the process in non-canonical autophagy. For example, cells may use autophagic structures to degrade or isolate foreign pathogens in a form of innate immunity known as xenophagy.[4]

An important aspect of autophagy that is yet poorly defined is how the cell chooses between target and non-target proteins, organelles, and pathogens. Or in other words, how does the cell create autophagosome structures specific for its appropriate tasks, whether they be in canonical or non-canonical autophagy. Clearly, selective autophagy must employ both protein and membrane components, and lipid metabolizing enzymes have been found to be critical in both the development of autophagosomes and in cargo selection.[1,3]

Recent work has shown that autophagy is induced by arachidonic acid (AA) liberated by cytosolic phospholipase A_2 ($cPLA_2$).[2] This polyunsaturated fatty acid is the substrate of the COXs and other critical signaling enzymes. Whether COX activity is required for AA induction of autophagy, however, has not been determined. Recently, our laboratory has discovered that seven proteins are translated from a transcript of the COX-1 gene using alternative translational methods (referred to as translational recoding). These mechanisms include the use of alternative start sites, ribosomal frame-shifting, and internal ribosomal entry sites.[3] In this dissertation, we

report that three of these proteins are binding partners of the vital autophagic regulator, autophagic-related protein 9a (ATG9a), and also localize with the auto-immune-associated protein nucleobindin (Nuc) around LLPSs.

Background

Macroautophagy

Macroautophagy is well understood in *S. cerevisea*; but over the past decade intense interest has focused on the more poorly understood process of mammalian macroautophagy due to its link to innate immunity,[4,5] cancer,[6] and many other pathological disorders.[7] In yeast and in mammals, macroautophagy is stimulated by stresses, such as nutrient deprivation[8] and hypoxia,[9] where large amounts of biomass are non-selectively engulfed and degraded to produce energy and substrates for metabolism. Under these conditions, the kinase mTOR (target of rapamycin) is inhibited, leading to release of the ATG13/ATG17 containing ULK1 complex from mTOR. The ULK1 complex then begins the nucleation step of autophagy through its activation of the Beclin-1 associated phosphatidylinositol-3 kinase class 3 (PI3KIII) complex. In the nucleation step, Beclin/PI3KIII complex metabolizes phosphatidylinositol-3-phosphate (PI(3)P) at or near the endoplasmic reticulum (ER) that evaginates the ER to form the omegasome, which becomes the site for autophagosome formation. Then PI(3)P recruits FYVE domain containing proteins/enzymes such as Double FYVE-domain containing protein 1 (DFCP1) and the ATG2-ATG18 complex. The E3-like ATG5-ATG12-ATG16L complex is then recruited to the

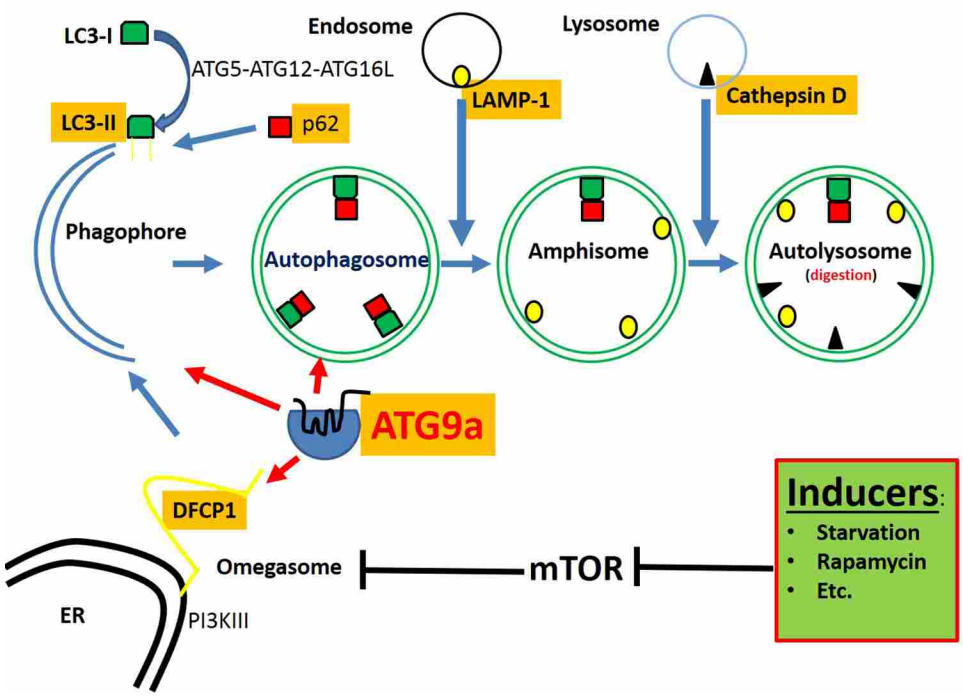

Figure 1: Pathway and critical components of macroautophagy. A schematic of the macroautophagy pathway with critical components. Upon stimulation of macroautophagy through inhibition of mTOR by starvation, PI3KIII metabolizes PI(3)P which recruits DFCP1 to the omegasome. The omegasome then develops into a phagophore where it is coated by LC3-II which aids in closure of the phagophore. Endosomes then fuse with the autophagosome to become an amphisome, LAMP-1 positive. The amphisome then fuses with a cathepsin D positive lysosome which is referred to as an autolysosome. At this stage, cargo within the autophagosome is digested for material and energy. Elements evaluated in this dissertation are highlighted with an orange background.

omegasome where it lipidates LC3-I to form phosphatidylethanolamine (PE) conjugated LC3-II. LC3-II coats the cup-shaped omegasome, at this stage of maturation termed a phagophore, and is essential for phagophore closure to form an autophagosome. Maturation of phagophore to autophagosomes occurs through elongation of the phagophore by incorporating membranes from multiple sources such as Golgi, ER, plasma, and mitochondria. ATG9a, a seven transmembrane protein, plays a critical role in recruiting these membranes to phagophore and autophagosomes.

Cargo to be contained in autophagosomes and ultimately digested may be added to the phagophore prior to closure. Alternatively, once autophagosomes have matured into double-membrane vesicles they fuse with cargo-carrying endosomes to form an amphisome. Amphisomes then fuse with lysosomes where cargo is digested by lysosomal enzymes. A diagram illustrating macroautophagy stimulated by nutrient deprivation and the important markers used to detect each step of the macroautophagic process used throughout this dissertation are shown in Figure 1.

Macroautophagic machinery is also employed in innate immunity by autophagosomes enveloping and digesting invading pathogens. Reference 10 provides an excellent overview of macroautophagy and provides examples of macroautophagic machinery used in innate immunity.

Non-canonical autophagy and innate immunity

In its strictest sense, xenophagy is a process by which invading microbes are engulfed by autophagosomes then fuse with lysosomes, for degradation.[11] This, therefore, is a type of autophagy. In a larger sense, xenophagy is an autophagic process associated with host defense whether through digestive (canonical) or non-digestive (non-canonical) mechanisms. The first evidence of this process was found when pathogen-associated molecular patterns (PAMPs) were reported to activate autophagy via Beclin-1 signaling.[12] Moreover, innate immune signals activated by invading organisms, such as interferon-γ (IFNγ),[13] were found to regulate autophagy by suppressing NFκB signaling.[14] A large body of work now shows microbe pathogenicity being effected by autophagy and these data are reviewed extensively by Deretic, V. et. al.[12]

With autophagy playing an important role in host defense, many microbes have evolved to counter or to even utilize autophagy for replication. In these processes, microbes often manipulate digestive macroautophagy to avoid destruction. For example, Herpesvirus counters

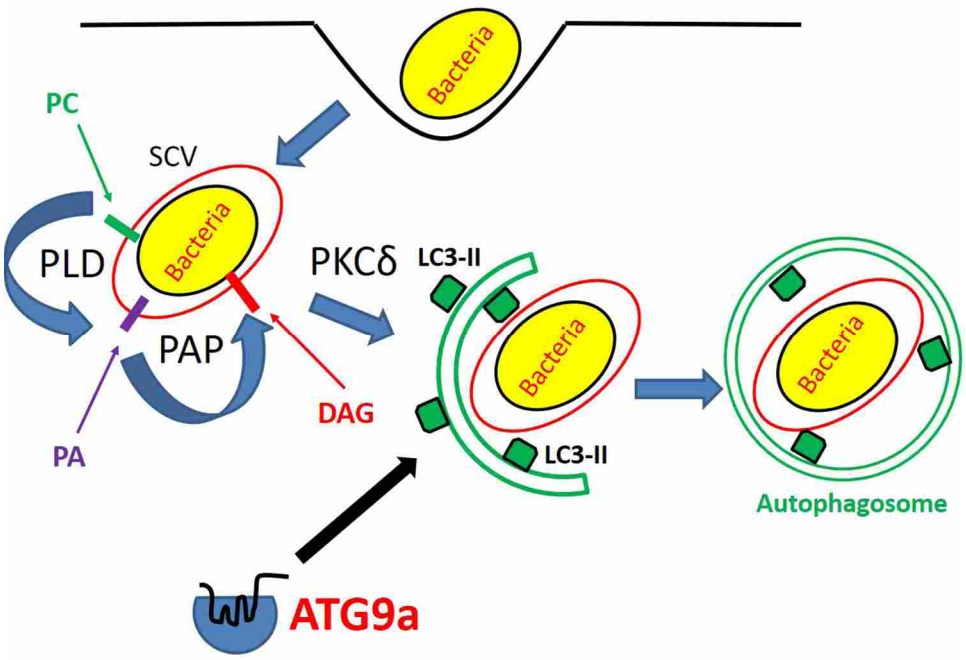

Figure 2: *Salmonella* evokes lipid remodeling in xenophagy. When *Salmonella* enters a host cell it forms a *Salmonella*-containing vacuole. In response to *Salmonella* binding, lipids of the vacuole remodel; phospholipase D (PLD) metabolizes phosphatidylcholine (PC) into phosphatidic acid (PA) that is then further modified by phosphatidic acid phosphatase (PAP) into diacylglycerol (DAG). DAG activates xenophagy through PKCδ stimulation. ATG9a is recruited to form the double membrane autophagosome that degrades the bacterium.

autophagic host defense by blocking autophagic induction through inhibiting Beclin-1 function by its viral protein ICP34.5.[15] Coxsackievirus B3 (CVB3) also blocks autophagic flux before autolysosome formation and uses non-digestive autophagosomes for viral assembly.[16] These autophagosomes become engorged with CVB3 viruses and form unique large structures termed megaphagosomes a type of LLPS. In contrast, Encephalomyocarditis virus (EMCV) actually induces autophagy, although this autophagy does not destroy the virus but acts as a means of delivery from the host cell.[17]

Cargo selection and lipid's role in autophagy

Just as in adaptive immunity, it is important for cells to distinguish between self and foreign invaders and to have precise systems to select subcellular components, including intracellular pathogens, for elimination. The most well-defined player in cargo selection is the autophagy receptor sequestrosome-1 (p62). This protein binds polyubiquitinated polypeptides and directs these proteins for degradation by tethering itself with its attached cargo to LC3-II situated on the membrane of phagophores.[18] When the phagophore closes cargo continues through amphisome formation and lysosome fusion to form autolysosomes, where complex and cargo are digested. This process is termed autophagic flux. Other autophagic cargo receptors are being identified for specific sub-forms of autophagy, such as the autophagic receptor Nix which is important for mitophagy (digestion of mitochondria).[19] Additionally, lipids are important for each step of the autophagic process by recruiting and/or regulating autophagic machinery.[20]

As mentioned above, metabolism of the lipid PI(3)P is critical in omegasome development through recruitment of autophagic proteins to the nucleation site. However, it is now clear that phosphatidyl inositol in its various phosphorylated forms plays multiple roles in autophagy. For example, class I PI3K (PI3KI) phosphorylates $PI(4,5)P_2$ to $PI(3,4,5)P_3$ that recruits activated protein kinase B (Akt) to activate the mTOR pathway.[21,8]

Non-inositol containing lipids are also important regulators of xenophagy. Phospholipase D (PLD) and phosphatidic acid phosphatase (PAP) sequentially produce the critical xenophagic lipid against *Salmonella Typhimurium* infection, diacyglycerol (DAG).[8] DAG generation activates protein kinase C isoform δ (PKCδ), which induces xenophagy through its downstream targets c-Jun N-terminal kinases (JNK) and NADPH oxidase (Figure 2).

Unsaturated fatty acids also appear to be critical for autophagy. Arachidonic acid is cleaved from the membrane by cytosolic phospholipase A_2 ($cPLA_2$) to induce autophagy in the rat macrophage cell line RAW246.7 and in primary human peripheral blood monocytes.[2] Additionally, overexpression of $cPLA_2$ induces autophagy by expressing IFNγ – an important signaling protein for xenophagy. Some specific downstream AA metabolites that induce autophagy were the lipoxygenase products leukotriene D_4 (LTD_4) and leukotriene E_4 (LTE_4) as well as the COX product prostaglandin D_2 (PGD_2). Oxygenated lipids, of which leukotrienes and prostaglandins are types, collectively are termed oxylipins. Oxylipins and the enzymes that generate them increasingly are being found to play roles in autophagy.[2]

Recently, our laboratory showed that the intron-1-retaining COX-1 splice variant, COX-3/COX-1b, is translationally recoded to produce multiple protein products.[2] Two of these products synthesize prostaglandins and have similar kinetics and pharmacological properties to COX-1. Three other products are un-glycosylated, do not participate in prostaglandin synthesis, and are detected in multiple rat tissues via Western blot (Appendix C). Figure 3 illustrates the protein products and their translational start sites described by our work, which is described in more detail in Appendix C.

In this dissertation, we demonstrate that the translationally recoded un-glycosylated forms of COX-3 proteins (denoted as rc57, rc50, and rc44 for their electrophoretic mobility) exhibit specific sub-cellular localizations and form a complex with the membrane organizing protein ATG9a at or near its N-terminus. This association is lost upon autophagy stimulation with rapamycin, indicating that the rcCOX/ATG9a complex is independent of macroautophagy. Moreover, this interaction is never found associated with the omegasome of macroautophagy. These, and other data, evaluating autophagic flux confirm that rcCOXs affect non-canonical

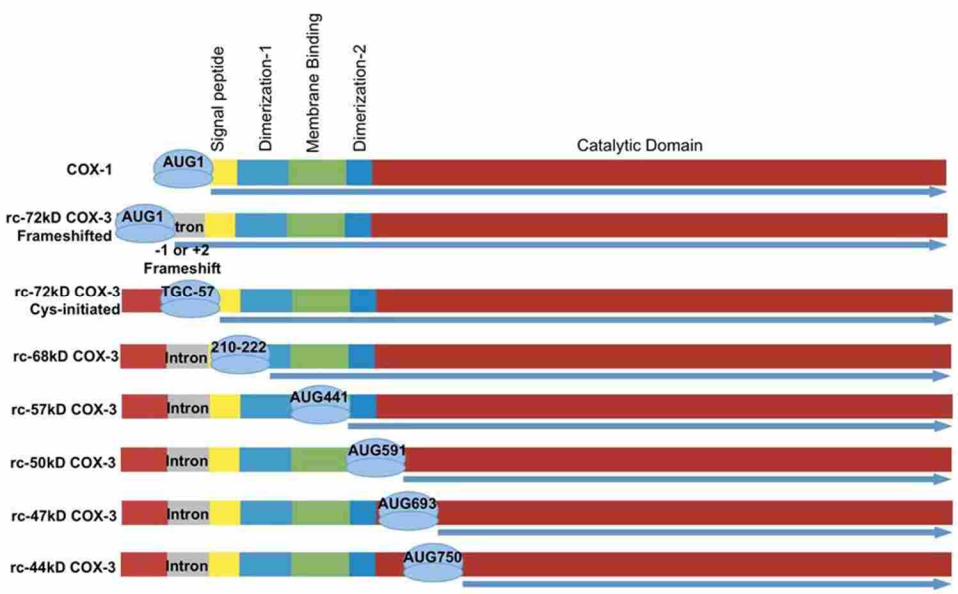

Figure 3: Diagram of recoded enzymes/proteins from COX-3 mRNA. Our laboratory previously determined that seven proteins were translationally recoded from rat COX-3 mRNA and that two of these are prostaglandin synthases. The rc72 kDa COX-3 proteins synthesize prostaglandins. Three of these recoded proteins--rc57, rc50, and rc44--are the main subjects of this research. Note the rc47 is translationally recoded from human COX-3. Image is from Dr. John Hunter.[3] Analogues of these proteins are also encoded by human COX-3 mRNA.

autophagy. Since this pathway is frequently associated with xenophagy we tested whether rcCOXs affect virus replication. We demonstrate that viral replication is differentially affected by rc57, rc50, and rc44, thus implicating rcCOXs in xenophagy.

Finally, we studied the biochemical effect of co-expressing rcCOX proteins with cytosolic nucleobindin (Nuc), which is also produced by recoding. Co-expression drives formation of LLPSs and this process is dependent on intrinsic oxylipin oxygenase activity of the rcCOX proteins as well as other factors we define.

References

1. Ravikumar, B.; Sarkar, S.; Davies, J. E.; Futter, M.; Garcia-Arencibia, M.; Green-Thompson, Z. W.; Jimenez-Sanchez, M.; Korolchuk, V. I.; Lichtenberg, M.; Luo, S.; Massey, D. C.; Menzies, F. M.; Moreau, K.; Narayanan, U.; Renna, M.; Siddiqi, F. H.; Underwood, B. R.; Winslow, A. R.; Rubinsztein, D. C., Regulation of mammalian autophagy in physiology and pathophysiology. *Physiol Rev* **2010,** *90* (4), 1383-435.

2. Qi, H. Y.; Daniels, M. P.; Liu, Y.; Chen, L. Y.; Alsaaty, S.; Levine, S. J.; Shelhamer, J. H., A cytosolic phospholipase A2-initiated lipid mediator pathway induces autophagy in macrophages. *J Immunol* **2011,** *187* (10), 5286-92.

3. Hunter, J. C. Multiple Recoding Mechanisms Produce Cyclooxygenase and Cyclooxygenase-Related Proteins from Frameshift-Containing COX-3/COX-1b Transcripts in Rat and Human. Brigham Young University, Brigham Young University, 2012.

4. Levine, B.; Mizushima, N.; Virgin, H. W., Autophagy in immunity and inflammation. *Nature* **2011,** *469* (7330), 323-35.

5. Deretic, V., Autophagy in immunity and cell-autonomous defense against intracellular microbes. *Immunol Rev* **2011,** *240* (1), 92-104.

6. Puissant, A.; Fenouille, N.; Auberger, P., When autophagy meets cancer through p62/SQSTM1. *Am J Cancer Res* **2012,** *2* (4), 397-413.

7. Shintani, T.; Klionsky, D. J., Autophagy in health and disease: a double-edged sword. *Science* **2004,** *306* (5698), 990-5.

8. Mehrpour, M.; Esclatine, A.; Beau, I.; Codogno, P., Overview of macroautophagy regulation in mammalian cells. *Cell Res* **2010,** *20* (7), 748-62.

9. Weerasekara, V. K.; Panek, D. J.; Broadbent, D. G.; Mortenson, J. B.; Mathis, A. D.; Logan, G. N.; Prince, J. T.; Thomson, D. M.; Thompson, J. W.; Anderson, J. L., Metabolic-Stress-Induced Rearrangement of the 14-3-3ζ Interactome Promotes Autophagy via a ULK1- and AMPK-Regulated 14-3-3ζ Interaction with Phosphorylated ATG9. *Mol. Cell. Bio.* **2014,** *34* (24), 4379-4388.

10. Reggiori, F.; Komatsu, M.; Finley, K.; Simonsen, A., Selective types of autophagy. *Int J Cell Biol* **2012,** *2012*, 156272.

11. Levine, B., Eating oneself and uninvited guests: autophagy-related pathways in cellular defense. *Cell* **2005,** *120* (2), 159-62.

12. Deretic, V.; Levine, B., Autophagy, immunity, and microbial adaptations. *Cell Host Microbe* **2009,** *5* (6), 527-49.

13. Tu, S. P.; Quante, M.; Bhagat, G.; Takaishi, S.; Cui, G.; Yang, X. D.; Muthuplani, S.; Shibata, W.; Fox, J. G.; Pritchard, D. M.; Wang, T. C., IFN-γ inhibits gastric carcinogenesis by inducing epithelial cell autophagy and T-cell apoptosis. *Cancer Res* **2011,** *71* (12), 4247-59.

14. Djavaheri-Mergny, M.; Amelotti, M.; Mathieu, J.; Besançon, F.; Bauvy, C.; Souquère, S.; Pierron, G.; Codogno, P., NF-kappaB activation represses tumor necrosis factor-alpha-induced autophagy. *J Biol Chem* **2006,** *281* (41), 30373-82.

15. Orvedahl, A.; Alexander, D.; Tallóczy, Z.; Sun, Q.; Wei, Y.; Zhang, W.; Burns, D.; Leib, D. A.; Levine, B., HSV-1 ICP34.5 confers neurovirulence by targeting the Beclin 1 autophagy protein. *Cell Host Microbe* **2007,** *1* (1), 23-35.

16. Kemball, C. C.; Alirezaei, M.; Flynn, C. T.; Wood, M. R.; Harkins, S.; Kiosses, W. B.; Whitton, J. L., Coxsackievirus infection induces autophagy-like vesicles and megaphagosomes in pancreatic acinar cells in vivo. *J Virol* **2010,** *84* (23), 12110-24.

17. Zhang, Y.; Li, Z.; Ge, X.; Guo, X.; Yang, H., Autophagy promotes the replication of encephalomyocarditis virus in host cells. *Autophagy* **2011,** *7* (6), 613-28.

18. Pankiv, S.; Clausen, T. H.; Lamark, T.; Brech, A.; Bruun, J. A.; Outzen, H.; Øvervatn, A.; Bjørkøy, G.; Johansen, T., p62/SQSTM1 binds directly to Atg8/LC3 to facilitate degradation of ubiquitinated protein aggregates by autophagy. *J Biol Chem* **2007,** *282* (33), 24131-45.

19. Kanki, T., Nix, a receptor protein for mitophagy in mammals. *Autophagy* **2010,** *6* (3), 433-5.

20. Dall'Armi, C.; Devereaux, K. A.; Di Paolo, G., The role of lipids in the control of autophagy. *Curr Biol* **2013,** *23* (1), R33-45.

21. Zoncu, R.; Efeyan, A.; Sabatini, D. M., mTOR: from growth signal integration to cancer, diabetes and ageing. *Nat Rev Mol Cell Biol* **2011,** *12* (1), 21-35.

Chapter 2

Recoded COXs complex with ATG9a, a vital component of autophagy

Abstract

Many components induce the development and progression of autophagosomes in their role of degrading target biomass. Lipids are one of these components vital to autophagosomes' development. One way lipids aid in autophagosomal development is in recruitment of autophagic machinery. The autophagic-related protein 9a (ATG9a) is a multi-transmembrane protein known to escort autophagic machinery and membrane to autophagosomes and is thus critical in autophagy.[1] Because of ATG9a's vital role in autophagy, others have intensively investigated its regulation and have identified binding partners and post-translational modifications of ATG9a.[8-9]

Through co-immunoprecipitations, confocal microscopy, and FRET techniques we show that rcCOX proteins (denoted as rc57, rc50, and rc44) form a complex with ATG9a at or near the amino terminus. This interaction is dependent on active target of rapamycin (mTOR), suggesting that it is important for non-canonical autophagic processes. We then show that rcCOXs are possibly involved in xenophagy by evoking differential effects on replication of encephalomyocarditis virus (EMCV).

Background

ATG9a is a transmembrane protein that shuttles between Golgi and autophagic structures

As stated in Chapter One, lipid composition of autophagosomes plays a critical role in both the recruitment of autophagic machinery and in the selection of cargo. Thus, enzymes that metabolize specific fatty acids, such as PI(3)P by PI3KIII, are important in the process of autophagy. Another important element in influencing membrane composition of

autophagosomes is the transport of lipids from Golgi, mitochondria, plasma membrane, and ER. This transport is performed by ATG9a.[1]

Currently, ATG9a is the only known autophagic protein with multiple transmembrane domains. In mammals, ATG9a contains six transmembrane domains and a glycosylation site at Arg99. Additionally, the amino terminus (first 67 amino acids) and carboxy terminus (last 343 amino acids) of ATG9a are both cytosolic.[2] In 2005, Yamada et. al. first identified two forms of human ATG9, designated as ATG9L1 and ATG9L2, and showed ATG9L1 to be ubiquitously transcribed in all tissues, whereas ATG9L2 was only expressed in placenta and pituitary gland.[3] When transiently transfected into COS7 cells, these forms were found perinuclear under normal cellular growth conditions; however, when cells were nutrient deprived, thus activating macroautophagy, ATG9a was in a cytosolic pattern and co-localized with LC3. Also, knockdown of ATG9a in HeLa cells decreased the number of autophagosomes under nutrient deprivation, suggesting a critical role for ATG9a in autophagy.[3]

Later confocal work demonstrated ATG9a localized specifically to trans-Golgi in HEK293 cells under basal conditions.[1] Upon activation of autophagy, ATG9a translocated from trans-Golgi and transiently interacted with the early endosomal marker Rab7, autophagosomal marker LC3, and phagophore marker DFCP1.[1,4] This transient interaction indicates that the action of ATG9a is in initiating and maturing the phagophore into autophagosomes and not as a structural component such as LC3-II.

Regulation of ATG9a is dependent on both protein binding and post-translational modifications

Through depletion experiments, it was shown that ULK1 is a major mobilizer of ATG9a.[5,1] It has been proposed that ULK1 initiates a pathway that activates ATG9a trafficking where the essential component to ATG9a lipid vesicle movement appears to be the motor protein

myosin II.[6] The method by which ATG9a removes membrane from cellular organelles may be accomplished through the membrane-curvature driving protein Bif-1.[7] Upon autophagy activation, Bif-1 co-localizes with ATG9a, ATG5, and LC3 in cytosol.[8,6] Knocking down Bif-1 in HeLa cells (specifically through its N-BAR domain) has been shown to cause fragmentation of Golgi in ATG9a trafficking and autophagosomal formation.[6]

An interesting form of regulation is by p38IP and p38α.[9] Binding of p38IP on the C terminus of ATG9a in starvation conditions causes ATG9a to translocate to the periphery of the cell. In complete medium, MAPK phosphorylates p38α, causing p38α to bind strongly to p38IP, which decreases its interaction with ATG9a. Thus MAPK activity plays a key role in preventing ATG9a translocation to the phagophore. Recently, ATG9a was also shown to be phosphorylated on the cytosolic C terminus at Ser761 by ULK1 and AMPK.[10] Phosphorylation of ATG9a occurred at low levels under rich medium conditions whereas it is phosphorylated by AMPK (independently of ULK1) under hypoxic and nutrient-deprived conditions. Phosphorylation, either under basal or hypoxic/nutrient-deprived conditions, causes 14-3-3ζ to bind to ATG9a. When this interaction is lost due to mutation of Ser761 to Ala autophagy is impeded in cells under hypoxic/nutrient deprived conditions illustrating the importance of 14-3-3ζ binding of ATG9a in autophagy.[10]

ATG9a is involved in innate immunity

Xenophagy is a very well documented process by which autophagic machinery (such as ATG9a) is utilized in innate immune host cell defense. In 2009, ATG9a was shown to be a suppressor of the anti-viral dsDNA response.[11] Studies with ATG9a knockout mice revealed that ATG9a suppressed stimulator of IFN genes (STING) from translocating from the ER to Golgi where STING assembles into a complex with TANK-binding kinase 1 (TBK1), activating genes

that promote innate immunity. Later, Kageyama et. al. showed ATG9a played a critical role in host cell defense in mouse embryonic fibroblasts (MEFs) infected with the bacterium *Salmonella typhimurium*.[12] *S. typhyimurium* develop in unique structures known as *Salmonella*-containing vacuoles (SCVs). LC3 then envelopes the SCV, independent of PI3KIII activity, indicating that in xenophagy LC3 recruitment does not require the macroautophagy lipid, PI(3)P. LC3 recruitment is also independent of ATG9a. Even though LC3 localization to SCV is independent of ATG9a and PI3KIII, ATG9a still played a critical role in the suppression of *S. typhimurium* growth. This is due to ATG9a's role in forming the autophagic double membrane around the SCV in the periphery of the cell. The authors concluded that recruitment of LC3 in certain xenophagic responses was independent of the formation of a canonical phagophore membrane, and that LC3 may in fact be recruited to "alternative target membrane"[12] but ATG9a is still required in the innate immune response through recruitment of autophagic machinery to the pathogen. The alternative target membrane was later found to be enriched in diacylglycerol (DAG).[13] Additionally, phospholipase D (PLD) and phosphatidic acid phosphatase (PAP) were shown to be required for DAG generation and xenophagy; hence, increasing the number of lipid metabolizing enzymes that influence autophagy.

In the present research, we describe a novel interactor of ATG9a that functions independently of macroautophagy. We further demonstrate via confocal microscopy that rcCOXs localize to cytosol, nucleus, Golgi, ATG9a vesicles, and autophagosomes but not to the macroautophagy related ER derived phagophores (omegasomes), endosomes, or lysosomes. We find that rcCOXs interact with the N terminus of ATG9a, an interaction abolished when macroautophagy is activated with rapamycin. We then show rcCOXs differentially effect EMCV replication indicating their role in innate immunity.

Materials and Methods

Materials

Antibodies used throughout this study are listed in Appendix B and primers used in this study are listed in Appendix A.

Cell culture

Chinese hamster ovary (CHO) cells were obtained from ATCC and grown in DMEM/F12 50:50 medium (Corning) with 10% fetal bovine serum (FBS [Gibco]) and 1% penicillin/streptomycin (Gibco) at 37° C and 5% CO_2 and used at passages below 20. Cells were passaged by washing the cells twice in phosphate buffered saline (10.4 mM Na_2HPO_4, 1.7 mM KH_2PO_4, 2.7 mM KCl, 136 mM NaCl pH: 7.4 [PBS]) and trypsinized (0.05% trypsin from Sigma-Aldrich) until cells detached and were seeded onto new plates.

Plasmid DNA purifiction

We used a Genelute plasmid mini-prep kit (Sigma-Aldrich) according to the instructions of the manufacturer for purification of plasmid DNA from transformed DH5α E. coli cells (Invitrogen). Transformed cells were grown in LB broth (Prepared by adding 10 g Bacto-Tryptone [BD], 5 g Bacto-Yeast Extract [BD], 10 g NaCl, and 100 mg Ampicillin [Fischer] into 1 L of water and sterilized by autoclave) overnight at 37° C with agitation at 250 rpm. After incubation, cells were pelleted at 3,000xg for 10 minutes. The LB broth was removed and pellets were resuspended in 200 µL of resuspension buffer (provided by kit). Cells were lysed by the addition 200 µL of lysis buffer (provided by kit). After inverting tubes twice 350 µL of neutralization buffer (provided by kit) was added and samples were again inverted. Cell debri was pelleted in a microcentrifuge for 10 minutes at 14,000 rpm. Supernatant was removed and transferred to mini-prep column provided by the kit (Sigma-Aldrich) and centrifuged again for 1

minute at 14,000 rpm. Then 750 µL of wash buffer was added to the column and centrifuged again as before. The column was dried by centrifugation for 2 minutes at 14,000 rpm. Elution buffer was added to dried columns and centrifuged at 14.000 rpm for 1 minute. DNA concentration was measured using Take3 module for the Synergy H4 Hybrid plate reader.

DC protein assay

DC protein assay kit was obtained from Bio-Rad. In this process, 5 µL sample was placed into wells of a 96-well plate. Then 25 µL of Reagent A, prepared by addition of 20 µL of reagent S into 1 mL of reagent A, was added to each sample and the reaction started by the addition of 200 µL of reagent B and allowed to incubate for 15 minutes at room temperature. Protein was measured at an absorbance of 750 nm using a Synergy H4 Hybrid plate reader. The measurements were compared to protein standards prepared by serial dilution of 2 mg/mL of BSA (Bio-Rad) to 0.05 mg/mL and then measured as described above.

Transient transfection

Transient transfections were performed using CHO cells which were seeded onto 6-well plates at a confluency of 70% in DMEM/F12 media with 10% FBS and allowed to incubate overnight at 37° C and 5% CO_2. After incubation, DNA was prepared by adding 1500 ng of DNA to DMEM/F12 to a total volume of 100 µL. Then 100 µL of lipofectamine solution (10 µL of lipofectamine [Invitrogen] into 90 µL of DMEM/F12) was added and rotated room temperature for 20 minutes. Cells were washed with DMEM/F12 and 600 µL of media was added to cells. Prepared lipofectamin/DNA solution was added to cells, to a total volume of 800 µL, and allowed to incubate for 2 hours at 37° C and 5% CO_2 in incubator. After incubation, 800 µL of DMEM/F12 media with 20% FBS was added, and cells were left to incubate at 37° C for an additional 22 hours.

Site-directed mutagenesis

Site-directed mutagenesis experiments were done using the Invitrogen Geneart site-directed mutagenesis kit. Primers (listed in Appendix A) were prepared for homologous recombination in which the forward primer contained the desired mutation and the reverse primer contained at its 5' end at least 12 nucleotides overlapping the 5' end of the forward primer. The PCR reaction was performed using platinum Pfx (Invitrogen) following the protocol provided, with 100 ng of DNA as template. Amplification was performed using a GeneAMP 9700 PCR system thermocycler (Applied Biosystems). After the polymerase was heat-activated at 94° C for 5 minutes, samples were amplified for 18 cycles, in which each cycle was the following: 30 seconds at 94° C, 30 seconds at melting temperature of the primers (usually 57° C), and amplicons extended at 68° C for 1 minute for every 1000 bp of DNA template. After 18 cycles, complete synthesis was assured by an extra 5 minutes of reaction at 68° C. Amplicons were then separated from template by DpnI digestion (New England Bio) for 1 hour at 37° C, heat inactivated at 80° C, electrophoresed on a 1% agarose gel in TBE buffer (0.18 M Tris, 0.1 M boric acid, 2 mM EDTA) with 0.0024% ethidium bromide, and visualized using UV light. Amplicons of the appropriate size were then excised from the gel and purified using a Qiagen Gel Extraction kit.

Purified amplicons were then circularized by homologous recombination using the Geneart site-directed mutagenesis module (Invitrogen) where amplicon was added to 5x reaction buffer, 10x recombination enzyme, and Dnase/Rnase free water to a final volume of 10 μL. The reaction was allowed to run for 10 minutes at room temperature. After the reaction, circularized amplicon was then transformed into chemical competent DH5α *E. coli* cells (Invitrogen).

Transformation of amplicons into *E. coli* was performed according to the protocol provided by Invitrogen. Briefly, DNA was incubated with the competent cells for 30 minutes on ice. After 30 minutes, cells were heat shocked at 42° C for 22 seconds and placed back on ice for 2 minutes. SOC media, provided by the Invitrogen kit, was added at 250 µL for every 50 µL of *E. coli* cells. Cells were then incubated for 1 hour at 37° C agitating at 250 rpm. After 1 hour incubation, bacteria were inoculated onto LB plates with 100 mg/L ampicillin and cultured at 37° C overnight. The following day, single colonies were picked and cultured in LB broth overnight at 37° C. DNA plasmids were then purified from bacteria.

Co-immunoprecipitation of ectopic ATG9a and rc57

CHO cells were transfected with a N-terminally hemagglutinin (HA)-tagged ATG9a (graciously provided by Dr. Tooze's laboratory at Cancer Research United Kingdom London Research Institute)[2] and Myc-tagged rc57 and then incubated for 24 hours. Cells were washed twice with 250 µL of TBS (100 mM Tris HCl, 150 mM NaCl pH 7.4) and cells were scraped into 500 µL of TBS with a cocktail of protease inhibitors (Roche). Cells on ice were then lysed by sonicating until cells were properly lysed (typically between 1-2 minutes) using a Heat Systems-Ultrasonics W-385 sonicator. Unlysed cells and nuclei were pelleted by centrifuging samples for 5 minutes at 4° C and 500xg. Supernatant was transferred to new Eppendorf tubes with or without digitonin (Sigma Aldrich) at a final concentration of 0.05%, and samples were solubilized via rotation at 4° C for 15 minutes. Protein was measured using BC assay as described above and equal amounts of protein were added into their respective Eppendorf tubes and diluted to 250 µL using wash buffer (100 mM Tris HCl, 150 mM NaCl pH 7.4 with protease inhibitors and 0.05% digitonin). Samples were incubated with 5 µL bead volumes of magnetic A/G beads (Thermo Scientific) coated with 2 µg of antibody against HA (Santa Cruz) or non-

specific antibody, such as against glutathione S transferase (GST) or Myc (Abcam). Samples, antibodies, and beads and were incubated together for 1 hour at 4° C on rotator. After incubation, beads were pelleted with a magnet and supernatant was removed. Beads were then washed twice with 25 bead volumes of TBS and electrophoresis sample buffer (50 mM Tris-HCl, 0.1% SDS [w/v], 0.4% glycerol [v/v], 0.01% bromophenol blue [w/v]) was added to elute protein from the beads. Polyacrylamide gel electrophoresis and immune-blotting was then performed.

Immunoblot analysis

Samples were incubated in sample buffer for 10 minutes at 65° C. Samples were then loaded onto 10% polyacrylamide/0.47% bis-acrylamide gels and electrophoresed in running buffer (100 mM Tris, 750 mM glycine, 1% [w/v] SDS) at 15 mAmp. Gels were then transferred onto nitrocellulose membrane (0.2 μm, BioRad) in transfer buffer (100 mM Tris, 750 mM glycine, 20% [v/v] MeOH) for 1 hour and 15 minutes at 100 V. Membranes were blocked in 2.5% milk in PBS for 1 hour at room temperature with gentle agitation and then incubated with primary antibody solution (primary antibodies in PBS and 0.1% milk) overnight at 4° C on a rotator. After overnight incubation, membranes were washed three times for 5 minutes each with PBST (PBS with 0.1% Tween 20) at room temperature with gentle agitation. Membranes were then incubated with secondary antibody (Li-Cor) in PBS for 1 hour with gentle agitation. After incubation, membranes were again washed 3 times in PBST and scanned by Odyssey Infrared Imaging Systems (Li-Cor Biosciences) and visualized using Odyssey software.

Collagenizing glass slides

Cover glass slides were collagenized by incubating 2 mL of collagen buffer (0.03 mg/mL of rat tail collagen I (Gibco) in MQ water with 0.115% glacial acetic acid v/v) for 1 hour in the

dark at room temperature. After hour incubation, collagen buffer was removed and glass slides were washed 3 times with 2 mL of PBS. Slides were allow to dry and stored in the dark at 4° C.

Confocal microscopy

Cells were washed three times in warm sterile filtered PBS and then fixed by 4% paraformaldehyde (Sigma Aldrich) in PBS for 15 minutes gently rocking at room temperature. After fixation, samples were washed three times in 1 mL of PBS and blocked for at least 30 minutes in PBST with 1% goat serum (Sigma Aldrich). After a 30 minute incubation, samples were again washed three times with 1 mL of PBS and incubated for at least 20 hours with 500 µL of primary antibody in PBST with 1% goat serum. After incubation, primary antibody solution was removed and cells were washed three times for 5 minutes each by gently rocking in warm PBS. Samples then incubated with 500 µL of secondary antibody against mouse, rabbit, or chicken IgG antibody and DAPI (Invitrogen) in PBST for 2 hours at room temperature in the dark. After the 2 hour incubation, secondary antibody was removed and samples were washed three times, 10 minutes each wash, in PBS gently rocked in the dark. After washes, slides were mounted with ProLong Gold antifade reagent (Life Technologies) and allowed to incubate in the dark over night at room temperature. Confocal micrographs were taken with an Olympus Fluoview 1000 confocal microscope mounted on an Olympus IX81 inverted microscope at 60x magnification. Sequential scans were taken with filter settings specific for the respective secondary antibodies utilized.

Acceptor photobleach FRET analysis

FRET was performed on cells in which ATG9a was tagged at its N-terminus with monomeric RFP (mRFP) which was kindly donated to us from Dr. Tooze's laboratory at Cancer Research United Kingdom London Research Institute and rc57 was tagged on a solvent exposed

internal loop with enhanced GFP (eGFP). Sample preparation followed the protocol outlined in the confocal microscopy section, without the addition of primary or secondary antibodies. FRET calculations were performed on an Olympus Fluoview 1000 confocal microscope mounted on an Olympus IX81 inverted microscope at 60x magnification. Acceptor photobleach FRET settings followed the manufacturer's presets utilizing the acceptor photobleach wizard for eGFP-mRFP pairing as donor and acceptor, respectively. After regions were assigned, acceptor fluorescence was bleached to 25% intensity and distances and efficiencies calculated by Olympus software. Förster distances were set to R_o = 4.7 nm, per Peter et al.[14] FRET efficiencies were calculated by $FRET\ Efficiency\ (E) = 1 - \frac{Prebleaching_{donor}}{Postbleaching_{donor}}$. Distances were calculated by $distance\ (r) = R_O * \left[\left(\frac{1}{E}\right) - 1\right]^{\frac{1}{6}}$. Averages for both distance and efficiencies were taken per region as reported, n = 10.

EMCV infection

CHO cells were transfected as described above and after 24 hours transfected cells were washed twice with 500 µL warm DMEM F-12. Then 200 µL of DMEM/F12 with EMCV at MOI of 1 was added and virus allowed to adsorb for 1 hour with gentle agitation every ten minutes. After adsorption, cells were washed twice with 500 µL of DMEM/F12 and cells were incubated with 2 mL of DMEM/F12 with 10% FBS for 36 hours in incubator at 37° C and 5% CO_2. After incubation, media was removed and filtered with 0.45 µm sterile filters (Thermo Scientific). Virus-containing media were stored in liquid nitrogen until plaque forming assays were performed.

Plaque forming assay

Cells were seeded onto 6-well plates for at least 12 hours with DMEM/F12 with 10% FBS and 1% Pen/Strep and were washed twice with DMEM/F12 with 10% FBS. Then 200 µL

of thawed virus serially diluted into sterile PBS was added to cells and allowed to adsorb for 1 hour with gentle agitation every 10 minutes. Afterwards, cells were washed twice with 500 µL of DMEM/F12 with 10% FBS and then 1% low melting point agarose in DMEM/F12 with 10% FBS was overlaid on the cells and agarose was allowed to solidify. One percent low melting point agarose was prepared by melting 2% low-melting point agarose in PBS and rapidly mixing it with an equal volume of DMEM/F12 with 20% FBS and immediately overlaying the solution onto the cells. Cells were allowed to incubate at 37° C in incubator for 36 hours. After incubation, plaques caused by virus infection were visualized by adding 200 µL of PBS with 5 mg/mL 3-(4,5-dimethylthiazol-2-yl)-2,5-diphenyltetrazolium bromide (MTT), incubated for 1 hour at 37° C and counted.

Results

Confocal microscopy of rcCOXs identifies a role in autophagy

The rcCOXs investigated in this study do not contain N-terminal signal peptides, we therefore hypothesized that they localize to cytosol and we tested this through confocal microscopy by imaging CHO cells transiently transfected with C-terminally FLAG-tagged rat rcCOX constructs labeled with anti-FLAG antibodies.

Confocal micrographs showed cells transfected with rc57 or rc50 to exhibit cytosolic distribution as well as a punctate pattern of localization, indicative of localizing to organelle structures (Figure 4A). We found two main populations of rcCOX puncta, one form was found near or around the nucleus, suggesting a Golgi-like pattern and the other found in the periphery suggesting non-Golgi organelles. We therefore dually-labeled CHO cells transiently transfected with rc57 or rc50 with antibodies against rcCOX, anti-FLAG antibody, and antibodies against lipid bodies (ADRP), mitochondria (Mitotracker), Golgi (mannosidase-II), or autophagosomes

(LC3-II) and imaged using confocal microscopy. We found the rc57 and rc50 puncta near the nucleus were positive for Golgi markers and puncta at the periphery were positive for the autophagosome marker.

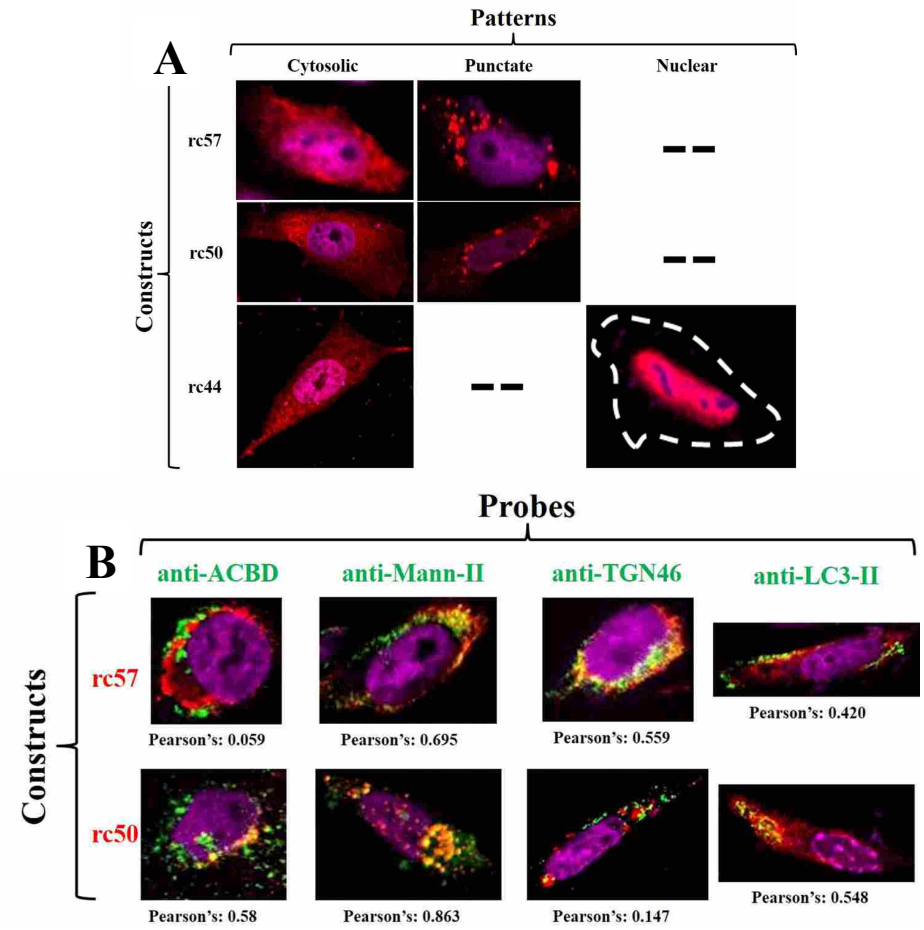

Figure 4: Sub-cellular localization of rc57, rc50, and rc44. A) FLAG-tagged rcCOX transcripts were transfected into CHO cells and visualized by confocal microscopy using antibodies against the FLAG tag. A) The rc57 and rc50 are punctate and cytosolic, while rc44 is found in the nucleus and cytosol. B) The rc57 and rc50 FLAG-tagged constructs were again transfected into CHO cells and cells were dually labeled with antibodies against FLAG peptide (rcCOX) and against either cis-Golgi (ACBD), intermediate Golgi (mannosidase-II), trans-Golgi (TGN46) or autophagosome (LC3-II) and imaged by confocal microscope. Purple: Nucleus (DAPI); Red: rcCOX; Green: Golgi, autophagosomes; and Yellow: rcCOX and marker co-localization.

We next tested for Golgi sidedness by dual-labeling CHO cells transfected with FLAG-tagged rc57 or rc50 with probes against the rcCOX proteins in combination with markers targeting either cis-Golgi (ACBD), intermediate Golgi (mannosidase II), or trans-Golgi (TGN46) apparati. Very little rc57 co-localized with cis-Golgi marker (Pearson's coefficient: 0.059). However, rc57 co-localized strongly with intermediate and trans-Golgi markers (Pearson's coefficient: 0.695 and 0.559 respectively). In contrast, rc50 co-localized with cis and intermediate Golgi markers (Pearson's coefficient: 0.58 and 0.863 respectively) more than trans-Golgi (Pearson's coefficient: 0.127) (Figure 4B). Unlike rc57 and rc50, rc44 did not exhibit a punctate pattern or localize to Golgi and autophagosomes but instead exhibited a cytosolic and intranuclear pattern (Figure 4A).

rcCOXs do not localize to amphisomes but rc50 associates with autolysosomes

Because rcCOXs co-localized with autophagosomes, we next determined if rcCOXs interacted with other autophagic organelles such as amphisomes or autolysosomes. We again transiently transfected CHO cells with FLAG-tagged rc57 or rc50 and dually labeled cells with antibodies against FLAG peptide or with antibodies against either LAMP-1 (amphisome marker) or cathepsin D (autolysosome marker) and imaged these via confocal microscopy. Neither rc57 nor rc50 co-localize with amphisomes (Figure 5). Similarly, rc57 did not co-localize with autolysosomes whereas rc50 did.

Permeabilization of cells shows rcCOXs are not intraluminal autophagosomal cargo

We next determined whether rc57 and rc50 were either intraluminal or on the cytosolic surface of Golgi and autophagosomes by permeabilizing the plasma membrane with digitonin which causes cytosolic proteins to leak from the cell. CHO cells were transfected with FLAG-tagged rc57, rc50, or rc44 for 24 hours and before being prepared for confocal imaging the cells

were treated with 20 μM digitonin in PBS for 10 minutes and washed three times with PBS.[15] We labeled cells with the cytosolic marker GAPDH, the intraluminal/membrane bound Golgi markers TGN46 or mannosidase-II, or the autophagosome marker LC3-II. We found digitonin treatment washed GAPDH from cytosol of CHO cells while the intraluminal/membrane bound Golgi markers continued localizing near the nucleus in a Golgi-like pattern and LC3-II in a punctate pattern, indicating digitonin permeabilized cells without disrupting organelle structure.

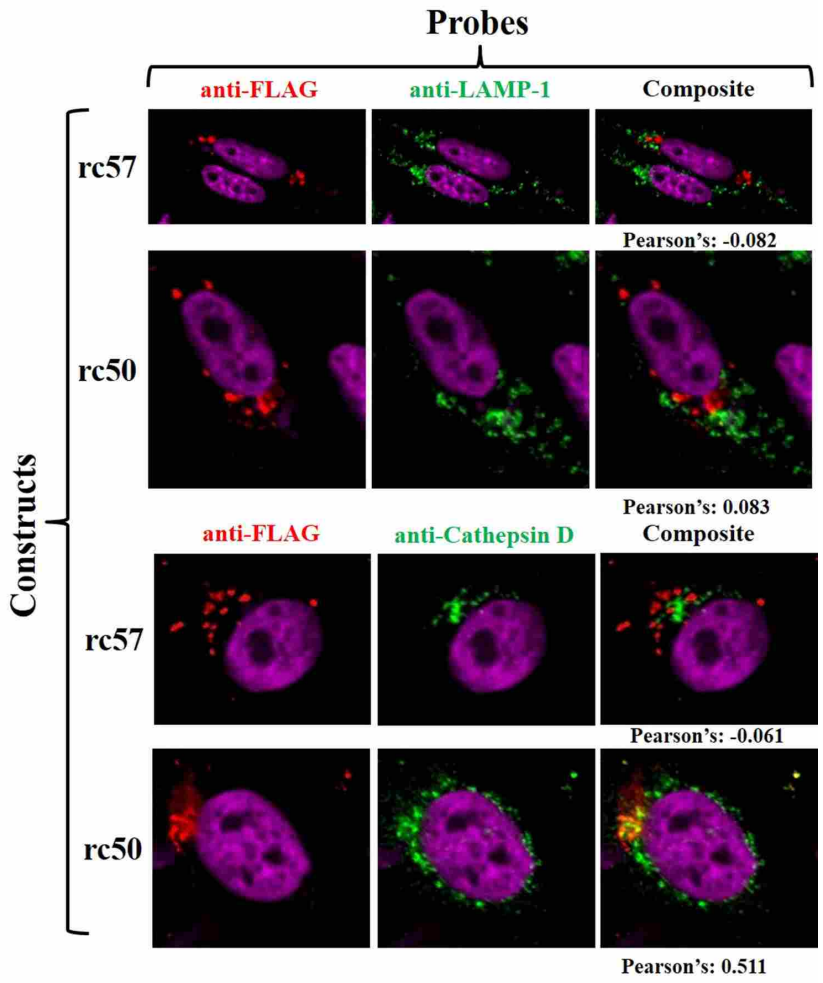

Figure 5: Recoded 57 and 50 do not localize to amphisomes while only rc50 localizes to autolysosomes. CHO cells transfected with either FLAG-tagged rc57 or rc50 and dually labeled with antibodies against the amphisome marker LAMP-1 or the autolysosome marker cathepsin D and imaged using confocal microscope. Purple: Nucleus (DAPI); Red: rcCOX; Green: LAMP-1 or cathepsin D; and Yellow: rcCOX and marker co-localization.

The same digitonin treatment removed rc57, rc50, and rc44 from cytosol along with cytosolic GAPDH indicating that rc57, rc50, and rc44 are associated with the cytosolic surface of Golgi. This treatment also removed most of the punctate localized rc57 and rc50; however, a few punctate structures remained (Figure 6).

We next determined whether these remaining punctate structures were Golgi or autophagosomes by dually labeling CHO cells transfected with rcCOXs against Golgi markers TGN46, mannosidase-II, autophagosome marker LC3-II, or autolysosomal marker cathepsin D. When these cells were treated with digitonin, we found that rc57 and rc50 ceased to co-localize with any Golgi markers. Similarly, digitonin treatment removed nearly all rc57 and rc50 from autophagosomes with only a few rc57 or rc50 positive autophagosomes surviving this treatment. Recoded 50 was also nearly all removed from autolysosomes (Figure 7). We concluded that these few instances where rc57 and rc50 co-localized to autophagosomes or autolysosome may represent rare examples where rcCOXs are autophagosomal cargo. Alternatively, these structures may represent a minority subset where rc57 and rc50 are more firmly attached to the cytosolic surface of membrane. Additionally, there were some punctate structures of rc57 and rc50 that survived digitonin treatment that did not co-localize with either Golgi or autophagosome markers. Together these results indicate that rc57 and rc50 are weakly bound to the cytosolic surface of Golgi and autophagosomes probably through interacting with either a membrane bound protein or membrane component on the surfaces of those structures. Additionally, rc57 and rc50 associate more strongly with a subset of autophagosomes and other non-autophagosomal vesicles.

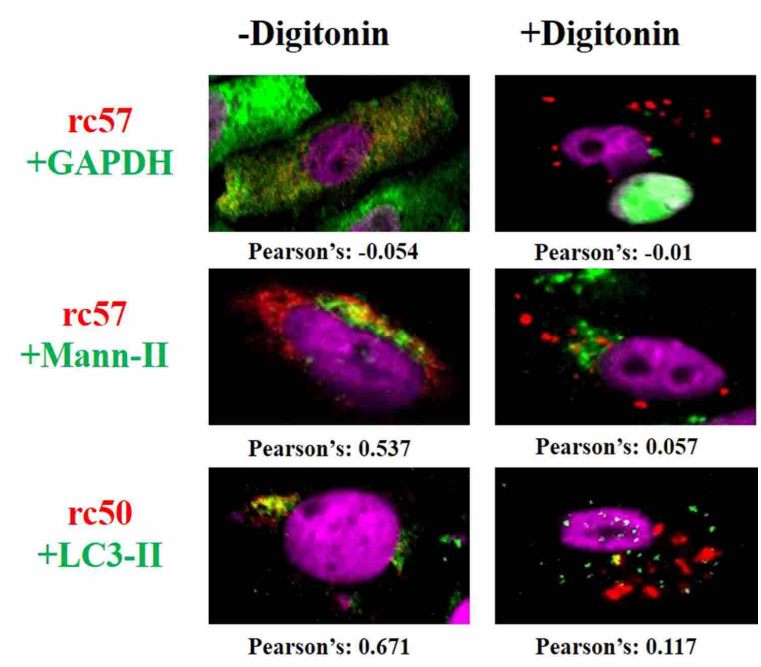

Figure 6: Cellular permeabilization shows rc57 and rc50 reside mainly on cytosolic surface of Golgi, autophagosomes, and autolysosomes. CHO cells transfected with rc57 or rc50 were permeabilized with digitonin and washed which removed cytosolic GAPDH, rc57, rc50, or rc44 from cells while organelle bound proteins LC3-II or mannosidase-II were retained. Purple: Nucleus (DAPI); Red: rcCOX; Green: GAPDH, LC3-II, mannosidase-II, or cathepsin D; Yellow: rcCOX and protein marker co-localization.

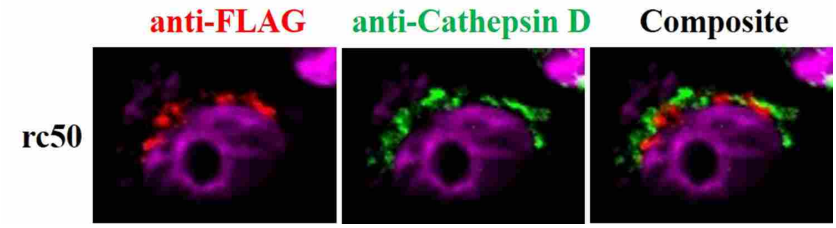

Figure 7: Digitonin treatment removes rc50 from autolysosomes. CHO cells transiently transfected with FLAG-tagged rc50 were treated with digitonin and dually probed against FLAG tag and cathepsin D. Purple: Nucleus (DAPI); Red: rcCOX and Green: cathepsin D.

rcCOXs co-localize with ATG9a vesicles

As the ATG9a, rc57, and rc50 localization pattern were similar, we hypothesized that rc57 and rc50 would localize to ATG9a. We co-transfected FLAG-tagged rc57, rc50, or rc44 with N-terminal mRFP labeled ATG9a, hereafter referred to as mRFP-ATG9a, and monitored co-localization by confocal microscopy. Near complete overlap of expression between rcCOXs and ATG9a was observed with Pearson's coefficients equal to 0.973, 0.954, and 0.928 for rc57, rc50, and rc44 respectively. The mRFP-ATG9a co-localized with rc57 and rc50 was particularly intense at two sites: near the nucleus (indicating accumulation at the Golgi) and at the periphery of the cell. The mRFP-ATG9a only co-localized with rc44 in the periphery of the cell when rc44 was cytosolic, but did not co-localize with rc44 when the latter protein was intranuclear (Figure 8A).

These results were further replicated when we assessed the localization of rc57, rc50, and rc44 with endogenous ATG9a using an anti-ATG9a antibody (Figure 8B). Again, a very high degree of overlap between rcCOXs and endogenous ATG9a was observed (Pearson's coefficient: rc57 = 0.74, rc50 = 0.73, rc44 = 0.66); however, when rc44 was nuclear, endogenous ATG9a was found in a punctate pattern in the periphery of the cell and no overlap occurred with rc44 (Pearson's coefficient: -0.13).

We next determined whether these ATG9a positive vesicles represent the digitonin insensitive vesicles observed in our previous digitonin experiment due to previous studies showing ATG9a is not washed from permeabilized cells.[2] We again permeabilized FLAG-tagged rcCOX transiently-transfected CHO cells with digitonin and dually labeled cells with antibodies against ATG9a and FLAG peptide. As observed before, the cytosolic pool of rc57 and rc50 washed from cells with digitonin treatment but a punctate pool persisted. These rcCOX

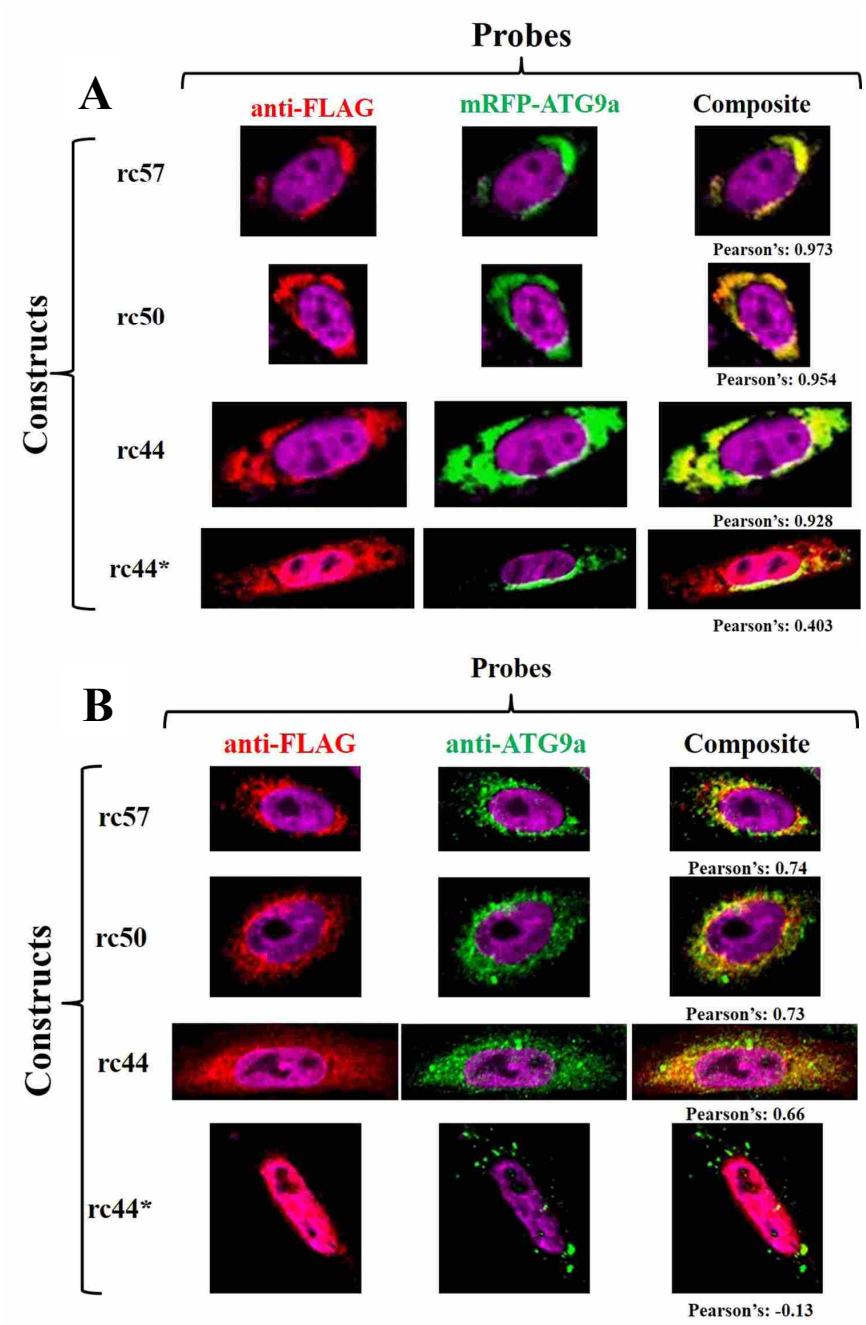

Figure 8: rcCOXs co-localize with ATG9a. A) mRFP-ATG9a was co-transfected with either FLAG-tagged rc57, rc50, or rc44 into CHO cells and labeled with antibodies against FLAG peptide, then visualized using a confocal microscope. B) FLAG-tagged rcCOX transcripts were transfected into CHO cells and co-localization between rcCOXs and endogenous ATG9a were visualized by confocal microscopy. * Images of rc44 in the nucleus. Purple: Nucleus (DAPI); Red: rcCOX; Green: ATG9a; and Yellow: rcCOX and ATG9a co-localization.

punctate structures co-localized with ATG9a, which demonstrates that the punctate structures are ATG9a vesicles and that the interaction between rc57 and rc50 with ATG9a is strong (Figure 9).

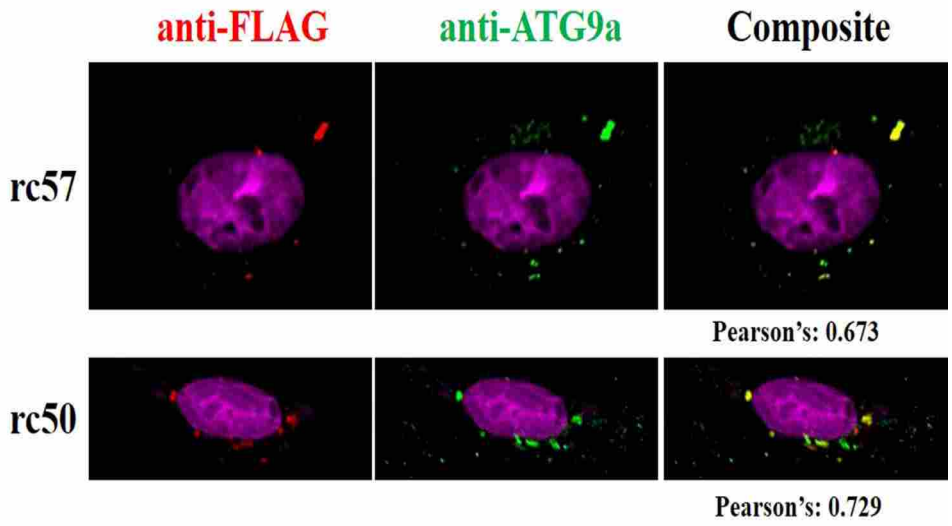

Figure 9: Digitonin treatment does not remove rcCOX from ATG9a. We again performed digitonin treatment of CHO cells transiently transfected with either FLAG-tagged rc57 or rc50 and dually labeled cells with antibodies against rcCOX (anti-FLAG) and against endogenous ATG9a. Purple: Nucleus (DAPI); Red: rcCOX; Green: ATG9a; and Yellow: rcCOX and ATG9a co-localization.

rcCOX binds near the N-terminus of ATG9a

Because confocal microscopy could not distinguish between a general co-localization and direct interaction between rcCOXs and ATG9a, we performed co-immunoprecipitation experiments to assess ATG9a binding. This was done by co-transfecting FLAG-tagged rc57 with N-terminal HA-tagged ATG9a and immuno-precipitating the ATG9a complex using anti-HA antibody. We found that rc57 co-immunoprecipitated with HA-ATG9a, demonstrating that these proteins, if not binding partners, are in the same protein complex (Figure 10).

We next examined the binding site of the rcCOX complex on ATG9a. Due to rcCOXs presence in cytosol, we hypothesized that rcCOX would form a complex either to the cytosolic amino or carboxyl terminus of ATG9a. We therefore truncated the last 343 amino acids of the

C-terminus of HA-tagged ATG9a (ATG9aΔC) and co-transfected this with FLAG-tagged rc57 into CHO cells which was subjected to HA antibody immunoprecipitating ATG9aΔC. Inspite of truncation of its C-terminus ATG9a continued to co-immunoprecipitate with rc57 (Figure 11). We attempted to confirm that the N-terminus was the rc57 binding site by truncating this region. However, after multiple attempts we were unable to achieve ATG9a expression when the cytosolic N-terminus was removed (data not shown).

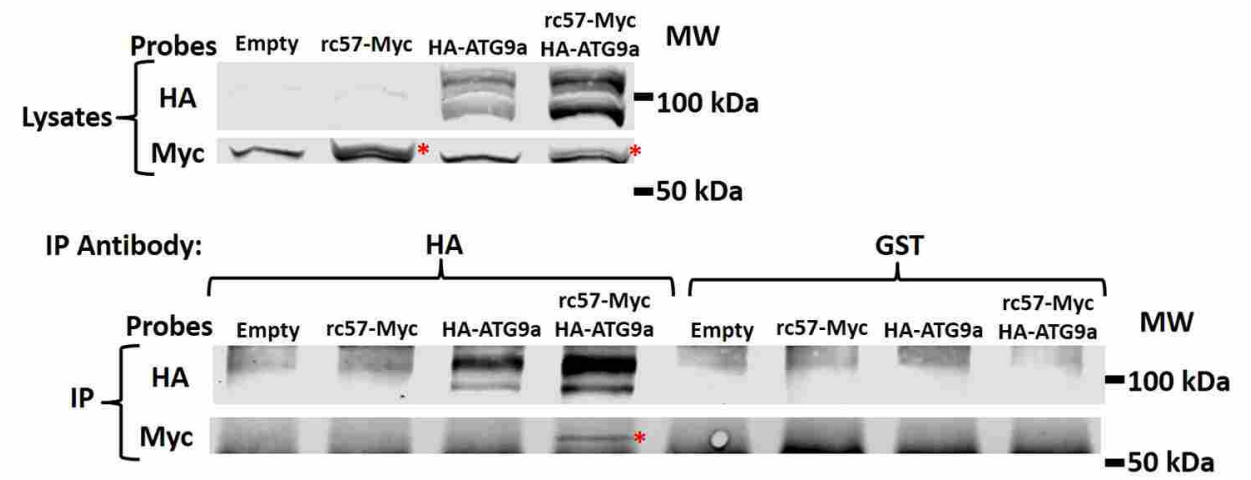

Figure 10: Recoded 57 co-immunoprecipitates with ATG9a. HA-tagged ATG9a was co-transfected with Myc-tagged rc57 in CHO cells and immunoprecipitated using antibodies against HA. Images are immunoblots probed using primary antibodies against HA (ATG9) and Myc (rc57) and visualized using secondary antibodies against mouse IgG (ATG9) and rabbit IgG (rc57). * denotes the Myc-tagged rc57. This is 1 image out of 3 experiments.

Next we tested whether the rcCOX binding site on ATG9a was cytosolic or intra-vesicular by permeabilizing CHO cells transiently transfected with internally eGFP-tagged rcCOX and mRFP-ATG9a and then adding trypsin to digest any cytosolic exposed peptide. Cells were live-imaged, and any fluorescence signal lost within one minute after addition of trypsin was considered to represent cytosolic location of the fluorochrome.[15] As previously reported by Young et. al.,[2] the mRFP signal of mRFP-ATG9a was lost after adding trypsin to permeabilized cells indicating the amino terminus of ATG9a is cytosolic. We replicated this

result when mRFP-ATG9a was transfected into CHO cells and subjected to trypsin treatment (Figure 12). However, when mRFP-ATG9a is co-transfected with rcCOXs, we found the N-terminal mRFP signal on ATG9a was largely protected from trypsin digestion, again suggesting rcCOX binds near the N terminus of ATG9a.

To confirm ATG9a-rcCOX complex formation, we then performed photobleach FRET confocal microscopy between ATG9a tagged at the N-terminus with mRFP and rcCOXs labeled with eGFP at an internal, solvent accessible loop. Energy transfer efficiency between the mRFP and eGFP was strong (rc57/ATG9a: 28%+/-4%; rc50/ATG9a: 27%+/-6%; and rc44/ATG9a: 38%+/-6%).[14,16] We also calculated the distance between the eGPF on rcCOXs and the mRFP

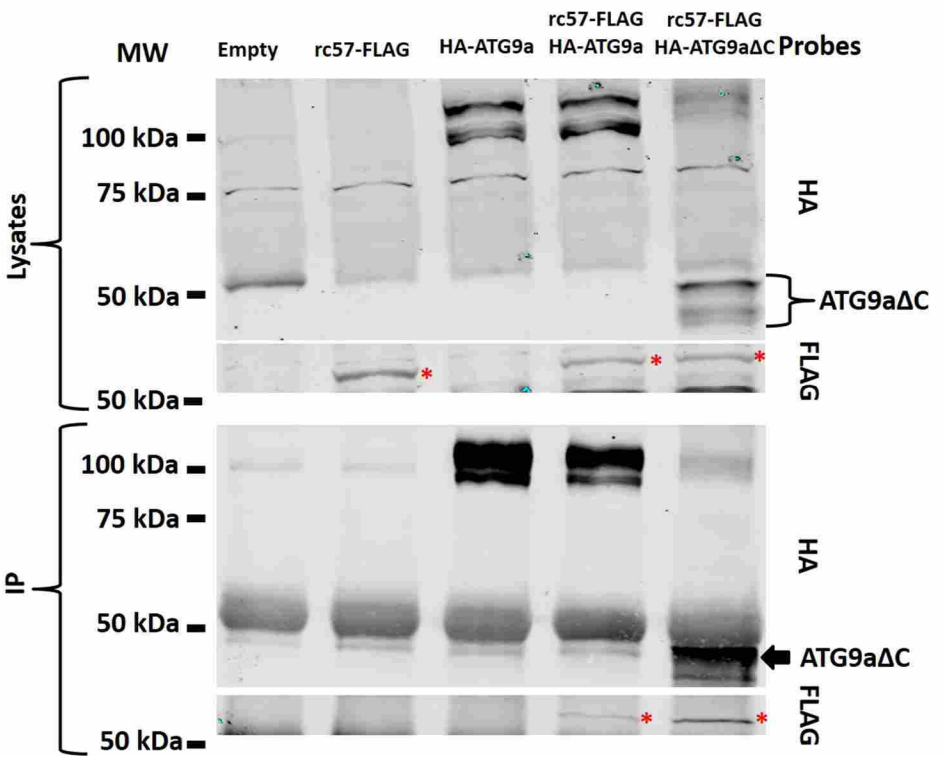

Figure 11: Recoded 57 co-immunoprecipitates with C-terminally truncated ATG9a. C terminally truncated HA-tagged ATG9a was co-transfected with rc57 into CHO cells with rc57 and immunoprecipitated by antibodies against HA. Lysates and elutions were immunobloted using antibodies against FLAG-tagged rc57 and HA-tagged ATG9. * denotes the rc57.

on ATG9a to be 7.0+/-0.6 nm (rc57/ATG9a), 7.0+/-0.5 nm (r50/ATG9a), and 7.3+/-0.4 nm (rc44/ATG9a). These data suggest binding of ATG9a to be located at or near the amino terminus (Figure 13).

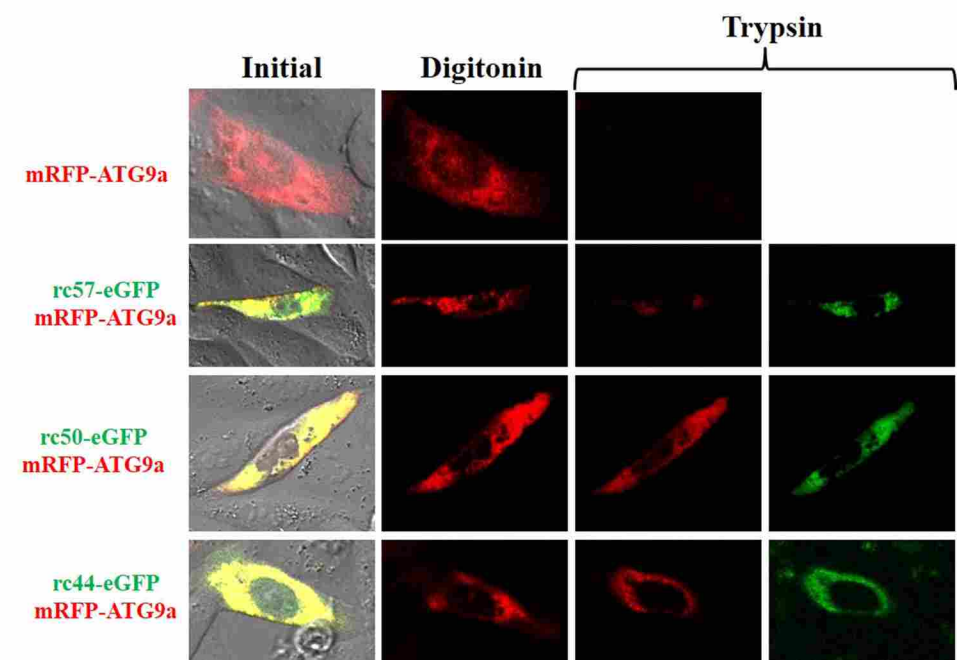

Figure 12: Recoded COXs protects cytosolic N-terminal mRFP tagged ATG9a from trypsin digestion. CHO cells were transfected with internally eGFP tagged rcCOX and N-terminally mRFP tagged ATG9a. Cells were live imaged using confocal microscopy and then permeabilized with digitonin solution and imaged after a minute of treatment. Then trypsin was added at a final concentration of 4 mM and again imaged after a minute of incubation with trypsin.[15] Green: eGFP-rcCOX; Red: mRFP-ATG9a; and Yellow: rcCOX and ATG9a co-localization.

rcCOXs do not co-localize with macroautophagic omegasomes

ATG9a transiently interacts with a host of autophagic components such as autophagosomes and omegasomes and is known to be required for omegasome formation. After our results showed rcCOXs' interaction with ATG9a, we next determined whether rcCOXs co-

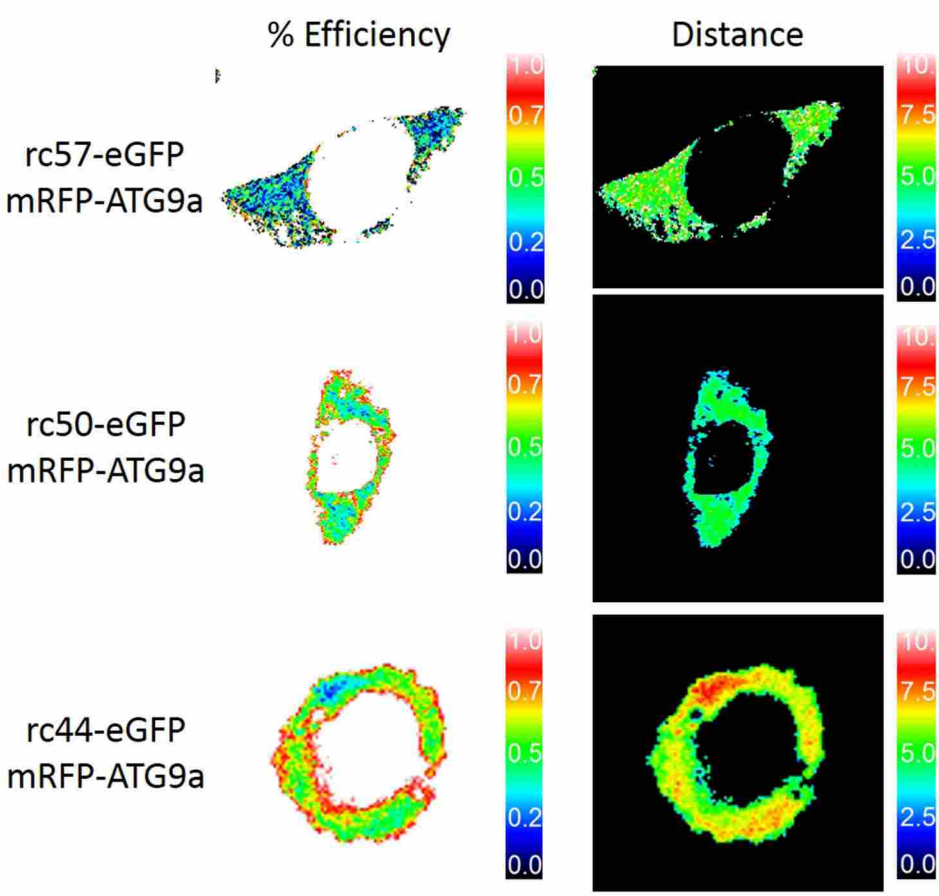

Samples	Distance (nm)	SEM	Efficiency	SEM
rc57/ATG9a	7.0	0.6	28%	4%
rc50/ATG9a	6.7	0.5	27%	6%
rc44/ATG9a	7.3	0.4	38%	6%

Figure 13: Photobleach FRET analysis reveals rcCOXs form a complex with ATG9a at or near the N terminus. CHO cells were co-transfected with internally eGFP-tagged rc57, rc50, or rc44 with N-terminally tagged mRFP ATG9a. Images are one example out of 10 illustrating the efficiency and calculation of distance between eGFP on rcCOX and mRFP on ATG9a. To the right of each image is a scale indicating either the distance or efficiency for each fluorescent signal. Table shows the average efficiencies and distances of 10 cells between the eGFP signal on rcCOXs and the mRFP signal on ATG9a.

localized with omegasomes. We co-transfected FLAG-tagged rc57 or rc50 transcipts with the GFP-tagged omegasome marker DFCP1 construct (graciously provided by Dr. Andersen at Brigham Young University, Provo, UT)[10] and labeled rcCOXs with antibodies against FLAG peptide, which was imaged by confocal microscopy. GFP-DFCP1 was found to be perinuclear as described by others, but rc57 and rc50 did not co-localize with GFP-DFCP1 (Figure 14). These data indicate that rcCOX translocation to autophagosome is not mediated through the omegasome or macroautophagic pathway, but may go instead to non-ER derived autophagosome organizing structures.

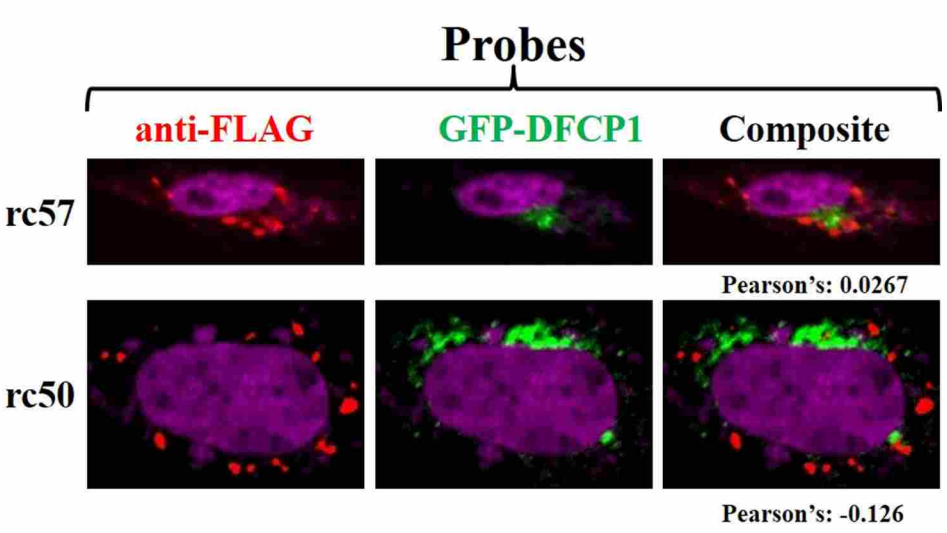

Figure 14: rcCOXs do not co-localize with DFCP1. CHO cells were co-transfected with GFP-labeled DFCP1 with either FLAG-tagged rc57 or rc50. Cells were prepped and viewed using confocal microscopy. Purple: Nucleus (DAPI); Red: rcCOXs and Green: GFP-DFCP1.

The rcCOX/ATG9a complex does not require COX catalytic residues

Because ATG9a is critical for membrane delivery and rcCOXs are potential oxylipin-synthesizing enzymes, we determined if rcCOX activity was important for ATG9a/rcCOX complex formation. We, therefore, mutagenized important catalytic residues and transiently

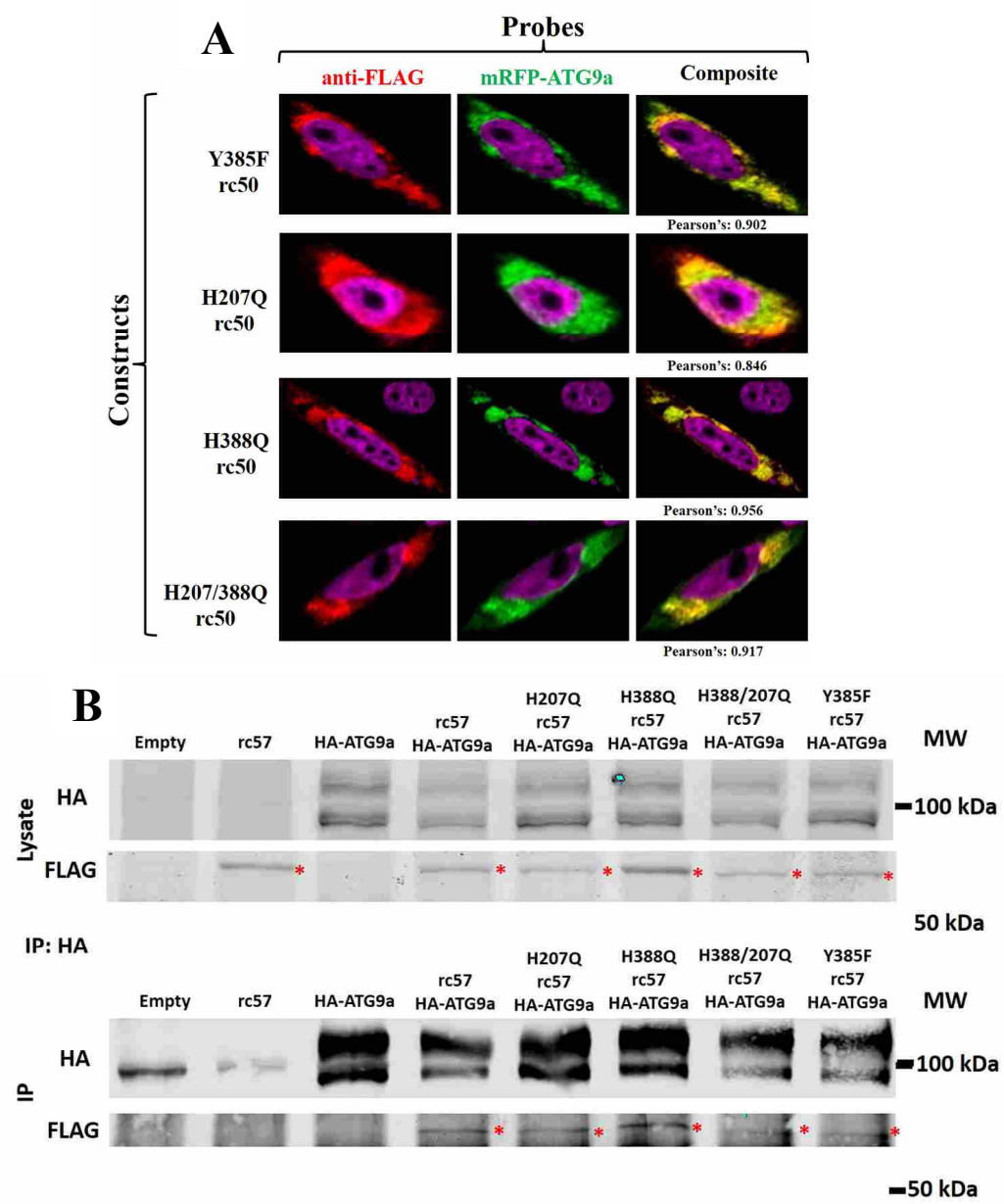

Figure 15: Recoded COX/ATG9a complex is independent of rcCOX activity. A) FLAG-tagged rc50 catalytic residues were mutated (H207Q, Y385F, H388Q, or H207/388Q) and these constructs were co-transfected with mRFP-ATG9a into CHO cells and probed with antibodies against FLAG peptide and imaged by confocal microscopy. Purple: Nucleus (DAPI); Red: rc50; Green: mRFP-ATG9a; and Yellow: rcCOX and ATG9a co-localization. B) FLAG-tagged rc57 with catalytic residues mutated were co-transfected with HA-ATG9a and immunoprecipitated using anti-HA antibodies. Lysates and elutions were immunoblotted using probes against FLAG and HA peptide.

co-transfected these constructs with either HA-ATG9a for immunoprecipitation or with mRFP-ATG9a for confocal imaging.

As described in more detail in Chapter 4, residues important for COX oxygenase activity are His388, His207, and Tyr385. We made the following four constructs: 1 - His388 was mutated to Gln (H388Q-rcCOX), 2 - His207 was mutated to Gln (H207Q-rcCOX), 3 - both His388 and His207 were mutated to Gln (H207/388Q-rcCOX), and 4 - Tyr385 was mutated to Phe (Y385F-rcCOX).[24, 25] Because rc44 does not contain a His207 only the His388 was mutated to Gln. These constructs were each co-transfected with mRFP-ATG9a and visualized by first probing with anti-FLAG antibodies and then imaging the cells with confocal microscopy.

All of the mutants – H388Q-rcCOXs, H207Q-rcCOXs, H207/388Q-rcCOXs, and Y385F-rcCOXs – continued to co-localize with mRFP-ATG9a in confocal microscopy images (Figure 15A). Furthermore, each mutated rcCOX construct also co-immunoprecipated with HA-ATG9a (Figure 15B). These data illustrate that rcCOX interaction with ATG9a is not dependent upon rcCOX activity.

mTOR inhibitor blocks rcCOX/ATG9a complex

Our DFCP1 results suggested that the rcCOX/ATG9a complex is formed for non-canonical autophagy and is independent of macroautophagy. We therefore transiently co-transfected FLAG-tagged rcCOXs with mRFP-ATG9a for 22 hours. Two hours before preparing cells for confocal microscopy we added 1 μM of the macroautophagy stimulating small molecule rapamycin. As reported, we observed upon addition of rapamycin that ATG9a mobilized to a cytosolic pattern indicative of macroautophagy activation (Figure 16).[10] However, rapamycin treatment abolished rc57, rc50, or rc44 co-localization with mRFP-ATG9a indicating the rcCOX/ATG9a complex is formed in a converse fashion to macroautophagy.

Interestingly, rapamycin treatment also caused rc44 to mobilize to a punctate pattern in the nucleus.

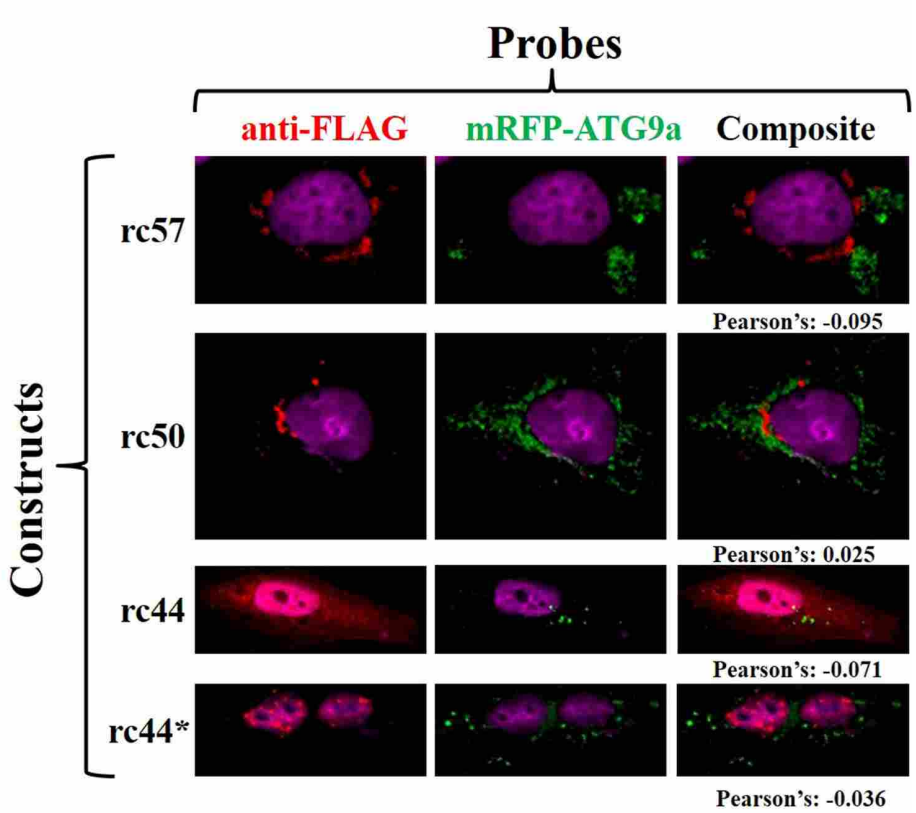

Figure 16: mTOR activity is important for rcCOX/ATG9a association. CHO cells transfected with mRFP-ATG9a and with either FLAG-tagged rc57, rc50, or rc44 were treated with 1 μM rapamycin for 2 hours before being prepared for confocal microscopy. Cells were labeled against FLAG peptide. * denotes cells where rc44 is nuclear and interestingly find rc44 is punctate. Purple: Nucleus (DAPI); Red: rcCOX and Green: mRFP-ATG9a.

rcCOXs' differential effect on EMCV replication

Due to the connection of rcCOXs to the critical membrane chaperone ATG9a and its disassociation from ATG9a during rapamycin treatment we hypothesized that rcCOX may play a role in non-canonical autophagy such as that associated with innate immunity against viral infection. We tested this by infecting CHO cells that had been transiently transfected with either rc57, rc50, rc44 or COX-3 with EMCV. After 36 hours post-infection the media was removed

and plaque-forming assay was performed to determine the number of cell-released virions. Virus replication from COX-3 transfected cells did not statistically change compared to empty vector transfected cells (Figure 17). However, we found that rc57 transfected CHO cells statistically impeded EMCV replication by ~40% (p-value=0.003) while rc50 statistically increased virion replication by ~50% (p-value=0.0002) and rc44 increased EMCV replication by 2-fold (p-value=0.004). These results support rcCOXs role in the innate immune response xenophagy.

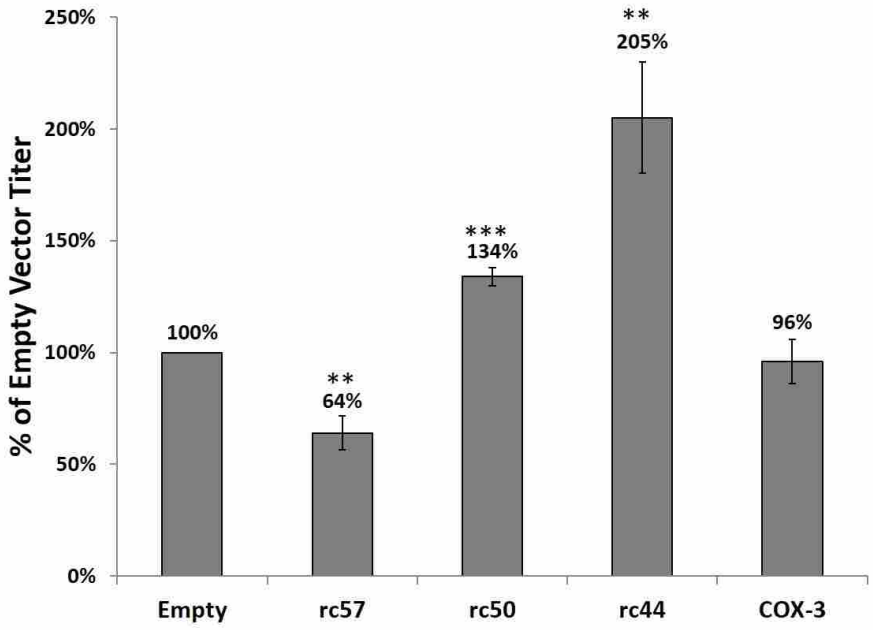

Figure 17: EMCV replication is affected by rcCOXs overexpression: Cells were transfected with rcCOX constructs for 24 hours and then infected with EMCV with a MOI of 1 and allowed to grow for 36 hours. Then media was removed and analyzed via plaque forming assays, arrow bars are averages and SEMS based on 2 experiments with 3 data points each. * = p-value<0.05; ** = p-value<0.01; and *** = p-value<0.001

Discussion

Despite containing overlapping portions of the primary sequence of COX-1; rc57, rc50, and rc44 each localize to distinct and separate sites in the cytoplasmic/nucleoplasmic compartment of the cell. Two of them target different domains of the cytoplasmic face of the

Golgi apparatus, with rc57 residing on the trans-medial face and rc50 on the cis-medial. Each protein additionally can be found in the cytosol. Likewise, rc44 resides in two locations: the cytosol and intranuclear compartment. This cytosolic/intranuclear pattern is similar to many transcription factors, which is intriguing since we previously showed that the carboxy-terminal region of COX-1 found in rc44 acts as a strong transcriptional transactivator in a yeast two-hybrid study.[17]

From one or both of their respective compartments (except for the intranuclear form of rc44), these proteins access and bind to the membrane-transporting protein ATG9a and eventually transit to the cytoplasmic surface of autophagosomes. This occurs independent of any oxylipin oxygenase activity possessed by these proteins. Furthermore, the autophagosomes formed through rcCOX/ATG9a transfer of membrane are destined for non-canonical autophagy as demonstrated by the facts that they are dependent on mTOR activity and they do not use the DFCP1-containing phagophore structure of macroautophagy. Yet, the autophagosomes associated with each rcCOX, while non-canonical, appear to be distinct in character as demonstrated by the fact that those associated with rc57 are non-digestive, whereas rc50-associated autophagosomes mature into autolysosomes with rc50 on their cytosolic surface.

The role of the Golgi residence of rc57 and rc50 is particularly relevant to non-canonical autophagy given the Golgi apparatus' association with xenophagy. For example, murine **i**mmunity-**r**elated **G**TPase family M (IRGM) is a cis-Golgi resident protein under basal conditions[18] but when RAW 264.7 cells are infected with pathogens such as *Mycobacterium tuberculosis*, IRGM translocates to localize with the *M. tuberculosis* and enhances mycobacterial phagosome maturation.[19] This translocation is dependent on the lipid mediators PI(3,4)P and

PI(3,4,5)P.[20] Although the autophagic machinery aided IRGM mycobacterial phagosome maturation, IRGM remained critical for degradation of bacteria in autophagy.[14]

Confocal microscopy, co-immunoprecipitation, and photobleach FRET results showed rcCOX binds to ATG9a at or near the cytosolic amino terminus. This binding occurred even in the presence of high concentrations of digitonin that solubilizes yet also stabilizes the confirmation of membrane proteins.[21]

These results provide a new type of binding partner are the most intriguing compared to the binding of other molecules to ATG9a since most ATG9a protein interactions occur at the C-terminus. For example, p38IP[9] and 14-3-3ζ[10], both interact with ATG9a's C-terminal region either under basal conditions and even more so when cells are undergoing macroautophagy due to nutrient deprivation and/or hypoxia. Yet we find that activation of macroautophagy through rapamycin causes the rcCOX/ATG9a complex to disassociate, indicating that the formation of this complex is not involved in macroautophagy, but is instead involved in other forms of autophagy such as xenophagy.

Other results supporting the notion that rcCOX-associated autophagosomes are involved with non-canonical autophagy is that we did not find rc57 and rc50 co-localizing with the amphisome marker LAMP-1. Instead, autophagosomes formed by rcCOX may be derived from Golgi or are seeded from other membrane in the cell's periphery. In either case, each has been shown to be a property of xenophagy. One possibility is that ATG9a, which has been known to recruit complexes and membrane to specific autophagic related structures,[12] is recruiting rc57 and rc50 to autophagosomes that may lack membrane or machinery important for fusion with endosomes, such as **s**oluble **N**SF **a**ttachment protein **re**ceptor (SNARE).[22]

Non-canonical autophagy is frequently evoked by invading organisms and we tested whether rcCOXs function in xenophagy by infecting CHO cells transiently transfected with rc57, rc50, or rc44 with EMCV and quantifying viral replication. We found that rc57 impedes viral replication while the rc50 and rc44 promotes it. We believe the fold-differences in viral replication caused by the various rcCOXs are a significant under-representation of their effects. Our estimates are limited by our transfection efficiency. Furthermore, we were unable to measure virus background caused by virus remaining from the initial infection done on the transfected cells. EMCV replication has been shown to be reliant on autophagy stimulation for delivery from the host cell.[23] We postulate that rc57 inhibits EMCV replication by forming autophagic structures that sequester EMCV within the cell, and the cell may die without EMCV fully assembling to an infectable virion. Recoded 50, in contrast, is shown to co-localize with cathepsin D indicating the rc50-formed autophagosomes may continue through autophagic flux, which could explain why we see a statistical increase in EMCV replication.[20] How rc44 positively influences viral replication is presently unknown, but is assumed to be through a mechanism separate from rc57 and rc50 since it does not localize to autophagosomes. Thus rcCOX proteins provide the cell with a potential repertoire of response proteins to invading organisms. The roles of rcCOXs' in autophagy provide a previously unexplored area of research. Paramount is our finding that rc57 and rc50 evoke the formation of non-canonical autophagosomes and may act as effectors of this critical process; such as involved in innate immunity and other physiologic phenomena.

References

1. Kim, J.; Huang, W. P.; Stromhaug, P. E.; Klionsky, D. J., Convergence of multiple autophagy and cytoplasm to vacuole targeting components to a perivacuolar membrane compartment prior to de novo vesicle formation. *J Biol Chem* **2002,** *277* (1), 763-73.

2. Young, A. R.; Chan, E. Y.; Hu, X. W.; Köchl, R.; Crawshaw, S. G.; High, S.; Hailey, D. W.; Lippincott-Schwartz, J.; Tooze, S. A., Starvation and ULK1-dependent cycling of mammalian Atg9 between the TGN and endosomes. *J Cell Sci* **2006,** *119* (Pt 18), 3888-900.

3. Yamada, T.; Carson, A. R.; Caniggia, I.; Umebayashi, K.; Yoshimori, T.; Nakabayashi, K.; Scherer, S. W., Endothelial nitric-oxide synthase antisense (NOS3AS) gene encodes an autophagy-related protein (APG9-like2) highly expressed in trophoblast. *J Biol Chem* **2005,** *280* (18), 18283-90.

4. Orsi, A.; Razi, M.; Dooley, H. C.; Robinson, D.; Weston, A. E.; Collinson, L. M.; Tooze, S. A., Dynamic and transient interactions of Atg9 with autophagosomes, but not membrane integration, are required for autophagy. *Mol Biol Cell* **2012,** *23* (10), 1860-73.

5. Zavodszky, E.; Vicinanza, M.; Rubinsztein, D. C., Biology and trafficking of ATG9 and ATG16L1, two proteins that regulate autophagosome formation. *FEBS Lett* **2013,** *587* (13), 1988-96.

6. Tang, H. W.; Wang, Y. B.; Wang, S. L.; Wu, M. H.; Lin, S. Y.; Chen, G. C., Atg1-mediated myosin II activation regulates autophagosome formation during starvation-induced autophagy. *EMBO J* **2011,** *30* (4), 636-51.

7. Takahashi, Y.; Meyerkord, C. L.; Hori, T.; Runkle, K.; Fox, T. E.; Kester, M.; Loughran, T. P.; Wang, H. G., Bif-1 regulates Atg9 trafficking by mediating the fission of Golgi membranes during autophagy. *Autophagy* **2011,** *7* (1), 61-73.

8. Takahashi, Y.; Coppola, D.; Matsushita, N.; Cualing, H. D.; Sun, M.; Sato, Y.; Liang, C.; Jung, J. U.; Cheng, J. Q.; Mulé, J. J.; Pledger, W. J.; Wang, H. G., Bif-1 interacts with Beclin 1 through UVRAG and regulates autophagy and tumorigenesis. *Nat Cell Biol* **2007,** *9* (10), 1142-51.

9. Webber, J. L.; Tooze, S. A., Coordinated regulation of autophagy by p38alpha MAPK through mAtg9 and p38IP. *EMBO J* **2010,** *29* (1), 27-40.

10. Weerasekara, V. K.; Panek, D. J.; Broadbent, D. G.; Mortenson, J. B.; Mathis, A. D.; Logan, G. N.; Prince, J. T.; Thomson, D. M.; Thompson, J. W.; Anderson, J. L., Metabolic-Stress-Induced Rearrangement of the 14-3-3ζ Interactome Promotes Autophagy via a ULK1- and AMPK-Regulated 14-3-3ζ Interaction with Phosphorylated ATG9. *Mol. Cell. Bio.* **2014,** *34* (24), 4379-4388.

11. Saitoh, T.; Fujita, N.; Hayashi, T.; Takahara, K.; Satoh, T.; Lee, H.; Matsunaga, K.; Kageyama, S.; Omori, H.; Noda, T.; Yamamoto, N.; Kawai, T.; Ishii, K.; Takeuchi, O.; Yoshimori, T.; Akira, S., Atg9a controls dsDNA-driven dynamic translocation of STING and the innate immune response. *Proc Natl Acad Sci U S A* **2009,** *106* (49), 20842-6.

12. Kageyama, S.; Omori, H.; Saitoh, T.; Sone, T.; Guan, J. L.; Akira, S.; Imamoto, F.; Noda, T.; Yoshimori, T., The LC3 recruitment mechanism is separate from Atg9L1-dependent membrane formation in the autophagic response against Salmonella. *Mol Biol Cell* **2011,** *22* (13), 2290-300.

13. Shahnazari, S.; Yen, W. L.; Birmingham, C. L.; Shiu, J.; Namolovan, A.; Zheng, Y. T.; Nakayama, K.; Klionsky, D. J.; Brumell, J. H., A diacylglycerol-dependent signaling pathway contributes to regulation of antibacterial autophagy. *Cell Host Microbe* **2010,** *8* (2), 137-46.

14. Peter, M.; Ameer-Beg, S. M.; Hughes, M. K.; Keppler, M. D.; Prag, S.; Marsh, M.; Vojnovic, B.; Ng, T., Multiphoton-FLIM quantification of the EGFP-mRFP1 FRET pair for localization of membrane receptor-kinase interactions. *Biophys J* **2005,** *88* (2), 1224-37.

15. Lorenz, H.; Hailey, D. W.; Lippincott-Schwartz, J., Fluorescence protease protection of GFP chimeras to reveal protein topology and subcellular localization. *Nat Methods* **2006,** *3* (3), 205-10.

16. van der Krogt, G. N.; Ogink, J.; Ponsioen, B.; Jalink, K., A comparison of donor-acceptor pairs for genetically encoded FRET sensors: application to the Epac cAMP sensor as an example. *PLoS One* **2008,** *3* (4), e1916.

17. Ballif, B. A.; Mincek, N. V.; Barratt, J. T.; Wilson, M. L.; Simmons, D. L., Interaction of cyclooxygenases with an apoptosis- and autoimmunity-associated protein. *Proc Natl Acad Sci U S A* **1996,** *93* (11), 5544-9.

18. Martens, S.; Sabel, K.; Lange, R.; Uthaiah, R.; Wolf, E.; Howard, J. C., Mechanisms regulating the positioning of mouse p47 resistance GTPases LRG-47 and IIGP1 on cellular membranes: retargeting to plasma membrane induced by phagocytosis. *J Immunol* **2004,** *173* (4), 2594-606.

19. Singh, S. B.; Davis, A. S.; Taylor, G. A.; Deretic, V., Human IRGM induces autophagy to eliminate intracellular mycobacteria. *Science* **2006,** *313* (5792), 1438-41.

20. Tiwari, S.; Choi, H. P.; Matsuzawa, T.; Pypaert, M.; MacMicking, J. D., Targeting of the GTPase Irgm1 to the phagosomal membrane via PtdIns(3,4)P(2) and PtdIns(3,4,5)P(3) promotes immunity to mycobacteria. *Nat Immunol* **2009,** *10* (8), 907-17.

21. Holden, P.; Horton, W. A., Crude subcellular fractionation of cultured mammalian cell lines. *BMC Res Notes* **2009,** *2*, 243.

22. Sarkar, S.; Carroll, B.; Buganim, Y.; Maetzel, D.; Ng, A. H.; Cassady, J. P.; Cohen, M. A.; Chakraborty, S.; Wang, H.; Spooner, E.; Ploegh, H.; Gsponer, J.; Korolchuk, V. I.; Jaenisch, R., Impaired autophagy in the lipid-storage disorder Niemann-Pick type C1 disease. *Cell Rep* **2013,** *5* (5), 1302-15.

23. Zhang, Y.; Li, Z.; Ge, X.; Guo, X.; Yang, H., Autophagy promotes the replication of encephalomyocarditis virus in host cells. *Autophagy* **2011,** *7* (6), 613-28.

24. Shimokawa, T.; Kulmacz, R. J.; DeWitt, D. L.; Smith, W. L., Tyrosine 385 of prostaglandin endoperoxide synthase is required for cyclooxygenase catalysis. *J Biol Chem* **1990,** *265* (33), 20073-6.

25. Shimokawa, T.; Smith, W. L., Essential histidines of prostaglandin endoperoxide synthase. His-309 is involved in heme binding. *J Biol Chem* **1991,** *266* (10), 6168-73.

Chapter 3

Recoded COXs and nucleobindin induce large LC3-II positive structures (LLPSs)

Abstract

Nucleobindin is a multi-domain protein associated with the auto-immune disease systemic lupus erythematosus (SLE).[6] One of these domains, an N-terminal signal peptide, directs Nuc translation into the ER where it is then further processed and secreted from the cell through the ER/Golgi pathway. Studies by Farquhar et. al. reported finding a cytosolic pool of Nuc[1] that was later shown to be involved in a host of physiological[2] and pathosphysiological[3] conditions. The manner in which cytosolic Nuc is translated into the cytosol has yet to be elucidated.

Past work in our laboratory has shown Nuc to interact with hypo/un-glycosylated COX but at the time of our work unglycosylated COX had yet to be identified.[4] Recently, we discovered unglycosylated proteins translationally recoded from the COX-1 splice variant, COX-3. This chapter focuses on the interaction between recoded COX proteins (rc57, rc50, and rc44) and recoded cytosolic Nuc. Furthermore, we determined through mutagenesis and confocal microscopy that translational recoding, which produces recoded COX proteins, also creates a cytosolic Nuc (cNuc) described by others. This cytosolic Nuc drives the production of large LC3-II positive structures (LLPSs), which is accentuated by co-transfection with rc57, rc50, or rc44. We also find that cNuc blocks autophagic flux at a point prior to amphisome formation.

Background

In 1998, our laboratory found that the C-terminus of non-glycosylated COX proteins interacts with an auto-immune associated protein, nucleobindin (Nuc). This was determined using yeast two-hybrid, co-immunoprecipitation, and pull-down assay studies.[4] However, non-

glycosylated COXs were unknown until Hunter et al., in our laboratory, found them in rat tissues and demonstrated that proteins of identical size were produced by translational recoding.[5] Because the rcCOX proteins contain potential Nuc interaction domains, we postulated that they may act as binding partners of Nuc. However, determining this required that we resolve a long-standing paradox regarding nucleobindin: how are nucleobindin proteins targeted to both the lumen of the ER/Golgi and to the cytosol? Solving this problem was essential to testing our hypothesis because only the cytosolic form of Nuc could interact with the cytosolic recoded COX proteins that Dr. Hunter[5] had identified.

Nucleobindin is a multi-domain protein with many physiological roles and two subcellular locations

Nucleobindin was identified as a protein bound to DNA in the extracellular matrix of mice (lpr/lpr) with the auto-immune disorder systemic lupus erythematosus (SLE).[6] It was further shown that DNA-bound Nuc elicited a SLE-like phenotype in mice when injected peritoneally.[7] Sequence analysis and protein structural studies found that Nuc contains a leucine zipper DNA binding domain[8] and two high affinity, calcium-binding EF-hands,[9] preceded by an N-terminal, cleavable signal peptide, which directs translation of the protein into the ER/Golgi secretory pathway. Indeed, confocal and subcellular fractionation experiments confirmed Nuc to reside in Golgi from where it is secreted.[10] These studies lead Farquhar and colleagues to postulate that Golgi-resident Nuc,[10] via its Ca^{2+}-binding EF hands regulates Ca^{2+} homeostasis in the Golgi lumen.[1] However, later studies found robust levels of Nuc in the cytosol where it binds $G_{\alpha i}$ proteins,[11,2] regulating their activity by inhibiting $G_{\alpha i1}$'s release of GDP.[12] Additionally, cytosolic Nuc also contains a serine protease active site at its C-terminus that is allosterically regulated by Zn^{2+} ions binding to sites near its N-terminus.[13]

Cytosolic Nuc has been found to regulate a number of pathways and physiological phenomena. For example, cytosolic Nuc negatively regulates the unfolded protein response (UPR) by inhibiting site-1-protease (S1P) cleavage of activating transcription factor 6 (ATF6).[14] The C-terminus of cytosolic Nuc also binds amyloid precursor protein (APP), leading to a decrease in APP levels in neuroblastoma cells.[15] Levels of Nuc in brains of those afflicted with Alzheimer's disease were shown to be substantially lower than those without Alzheimer's disease of the same age.[3] Thus Nuc's multiple domains help it to be utilized in multiple roles in cellular signaling and immunity.

Cytosolic nucleobindin occurs through translational recoding

Cytosolic Nuc found in AtT-20, NRK, and REF cells constituted 20%, 50%, and 10%, respectively,[10] of total Nuc in these cells; whereas CHO cells stably expressing Nuc exhibited over 60% of Nuc in cytosol and 40% in membrane (i.e. ER/Golgi).[2] Therefore, the question we faced was how these cytosolic pools are created given Nuc's consensus N-terminal signal peptide, which should shunt its translation into the lumen of ER.

We show here that a cytosolic Nuc (cNuc) is translationally recoded at an internal initiation site located near the cleavage site of the signal peptide, producing a protein of the correct size of cytosolic Nuc observed in cells and tissues. Remarkably, expression of transiently transfected cNuc in CHO cells induces the formation of large LC3-II positive structures (LLPSs) We refer to these structures as LLPSs due to their similarity to structures induced by coxsackievirus B3 (CVB3) in rat acinar cells.[16] Expression of rcCOXs with cNuc potentiates the creation of LLPSs, resulting in the co-localization of rcCOX and Nuc onto these large structures.

Materials and Methods

Cell culture, site-directed mutagenesis, transient transfection, confocal imaging, DC protein assay, and immunoblot analysis are described in the Materials and Methods section of Chapter 2.

Sample preparation for p62 immunoblot analysis

Cells transiently transfected with constructs of interest were washed in 500 µL of PBS and then scrapped into RIPA buffer (50 mM Tris pH 8.0, 150 mM NaCl, 1% NP-40, 0.5% deoxycholate, 0.1% SDS). Cells were lysed by triggering the samples with a 25-gauge needle 11 times. Material was pelleted in microcentrifuge at 4° C for 15 minutes at 14,000 rpm. Supernatant was placed into a fresh Eppendorf and protein measured using DC assay and prepared for immunoblot analysis.

Results

Site-directed mutagenesis demonstrates that cNuc is a recoded form of Nuc

We performed site-directed mutagenesis on Nuc to determine whether cNuc is formed by recoding mechanisms similar to rcCOXs. Due to reports of cNuc having electrophoretic mobility essentially identical to fully processed Nuc, we focused on possible recoding codons near the cleavage site of the signal peptide. Within the signal peptide region, an AUG two codons away from the signal peptide cleavage site is conserved in both mouse and rat Nuc but not in human. Myc-tagged Nuc constructs were prepared by mutating the initiating AUG (M1K-Nuc) and/or the signal peptide AUG to AAA (M1/19K-Nuc, M19K-Nuc). These constructs were compared to a construct utilized in past studies to represent cNuc where the signal peptide is removed and an artificial AUG is placed before the cleavage site. These constructs were

transiently transfected into CHO cells and protein products' electrophoretic mobility were analyzed using Western blot (Figure 18).

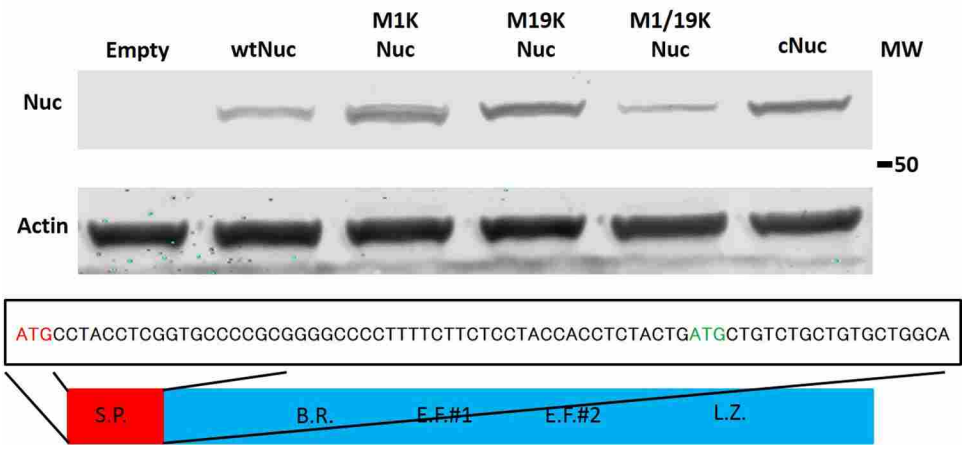

Figure 18: Mutagenesis reveals Nuc is recoded near the N-terminus. An illustration showing the different domains of Nuc (S.P.=signal peptide; B.R.=COX binding region ; E.F.=EF hand; L.Z.=leucine zipper) and the nucleotide sequence of the N-terminus of mouse Nuc (wtNuc) with a possible ATG codon (green) within the signal peptide where recoding could produce a cytosolic Nuc. We therefore made constructs where the initiating Met (M1K-Nuc), the internal ATG codon found in the signal peptide (M19K-Nuc), or both Met codons (M1/19K-Nuc) of Myc-tagged Nuc were mutated to AAA and transiently transfected into CHO cells and immunoblots were probed with antibodies against Myc tag and actin. Translated products of the mutants were compared to wtNuc and cNuc.

Mutation of the initiating Met (M1K-Nuc) produced a highly expressed doublet of the approximate size of fully process wild type Nuc (wtNuc). This finding suggested two potential start sites immediately downstream of the initiating Met. When we mutated both the initiating Met and Met19 (M1/19K-Nuc), protein expression was reduced and only a single protein remained. As expected, mutations of Met19 continued to produce a protein with similar size to wtNuc. Together, these data suggest two potential translational recoding start sites, Met19 and another nearby non-AUG codon which are efficiently translated to create cNuc.

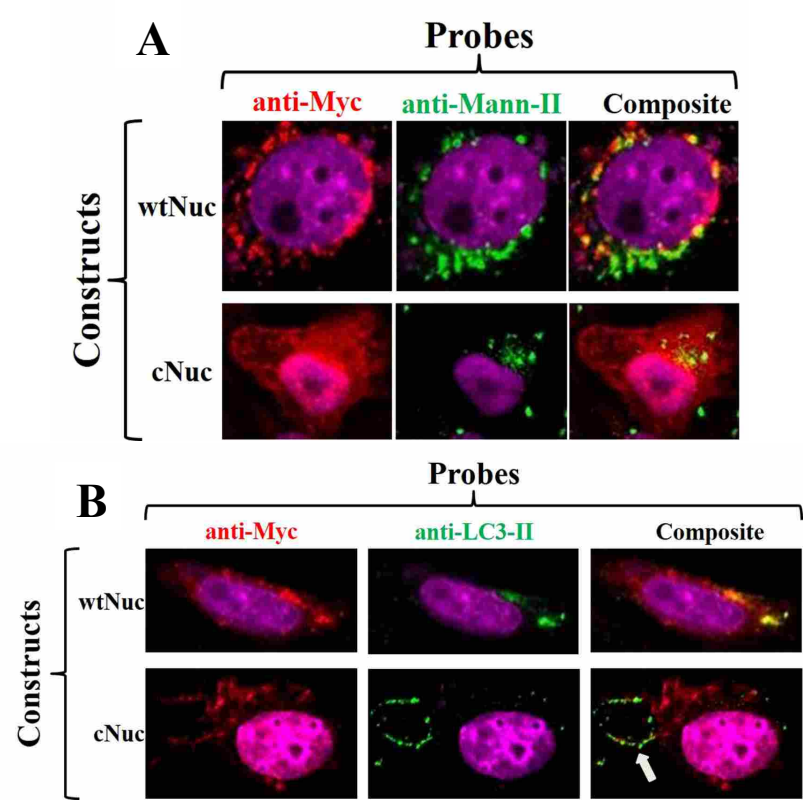

Figure 19: Localization pattern of cNuc and wtNuc. Myc-tagged wtNuc and cNuc constructs were transiently transfected into CHO cells and localization patterns were probed using antibodies against Myc, A) mannosidase-II (Golgi), and B) LC3-II (autophagosomes) then imaged using confocal microscopy. White arrows point toward LLPS. Purple: Nucleus (DAPI); Red: cNuc; Green: LC3-II and mannosidase-II; and Yellow: cNuc and protein marker co-localization.

We next analyzed localization patterns for each of the constructs using confocal microscopy. We found wtNuc in a punctate pattern and cNuc in the cytosol as described by Miura et. al. (Figure 19A).[8, 9] Interestingly, we also found cNuc co-localized with LC3-II around LLPSs in 30% of transfected cells but we never detected these LLPSs in wtNuc transfected cells (Figure 19B). We also noted that both the M1K-Nuc and M1/19K-Nuc constructs had similar cytosolic localization patterns and similar induction of LLPSs (around 30% each) as cNuc (Figure 20). We also found smaller LLPSs formed in M19K-Nuc transfected cells but only

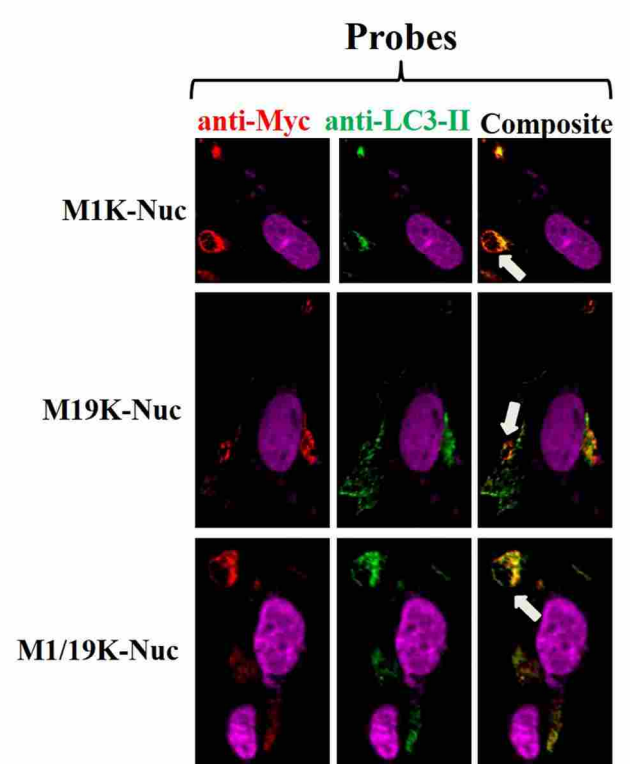

Figure 20: Recoded Nuc drive LLPS production. Myc-tagged M1K-Nuc, M19K-Nuc, and M1/19K-Nuc were transiently transfected into CHO cells and dually probed with antibodies against Myc peptide and LC3-II. White arrows point to LLPSs. Purple: Nucleus (DAPI); Red: cNuc; Green: LC3-II; and Yellow: cNuc and LC3 co-localization.

~10% of transfected cells contained dysmorphic LLPSs. These results indicate that a cytosolic pool of Nuc described by others can be formed through recoding mechanisms similar to rcCOXs.

Recoded COXs translocate with cNuc to LLPSs and act synergistically to drive their formation

Previously, we showed COX and Nuc interaction was dependent on COX being hypo/un-glycosylated.[4] We, therefore, hypothesized that rc57, rc50, and rc44, being unglycosylated and cytosolic, would co-localize and/or interact with cNuc. We confirmed this by co-expressing Myc-tagged cNuc with FLAG-tagged rcCOXs, rc57 and rc50, both translocated from Golgi to co-localize with cNuc around LLPSs (Figure 21-22). Likewise, rc44 co-localized with cNuc around LLPSs. While 30% of cNuc transfected cells developed a LLPS, 60% of rcCOX/cNuc

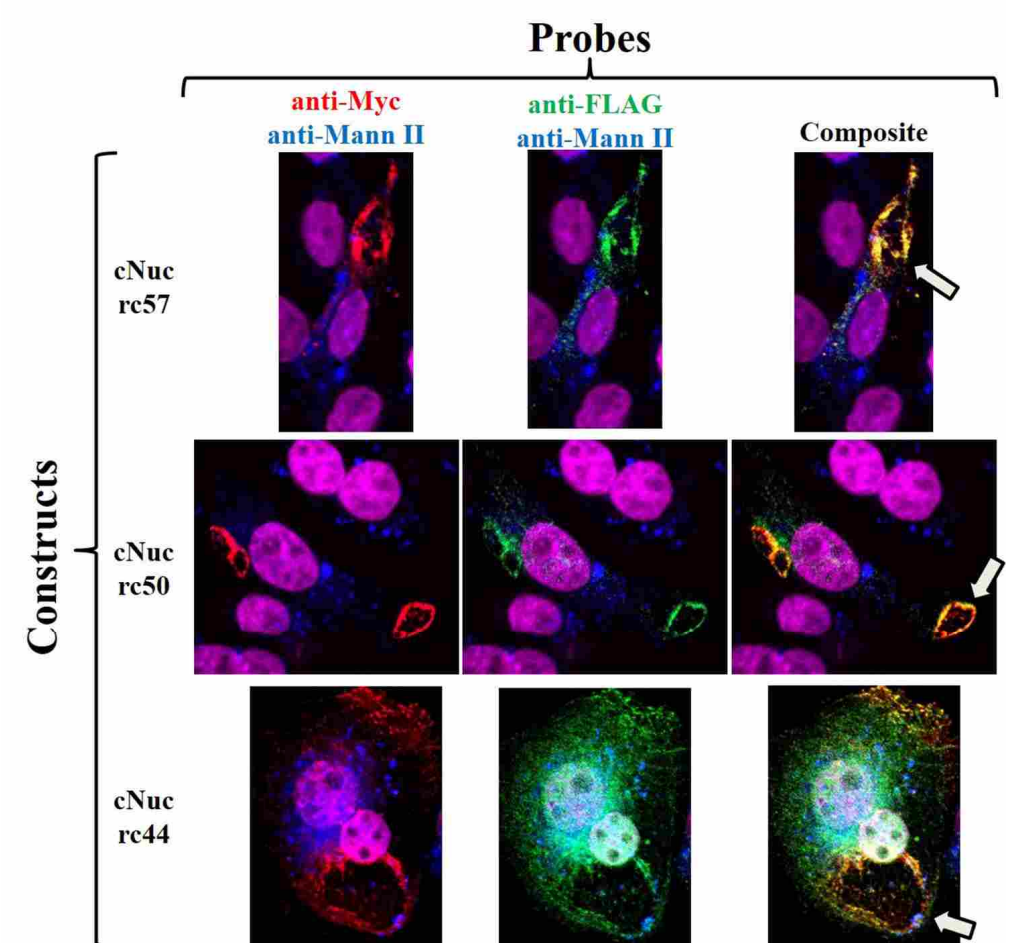

Figure 21: Recoded COXs translocate from Golgi to co-localize with cNuc at LLPSs. We co-transfected rcCOXs and cNuc into CHO cells and labeled with antibodies against FLAG (rcCOX), Myc (cNuc), and Golgi (mannosidase-II) and imaged using confocal microscopy. White arrows point to LLPSs. Purple: Nucleus (DAPI); Red: cNuc; Green: rcCOX; Blue: Golgi; and Yellow: cNuc and rcCOX co-localization.

co-transfected cells contained a LLPS. LLPSs were usually found near the plasma membrane when cNuc was co-expressed with rc57 or rc50 while rc44/cNuc-formed LLPSs were situated near the nucleus. In each transfection experiment, only a subset of cells take up and express DNA; however, LLPSs never formed in non-transfected cells within the experiments or in empty vector-transfected cells, suggesting that LLPS formation by cNuc or rcCOX with cNuc is dependent on cell autonomous activity of these proteins.

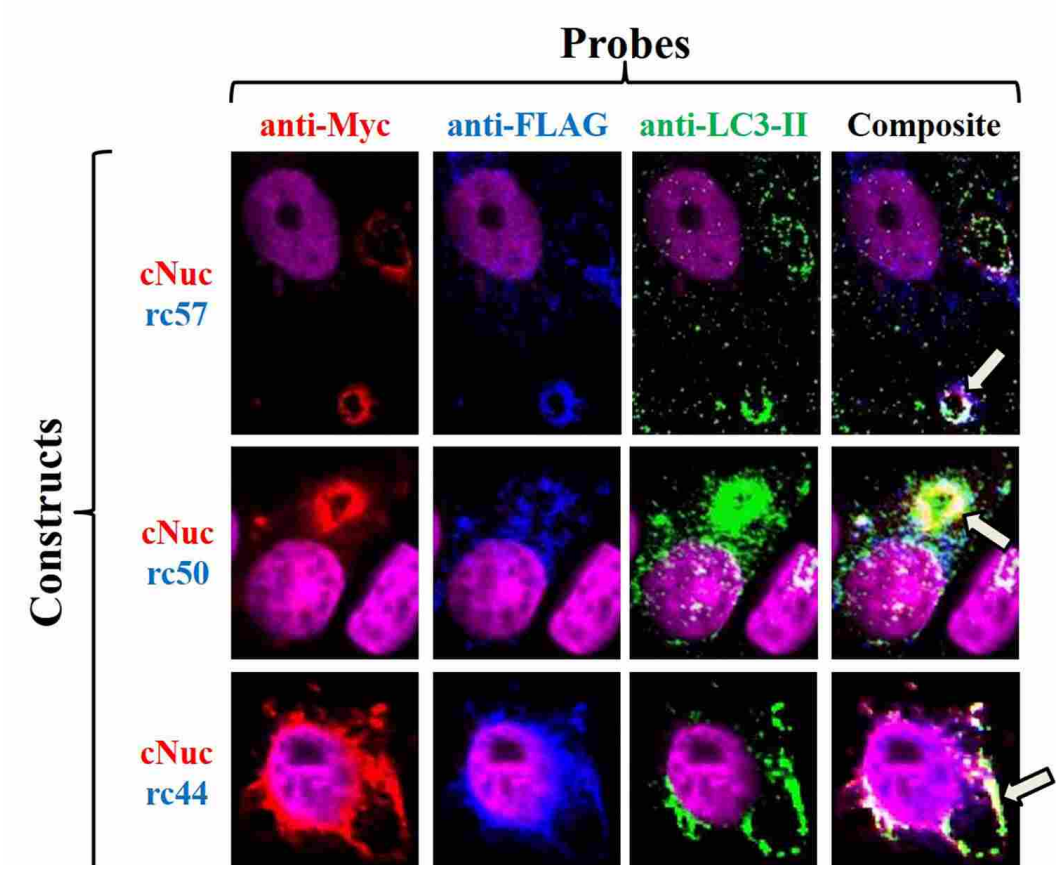

Figure 22: rcCOXs and cNuc co-localize with LC3-II at LLPSs. We confirmed the large vesicles were LLPSs by co-transfecting rcCOXs with cNuc into CHO cells and labeling them with antibodies against FLAG (rcCOX), Myc (cNuc), and LC3-II (autophagosomes). These were imaged using confocal microscopy. White arrows point to LLPSs. Purple: Nucleus (DAPI); Red: cNuc; Green: LC3-II; Blue: rcCOX; Yellow: co-localization between Nuc and rcCOX; and White: co-localization between LC3-II, rcCOX, and cNuc.

Co-transfection of cNuc abolishes interaction between rcCOX and ATG9a

In seeing rc57 and rc50 relocate from Golgi to co-reside with cNuc around LLPSs, spurred us to investigate whether interaction between rcCOX and ATG9a continued at LLPSs. Therefore, we transiently transfected Myc-tagged cNuc and FLAG-tagged rcCOXs into CHO cells – labeled cells with antibodies against cNuc, rcCOX, and endogenous ATG9a – and imaged the cells using confocal microscopy. We found that rc57, rc50, and rc44 co-localized with cNuc

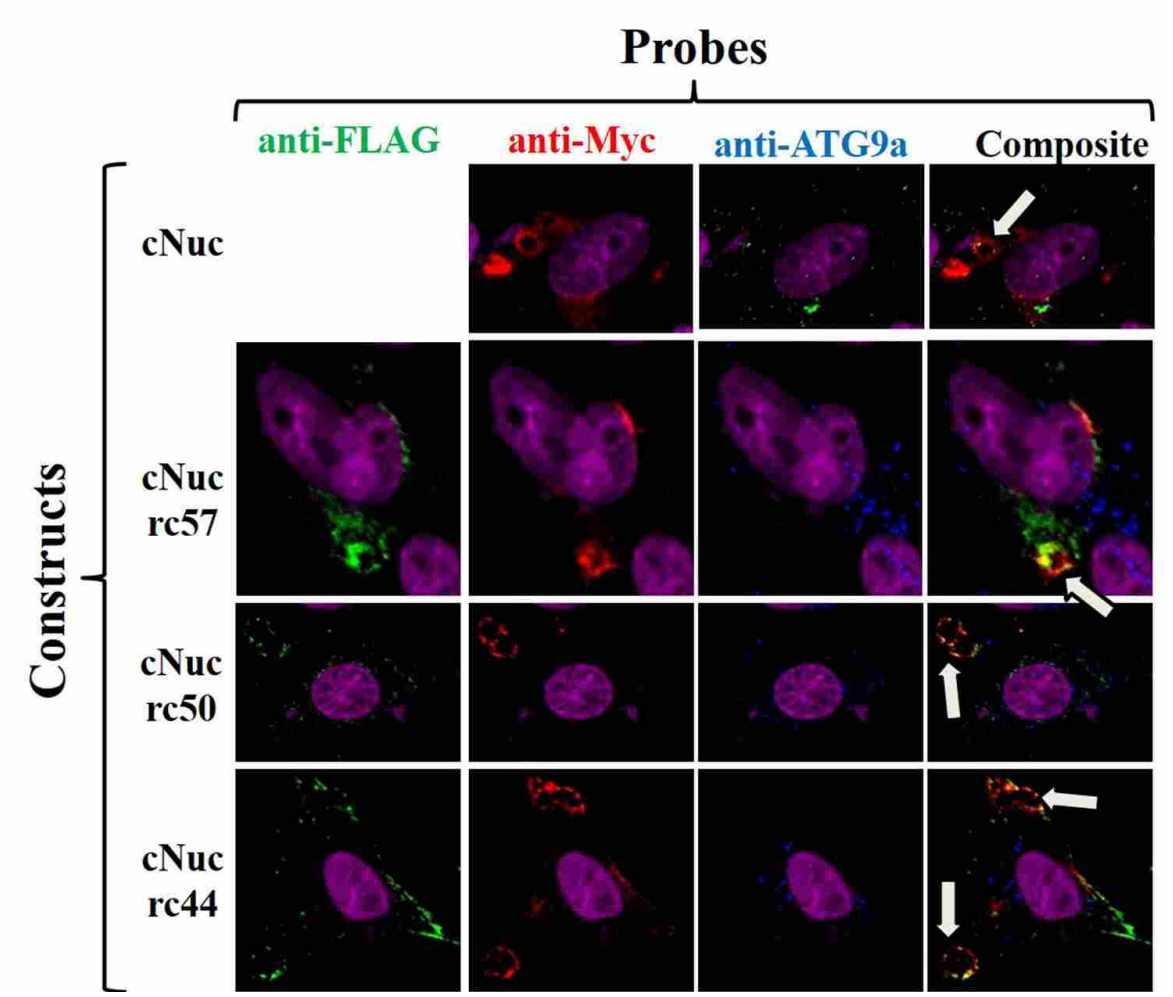

Figure 23: ATG9a does not co-localize with cNuc or rcCOX/cNuc formed LLPSs. We transiently transfected CHO cells with Myc-tagged cNuc or Myc-tagged cNuc with FLAG-tagged rcCOXs and after 24 hours fixed the cells and labeled cells against ATG9a, Myc, and FLAG peptide. White arrows indicate LLPSs. Purple: Nucleus (DAPI); Red: cNuc; Green: rcCOX; Blue: ATG9a; and Yellow: cNuc and rcCOX co-localizaion.

around LLPSs as reported above, but endogenous ATG9a did not co-localize to rcCOX/cNuc-formed LLPSs (Figure 23).

cNuc blocks autophagic flux before amphisome formation

Because autophagic flux is disrupted in LLPSs associated with CVB3 infection of rat pancreatic acinar cells, we assessed autophagic flux in rcCOX/cNuc transfected cells. Because

p62 is typically digested in canonical autophagy, accumulation of p62 is a marker for autophagic flux disruption. Analysis of p62 revealed that, 24 hours after transfection, p62 accumulation occurred in CHO cells overexpressing cNuc alone and cNuc with rc57, rc50, or rc44 (Figure 24) but p62 accumulation did not occur in cells overexpressing rc57, rc50, or rc44.

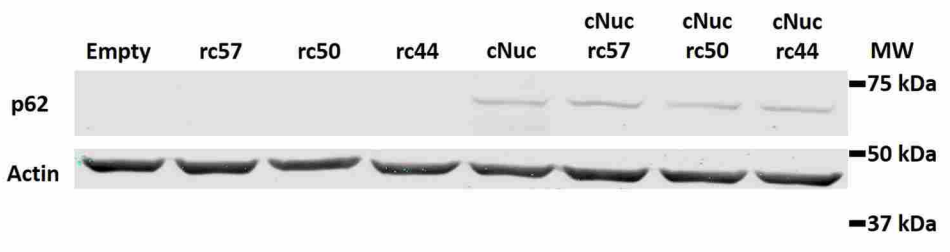

Figure 24: Cytosolic Nuc causes accumulation of p62. Western blot of rcCOX and/or cNuc transiently transfected CHO cell lysates probed with antibodies against p62 and actin, loading control marker.

We next determined if autophagic flux is blocked before autolysosome formation by transfecting Myc-tagged cNuc with FLAG-tagged rcCOXs into CHO cells and probing the cells with antibodies against Myc peptide, FLAG peptide, and the autolysosome marker cathepsin D. Cathepsin D was found in a punctate fashion throughout the cells but did not co-localize with cNuc/rcCOX-formed LLPSs, indicating that flux is blocked before autolysosome formation (Figure 25). We also observed LAMP-1 in a punctate pattern throughout the cell but LAMP-1 also did not co-localize around LLPSs. Combined, these data indicate that autophagic flux disruption occurs before amphisome formation (Figure 26).

Because a lack of fusion of LAMP-1 positive endosomes could result from defects in endosome formation, we then checked to see if endocytosis was disrupted by cNuc/rcCOX co-transfection, by co-transfecting cells as described above and incubating cells with 1 μm FluoSpheres® carboxylate-modified (540/560) beads (Life Technologies) for 22 hours. We washed the cells twice with PBS and prepared cells for confocal imaging as described earlier.

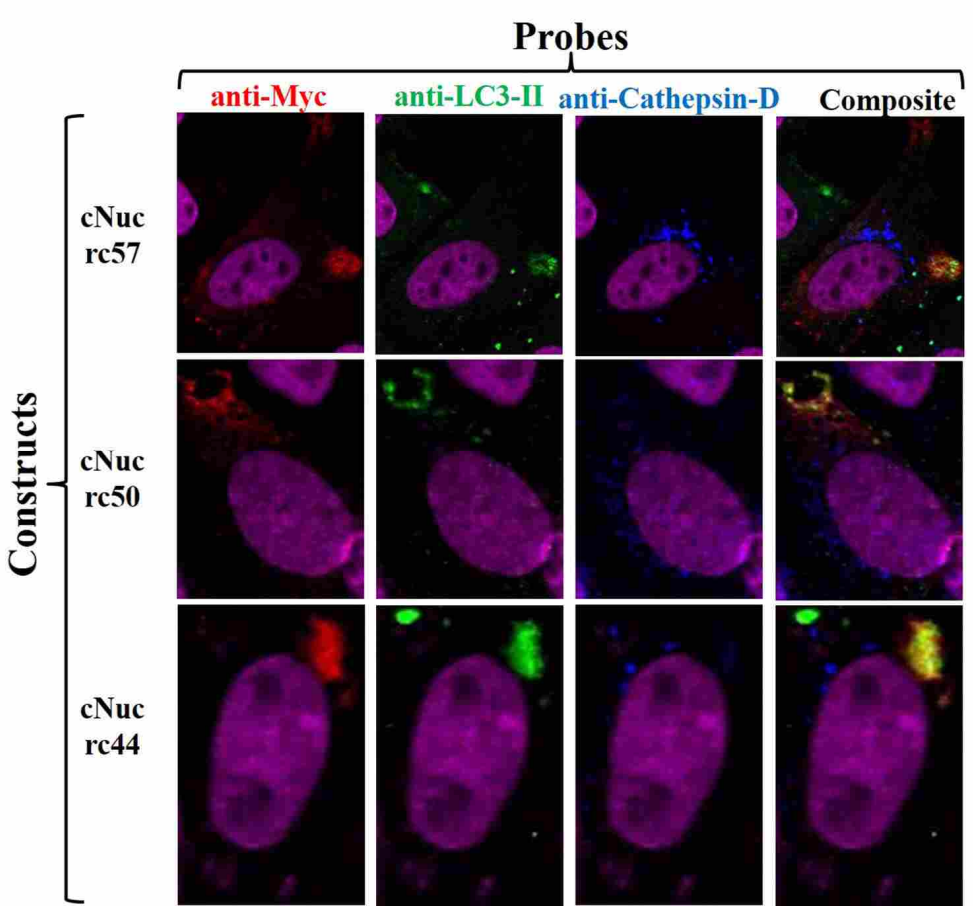

Figure 25: Autophagic flux is blocked before autolysosome formation. We tested whether autophagic flux is disrupted before autolysosome by transiently transfecting rcCOXs with cNuc and imaging the cells using confocal microscopy with antibodies probed against cNuc (Myc), rcCOX (FLAG), and the autolysosome marker cathepsin-D. Purple: Nucleus (DAPI); Red: cNuc; Green: rcCOX; Blue: cathepsin D; and Yellow: cNuc and LC3 co-localization.

We found that cells co-transfected with cNuc and rcCOX contain beads indicating that endocytosis is unabated. However, we did not find the beads within the LLPSs. The lack of beads within LLPSs again shows that they do not fuse with beads containing endosomes, supporting our results with LAMP-1 that endosome fusion to these structures is blocked (Figure 27).

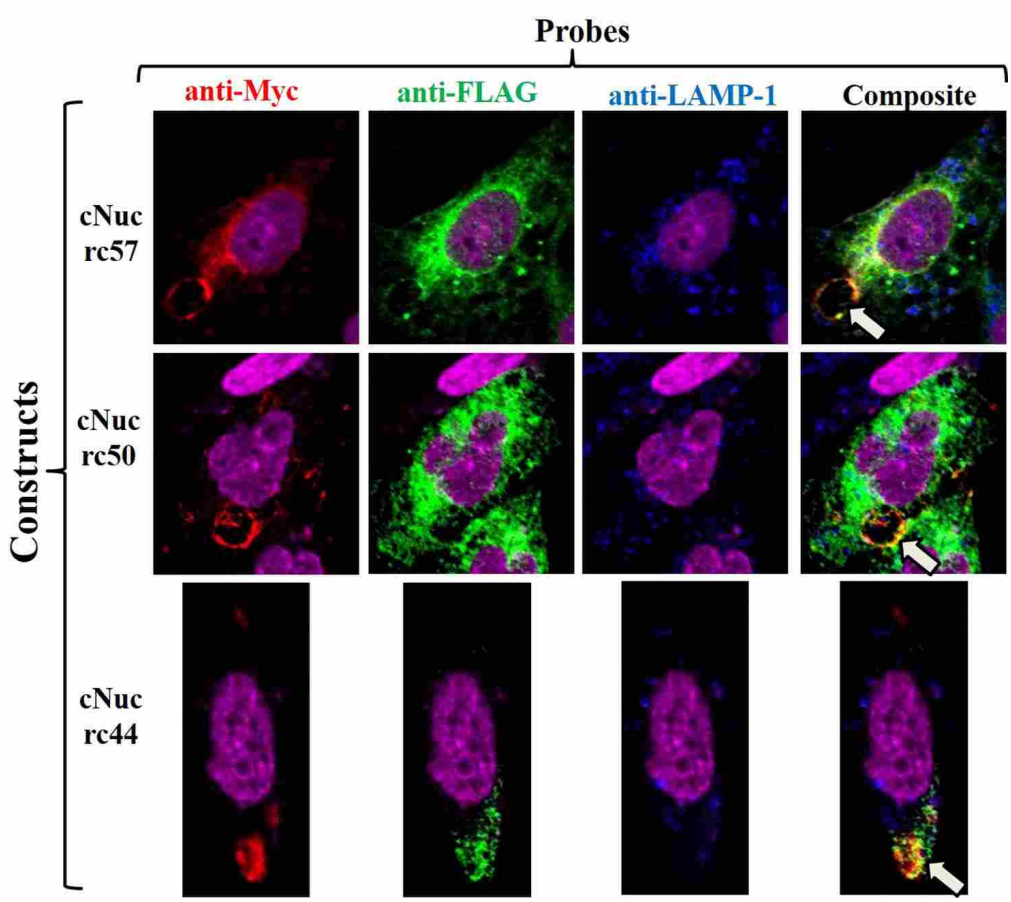

Figure 26: Autophagic flux is blocked before amphisome formation. Confocal images of CHO cells transiently transfected with FLAG-tagged rcCOXs and Myc-tagged cNuc and probed with antibodies against FLAG peptide, Myc peptide, and the amphisome marker LAMP-1. White arrow points to LLPSs. Purple: Nucleus (DAPI); Red: cNuc; Green: rcCOX; Blue: LAMP-1; and Yellow: cNuc and rcCOX co-localization.

Discussion

Since the development of ribosomal profiling (a technique wherein ribosomes are stalled on the mRNA either during translation initiation or elongation) our understanding has dramatically increased regarding the extent to which mRNA is translationally recoded.[17] Translational recoding, through ribosomal frameshifting or an alternative start codon, translates modified proteins which may have different functions or localizations from the cap-dependent translated product. This increases protein diversity. One important example is fibroblast growth

factor 2 (FGF2)[18] where there are five translationally recoded products.[19,20,21] Fully translated FGF2 contains a nuclear localization signal (NLS) that four of the alternatively translated isoforms retain and is therefore localized to the nucleus where it activates genes in an intracrine manner.[22] The fifth and smallest isoform lacks the NLS and activates its target genes in an autocrine or paracrine fashion. Thus, removing a specific polypeptide signal (in this case the NLS) by translational recoding, caused FGF2 gene products to not only localize to different compartments of the cell but also to function differently.

Here we document another instance where an mRNA, Nuc, is translationally recoded to produce proteins with differing localization and function compared to cap-dependent translated Nuc.

We provide evidence that the mechanism for generating cytosolic Nuc occurs via translational recoding. Surprisingly, we discovered that cNuc but not wtNuc evoked LLPS production. These structures were also produced by M1K-Nuc, M19K-Nuc, and M1/19K-Nuc constructs. We speculate that the mutation of Met19 to Lys may induce some translation of cNuc resulting in a low, but detectable production of LLPSs that are smaller than those driven by robust cNuc expression. Further work is needed to define the precise initiation sequence that produces the cNuc proteins, as the M1K and M1/19K-Nuc constructs indicate there are two potential sites in close proximity. Recoding of COX proteins, have demonstrated that in some instances a short region of RNA sequence rather than a specific codon, acts as the initiation of translocation. Also, the cellular signal/environment that induces translation of recoded Nuc proteins needs to be defined.

Our laboratory previously found the immunity-associated protein Nuc to be a binding partner of COX and here we show that a recoded form of Nuc, cNuc, co-localizes with rcCOXs around LLPSs. Recoded COXs also cause an increase in the number of transfected cells to form LLPSs. Until recently, LLPSs were found to occur during coxsackieviral infection[16] and other non-canonical phenomena.[23] Here we are able to observe the formation LLPSs in the absence of infectious agents, thus providing another system for studying the molecular mechanisms of

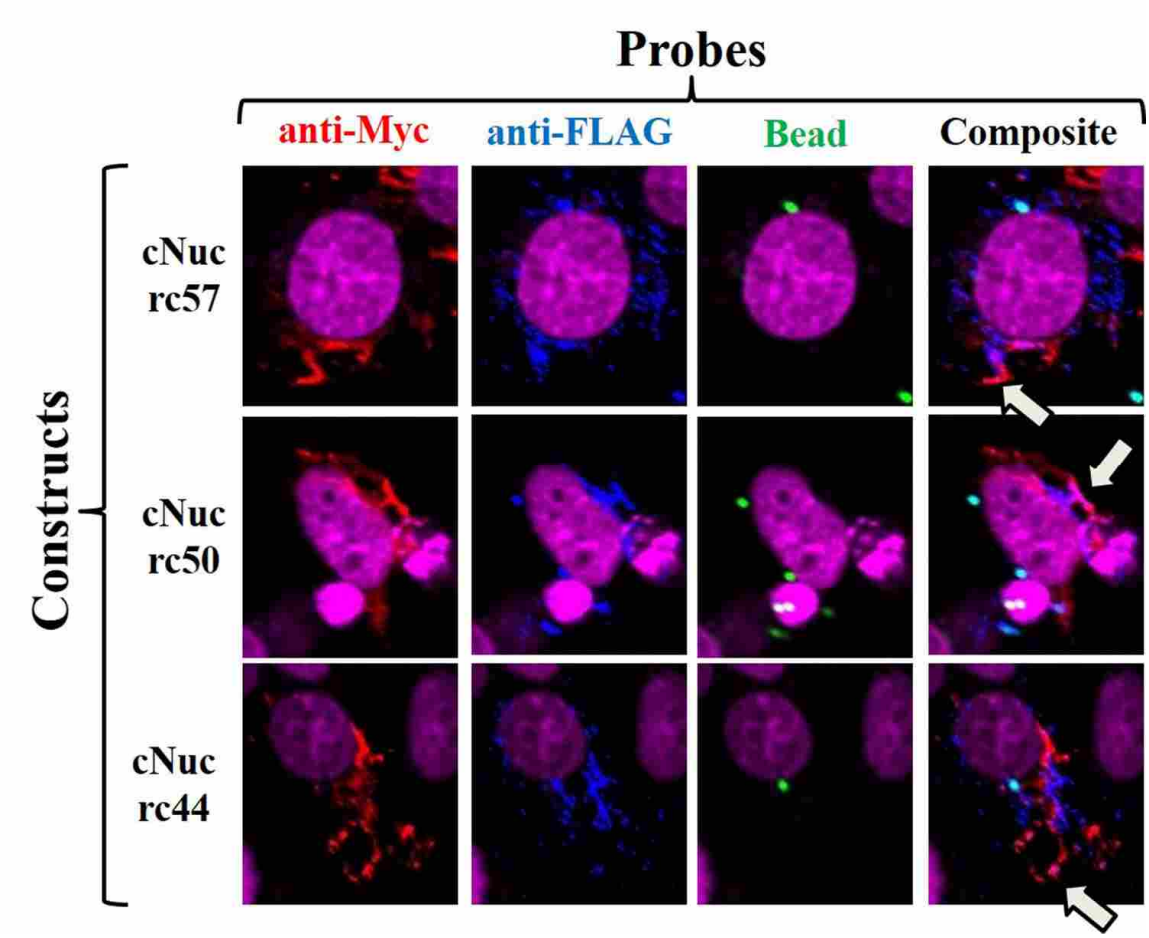

Figure 27: Endocytosed beads are not found within LLPSs. We used another technique to determine if autophagic flux disruption occurred before amphisome formation. We transfected CHO cells with rcCOXs and/or cNuc and incubated the cells with 1.0 µm diameter FluoSpheres (Life Technologies) for 22 hours. White arrows point to LLPSs. Red: cNuc; Blue: rcCOX; Green: beads; and Purple: cNuc and rcCOX co-localization.

LLPS formation. Whether mammalian cells utilize this phenomenon for other biological processes has yet to be determined.

It is also important to consider the correlation between LLPSs and autophagic flux disruption. We found cNuc both formed LLPSs and blocked autophagic flux; however, LLPSs lacked both the autolysosome marker cathepsin-D and the amphisome marker LAMP-1. This indicates that autophagic flux is blocked before amphisome formation. The mechanism by which cNuc blocks autophagic flux needs further investigation. Recently, Jaenisch's group showed that defective amphisome formation in Niemann-Pick type C1 (NPC1) disease is due to mutations of NPC1 gene that impede SNARE complex formation, which is important for autophagosome/endosome fusion, the step that appears to be disrupted in our studies.[24] One possibility is that cNuc interacts with SNARE proteins directly and impedes their role in organelle fusion. Due to cNuc's interaction with $G_{\alpha i}$,[11, 2] another possibility is that activation/inhibition of signaling pathways would lead to the expression of enzymes/effectors that produce LLPSs. Finally, we have discovered another function for the Nuc gene in the blockage of digestive autophagy which results in accumulation of p62.

References

1. Lin, P.; Yao, Y.; Hofmeister, R.; Tsien, R. Y.; Farquhar, M. G., Overexpression of CALNUC (nucleobindin) increases agonist and thapsigargin releasable Ca2+ storage in the Golgi. *J Cell Biol* **1999,** *145* (2), 279-89.

2. Lin, P.; Fischer, T.; Weiss, T.; Farquhar, M. G., Calnuc, an EF-hand Ca(2+) binding protein, specifically interacts with the C-terminal alpha5-helix of G(alpha)i3. *Proc Natl Acad Sci U S A* **2000,** *97* (2), 674-9.

3. Lin, P.; Li, F.; Zhang, Y. W.; Huang, H.; Tong, G.; Farquhar, M. G.; Xu, H., Calnuc binds to Alzheimer's beta-amyloid precursor protein and affects its biogenesis. *J Neurochem* **2007,** *100* (6), 1505-14.

4. Ballif, B. A.; Mincek, N. V.; Barratt, J. T.; Wilson, M. L.; Simmons, D. L., Interaction of cyclooxygenases with an apoptosis- and autoimmunity-associated protein. *Proc Natl Acad Sci U S A* **1996,** *93* (11), 5544-9.

5. Hunter, J. C. Multiple Recoding Mechanisms Produce Cyclooxygenase and Cyclooxygenase-Related Proteins from Frameshift-Containing COX-3/COX-1b Transcripts in Rat and Human. Brigham Young University, Brigham Young University, 2012.

6. Kanai, Y.; Kyuwa, S.; Miura, K.; Kurosawa, Y., Induction and natural occurrence of serum nucleosomal DNA in autoimmune MRL/lpr/lpr mice: its relation to apoptosis in the thymus. *Immunol Lett* **1995,** *46* (1-2), 207-14.

7. Kanai, Y.; Takeda, O.; Miura, K.; Amagai, M.; Kaneko, T.; Kubota, T.; Tanuma, S.; Kurosawa, Y., Induction of autoantibodies in normal mice by injection of nucleobindin and natural occurrence of antibodies against nucleobindin in autoimmune MRL/lpr/lpr mice. *Immunol Lett* **1995,** *45* (1-2), 35-42.

8. Miura, K.; Titani, K.; Kurosawa, Y.; Kanai, Y., Molecular cloning of nucleobindin, a novel DNA-binding protein that contains both a signal peptide and a leucine zipper structure. *Biochem Biophys Res Commun* **1992,** *187* (1), 375-80.

9. Miura, K.; Kurosawa, Y.; Kanai, Y., Calcium-binding activity of nucleobindin mediated by an EF hand moiety. *Biochem Biophys Res Commun* **1994,** *199* (3), 1388-93.

10. Lin, P.; Le-Niculescu, H.; Hofmeister, R.; McCaffery, J. M.; Jin, M.; Hennemann, H.; McQuistan, T.; De Vries, L.; Farquhar, M. G., The mammalian calcium-binding protein, nucleobindin (CALNUC), is a Golgi resident protein. *J Cell Biol* **1998,** *141* (7), 1515-27.

11. Lin, P.; Fischer, T.; Lavoie, C.; Huang, H.; Farquhar, M. G., Calnuc plays a role in dynamic distribution of Galphai but not Gbeta subunits and modulates ACTH secretion in AtT-20 neuroendocrine secretory cells. *Mol Neurodegener* **2009,** *4*, 15.

12. Kapoor, N.; Gupta, R.; Menon, S. T.; Folta-Stogniew, E.; Raleigh, D. P.; Sakmar, T. P., Nucleobindin 1 is a calcium-regulated guanine nucleotide dissociation inhibitor of G{alpha}i1. *J Biol Chem* **2010,** *285* (41), 31647-60.

13. Kanuru, M.; Raman, R.; Aradhyam, G. K., Serine protease activity of calnuc: regulation by Zn2+ and G proteins. *J Biol Chem* **2013,** *288* (3), 1762-73.

14. Tsukumo, Y.; Tomida, A.; Kitahara, O.; Nakamura, Y.; Asada, S.; Mori, K.; Tsuruo, T., Nucleobindin 1 controls the unfolded protein response by inhibiting ATF6 activation. *J Biol Chem* **2007,** *282* (40), 29264-72.

15. Gupta, R.; Kapoor, N.; Raleigh, D. P.; Sakmar, T. P., Nucleobindin 1 caps human islet amyloid polypeptide protofibrils to prevent amyloid fibril formation. *J Mol Biol* **2012,** *421* (2-3), 378-89.

16. Kemball, C. C.; Alirezaei, M.; Flynn, C. T.; Wood, M. R.; Harkins, S.; Kiosses, W. B.; Whitton, J. L., Coxsackievirus infection induces autophagy-like vesicles and megaphagosomes in pancreatic acinar cells in vivo. *J Virol* **2010,** *84* (23), 12110-24.

17. Atkins, J.; Gesteland, R., *Recoding: Expansion of Decoding Rules Enriches Gene Expression*. Springer: 2010; Vol. 24.

18. Touriol, C.; Bornes, S.; Bonnal, S.; Audigier, S.; Prats, H.; Prats, A. C.; Vagner, S., Generation of protein isoform diversity by alternative initiation of translation at non-AUG codons. *Biol Cell* **2003,** *95* (3-4), 169-78.

19. Prats, H.; Kaghad, M.; Prats, A. C.; Klagsbrun, M.; Lélias, J. M.; Liauzun, P.; Chalon, P.; Tauber, J. P.; Amalric, F.; Smith, J. A., High molecular mass forms of basic fibroblast growth factor are initiated by alternative CUG codons. *Proc Natl Acad Sci U S A* **1989,** *86* (6), 1836-40.

20. Florkiewicz, R. Z.; Sommer, A., Human basic fibroblast growth factor gene encodes four polypeptides: three initiate translation from non-AUG codons. *Proc Natl Acad Sci U S A* **1989,** *86* (11), 3978-81.

21. Arnaud, E.; Touriol, C.; Boutonnet, C.; Gensac, M. C.; Vagner, S.; Prats, H.; Prats, A. C., A new 34-kilodalton isoform of human fibroblast growth factor 2 is cap dependently synthesized by using a non-AUG start codon and behaves as a survival factor. *Mol Cell Biol* **1999,** *19* (1), 505-14.

22. Vagner, S.; Touriol, C.; Galy, B.; Audigier, S.; Gensac, M. C.; Amalric, F.; Bayard, F.; Prats, H.; Prats, A. C., Translation of CUG- but not AUG-initiated forms of human fibroblast growth factor 2 is activated in transformed and stressed cells. *J Cell Biol* **1996,** *135* (5), 1391-402.

23. Ceru, S.; Layfield, R.; Zavasnik-Bergant, T.; Repnik, U.; Kopitar-Jerala, N.; Turk, V.; Zerovnik, E., Intracellular aggregation of human stefin B: confocal and electron microscopy study. *Biol Cell* **2010,** *102* (6), 319-34.

24. Sarkar, S.; Carroll, B.; Buganim, Y.; Maetzel, D.; Ng, A. H.; Cassady, J. P.; Cohen, M. A.; Chakraborty, S.; Wang, H.; Spooner, E.; Ploegh, H.; Gsponer, J.; Korolchuk, V. I.; Jaenisch,

R., Impaired autophagy in the lipid-storage disorder Niemann-Pick type C1 disease. *Cell Rep* **2013,** *5* (5), 1302-15.

Chapter 4

Large LC3-II positive structure (LLPS) formation is affected by rcCOX redox activity and requires oxylipin metabolism

Abstract

Early in evolutionary history cells acquired iron-containing enzymes to deactivate radical oxygen species. These enzymes then evolved to be major components of innate immunity, such as cyclooxygenases and lipoxygenases. The manner in which these enzymes activate innate immune responses is through the oxygenation of unsaturated fatty acids, which in turn act as signaling molecules. Cyclooxygenase-mediated oxygenation of unsaturated fatty acids is accomplished through radical chemistry in which important catalytic residues Tyr385, His388, and His207 are critical (residue numbering based upon ovine COX-1).[2]

We utilize site-directed mutagenesis and prostaglandin synthesis activity assays to show that most methionines (Mets) that encode the translation of rcCOXs are not essential for cyclooxygenase activity of COX-1. Through molecular modeling, we also find that rcCOXs resemble peroxidase-cyclooxygenase enzymes from plants in that they lack dimerization domains and are non-glycosylated. We demonstrate that rcCOXs are oxylipin generating enzymes by mutating important catalytic residues of the COX gene which, in turn, inhibits rcCOX/cNuc formation of LLPSs.

To determine the substrate source for rcCOX activity we found that $cPLA_2$, an enzyme that releases COX substrate arachidonic acid (AA) from membrane, is vital for LLPS formation. Additionally, one or more endogenous oxygenase enzymes appear to act in place of rcCOX, but to a lesser degree when cNuc is expressed in the absence of rcCOXs. Using LLPS as a marker for intracellular rcCOX oxygenase activity, we tested a variety of drugs and show acetaminophen

and LOX5 specific inhibitors blocked rc57/cNuc LLPS formation but not LLPS formation potentiated by the endogenous oxygenase. However, a LOX15 specific inhibitor inhibited both rc57/cNuc and endogenous oxygenase stimulated LLPS formation. Combined, these results indicate rcCOXs possess unique oxylipin enzymatic capabilities relative to the endogenous enzyme and that LLPS formation evoked by rcCOXs or the endogenous enzyme, depend on LOX15.

Background

Early earth's highly oxygenated environment led organisms to evolve enzymes that deactivate highly reactive oxygen species (ROSs) for survival. These early enzymes diversified and evolved into multiple superfamilies, one such is the peroxidase-cyclooxygenase superfamily, which spans both prokaryotic and eukaryotic domains and is involved in a host of cellular processes from embryonic development to its major role in innate immunity. Recent construction of phylogenetic relationships reveals that the peroxidase-cyclooxygenase superfamily follows the birth-and-death model of evolution.[3] In this model, organisms develop gene duplications of oxygenase gene precursors (birth) resulting in functional genes and genes that are inactive or not expressed (pseudogenes or death). Peroxidase-cyclooxygenases utilize heme as a cofactor that is creviced in conserved alpha helices denoted as the peroxidase site. Utilizing the heme, they oxygenate substrates through chemistry producing a substrate radical. The oxygenation active site for these enzymes typically are distinct from, but relies upon the peroxidase site. Oxygenated lipids created at the oxygenation site are then reduced at the peroxidase site to form the final product. This reductive step is important for priming oxygenase activity.[2] Key residues conserved in the peroxidase site, histidine ligands which coordinate with heme, are essential for the redox chemistry that occurs at both the oxygenation and peroxidase

sites. The oxygenase site is where substrate, typically an unsaturated fatty acid, is activated to a lipid radical. This site contains an invariant Tyr that is converted into a tyrosyl radical, generating the lipid radical that reacts with O_2 resulting in oxygenation of the substrate.

Using genome sequencing, prokaryotic cyclooxygenase like-peroxidases (CLPs) have been discovered in *Mycobacterium vanbaalenii*, *Nitrosomas europeaea*, and *Streptomyces avaermitilis*.[4,5] These CLPs are described from ancestral genes of *Homo sapien* COX.[3] Very little is known about the structure of bacterial CLPs and the role they play in cellular survival. However, whole-genome sequencing techniques showed *N. europeaea* CLP mRNA expression is induced when the bacterium is stressed, such as by toxic levels of cyanide.[5]

Currently, CLPs have also been discovered in an array of plant and fungal species where their main role has been defense against invading pathogens,[11] but their expression is also important for development.[12] The CLP, pathogen-inducible oxygenase (PIOX), is induced in tobacco leaves when the bacteria *Erwinia amylovora* invades a host cell.[6] The flowering plant *Arabidopsis thaliana* contains a CLP, α-dioxygenase (Ata-DiOx), which is well characterized and shown through crystallography to have high secondary structure homology to mammalian COX.[7] The CLP from Ata-DiOx contains peroxidase and oxygenase sites, but it lacks both the epithelial growth factor (EGF) domain necessary for dimerization, and a signal peptide, important for translation into the endoplasmic reticulum (ER), found in mammalian COX. Interestingly, cytosolic Ata-DiOx CLP is active in an array of different expression systems (such as *E. coli*) and is not dependent upon glycosylation, a mammalian COX post-translational modification required for activity.[8]

CLPs are also formed in fungi in which take-all fungi (fungi that cause root rot in plants) have a CLP denoted as 7,8-linoleate diol synthase (7,8-LDS) that has been cloned,[9]

characterized,[10] and shown to form oxylipins like mammalian COX.[11] These oxylipins are important for both the development and the pathogenicity of take-all fungi.[12,13]

Thus, in unicellular and multicellular organisms CLPs are being discovered that bear structural similarity to COXs even though they are cytosolic in nature. Their roles appear to be diverse, but frequently involve functions in innate immunity and development. The roles COX performs in mammals extend beyond innate immunity and reproduction. There are two isoforms denoted as COX-1 and COX-2.[14] COX-1 plays a role in innate immunity by inducing thrombosis[15] upon injury which encloses and facilitates the elimination of invading pathogens.[16] COX-2 the inducible form, is involved in a number of physiological roles including but not limited to angiogenesis,[17] follicle release,[18] pyresis,[19] and inflammation.[20] COX-2 has also been implicated in a number of pathophysiological disorders such as arthritis[21] and cancer,[22,23] in which COX-2 regulation is impaired and is overexpressed causing chronic inflammation.

In addition to containing cyclooxygenases, eukaryotes and prokaryotes also possess other oxylipin-generating enzymes. One of these is the iron containing peroxidase family of lipoxygenases. Lipoxygenases (LOXs) are found in unicellular organisms such as *Chlorella*[24] but also in an array of plants, fungi, and animals.[25] In many instances, organisms will contain multiple genes that encode different lipoxygenases that are designated by the carbon number of arachidonic acid that each oxygenates.[26,27] For instance, LOX5 gene encodes a lipoxygenase that typically oxygenates carbon 5 on arachidonic acid while LOX15 typically oxygenates carbon 15.

Oxygenation of lipid substrate in LOX metabolism begins when the iron is oxidized to the ferric state. At this point ferric iron radicalizes the substrate whereupon the ferric iron is reduced to the ferrous state.[28] Oxygen then reacts with the radicalized substrate to form a peroxyl group that forms the intermediate product, hydroperoxy eicosatetraenoic acid (HPETE).

The peroxyl group is then reduced by the LOX ferrous iron to form either the final product, hydroxyl eicosatetraenoic acid (HETE) or an intermediate product that is further isomerized by downstream enzymes. Due to the use of reactive radical chemistry in LOX product synthesis, LOX enzymes, especially reticulocyte LOX15, are shown to self-deactivate similar to COX.[29,30]

LOX substrates include free fatty acids such as arachidonic acid and esterified membrane bound lipids. Oxygenation of free fatty acids are sometimes conjugated to peptides (such as in generation of cysteinyl leukotrienes) that cause bronchoconstriction and are a source of the pathological disorder asthma.[31] However, LOXs can also act on esterified fatty acid in membranes to cause membrane reorganization rather than creating a diffusible signaling molecule. For example, LOX15 peroxidizes esterified membrane lipids, such as glycero-phospholipids and cholesteryl-esters, which induces structural changes that causes both red cell maturation[32] and oxidation of low density lipoprotein in atherosclerosis.[33] Membrane modifications by LOX15 have also been connected to mitochondrial cargo loading in autophagy.[45]

Biological roles of lipoxygenases have been difficult to ascertain due to lack of obvious phenotypic changes in LOX gene knockout mice.[34] These results indicate pathway redundancy where multiple enzymes catalyze specific lipoxygenase products or may even play their roles. Like COXs and cytochrome P-450, LOXs react to physiological and pathological stresses and are shown to be involved in but not limited to inflammation,[35,36] cell adhesion,[37] and processes involving development[49] and innate immunity.[48]

Materials and Methods

Cell culture, site-directed mutagenesis, transient transfection, and confocal microscopy procedures used in this chapter are discussed in the Materials and Methods section in Chapter 2.

Prostaglandin Synthesis Activity Assay

CHO cells were transiently transfected with constructs as described above and allowed to incubate at 37° C and 5% CO_2 for 24 hours. After 24 hours, cells were washed twice with 500 µL of DMEM F/12 media and 500 µL of reaction solution (30 µM arachidonic acid in DMEM F-12) and incubated at 37° C and 5% CO_2 for 30 minutes. PGE_2 synthesis was then measured by anti-PGE_2 radioimmunoassay. Cellular media (100 µL) was placed into 10 mL glass tubes with 100 µL of 50 mM Tris HCl pH 7.5. Then 100 µL of antibody solution (1 vial of anti-PGE_2 antibody (Sigma) was dissolved into 10 mL of 50 mM Tris HCl, pH 7.4), 100 µL of tracer solution (7.5 µL of tritiated PGE_2 from Perkin Elmer placed into 10 mL of 50 mM Tris HCl, pH 7.4) and 100 µL of 50 mM Tris HCl, pH 7.5 was added to each sample tube. Each sample was measured in triplicate. A standard curve was prepared by serially diluting PGE_2 (Sigma Aldrich) into 50 mM Tris HCl, pH 7.4, to concentrations between 200 ng/mL to 0.098 ng/mL. Then 100 µL of standard was placed into a 10 mL glass vial with 100 µL of tracer, 100 µL of antibody solution, 100 µL of DMEM F/12 and 100 µL of 50 mM Tris HCl pH 7.4. Samples and standards were vortexed and allowed to incubate overnight at 4° C.

The next day, 200 µL of charcoal solution (0.1 g of dextran and 0.5 g of charcoal added and mixed in 25 mL of 50 mM Tris HCl pH 7.4) was added to each sample and standard, vortexed, and incubated for 10 minutes at 4° C. Charcoal was then sedimented via centrifugation for 10 minutes at 4° C and 1000xg. Then 400 µL of the supernatant was transferred to 3 mL of Ecoscint A scintillation cocktail (National Diagnostic) in scintillation vials (Perkin Elmer), mixed, and counted by a Tri-carb counter (Perkin Elmer). Data were analyzed using GraphPad (Prism) by calculating a best fit dose-response curve using standards prepared above and calculating the concentration of PGE_2 in each sample.

Cellular drug assay

Stock concentration of drugs were prepared in DMSO and stored at -80° C. On the day of treatment, drugs were thawed and added to CHO cells that were transiently transfected as described in Chapter 2 at the 20% FBS addition step. Cells were incubated with drugs for 22 hours at 37° C. Cells were then washed three times with PBS and prepared for confocal microscopy and imaged as described in Chapter 2.

Results

Evolutionary evaluation of methionines responsible for rcCOX recoding and their roles in cyclooxygenase catalysis

Initiating Mets of rc57, rc50, and rc44 proteins in the COX-1 primary sequence are highly conserved in multiple species (Figure 28), indicating these Met are important for COX gene function. To test whether the evolutionary conservation of the initiating Met for rc57, rc50, and rc44 is due to their requirement for prostaglandin synthesis, we mutated each rat COX-1 Met to Ala (constructs denoted as M57A-COX-1, M50A-COX-1, and M44A-COX-1). Then we transiently transfected these constructs into CHO cells and measured COX-1 activity (by PGE_2 production) using radio-immunoassay. The results are shown in Figure 29. There is a ~60% decrease in activity in the M57A-COX-1 construct compared to wild type COX-1 (p-value=1.986E-8), but no statistical difference in activity between wild type COX-1 and the M50A-COX-1 and M44A-COX-1 constructs. To test whether the inhibition in M57A-COX-1 activity was due to loss of rc57 protein, which can be recoded from COX-1 mRNA,[38] we titrated a construct that only produces the rc57 with the M57A-COX-1 construct and performed an activity assay to determine if activity is restored. We found that activity was not restored with titration of the rc57 construct with the M57A-COX-1 transcript. This indicates the initiating Met

of rc57 is important for COX-1 activity and that some of its conservation is due to a structural role that affects catalysis. The initiating Met of the rc50 and rc44 are not important for COX-1 activity and, therefore, their evolutionary conservation may be due to other functions, including being the translational initiation Met codon for rc50 and rc44.

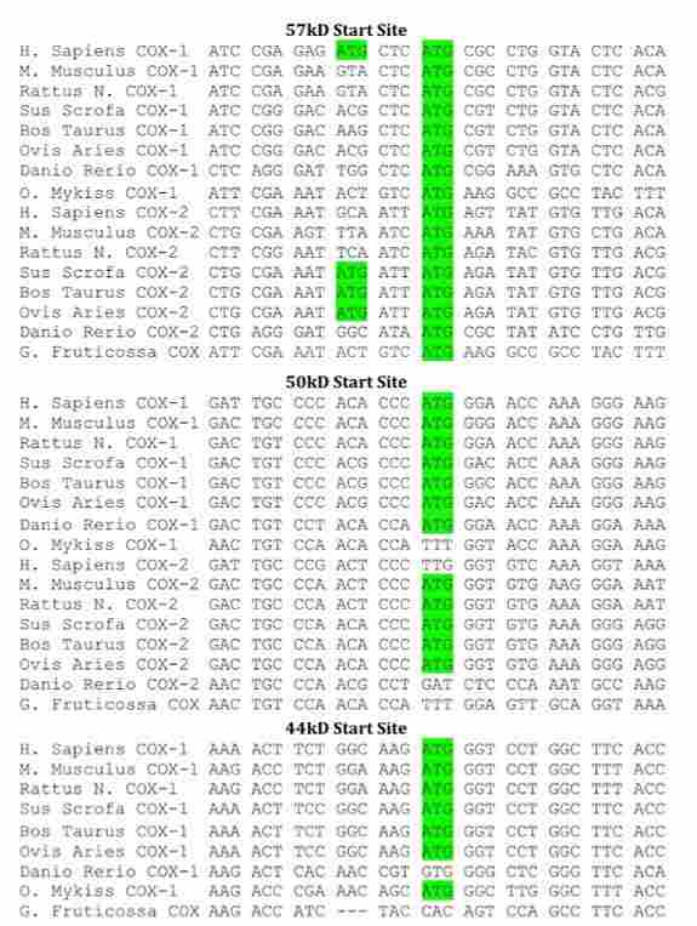

Figure 28: Evolutionary conservation of initiating Met of rc57, rc50, and rc44. Most species contain Met codons that initiate translation of the rc57, rc50, and rc44. Met codons are highlighted in green showing high conservation. Image was prepared by Dr. John Hunter[23] and edited by me.

Structural comparison of CLPs and rcCOXs reveals evolutionary similarities

The tertiary structure prediction program I-TASSER generates 3D structures based upon a threading/fold recognition methodology.[39] As a first step to understand rcCOX structure, we used this program to predict structures for rc57, rc50, and rc44.[40] These predicted structures were then compared to known or predicted Protein Data Base (PDB) crystal structures of non-mammalian CLP/COX enzymes.[41]

The top ten templates utilized by I-TASSER for predicting the tertiary structure of the rcCOXs are listed in Table 1. Predictably all 10 templates used were of COX-1 or COX-2 PDB files, due primarily to sequence homology to rcCOXs. Table 1 also illustrates the proteins I-

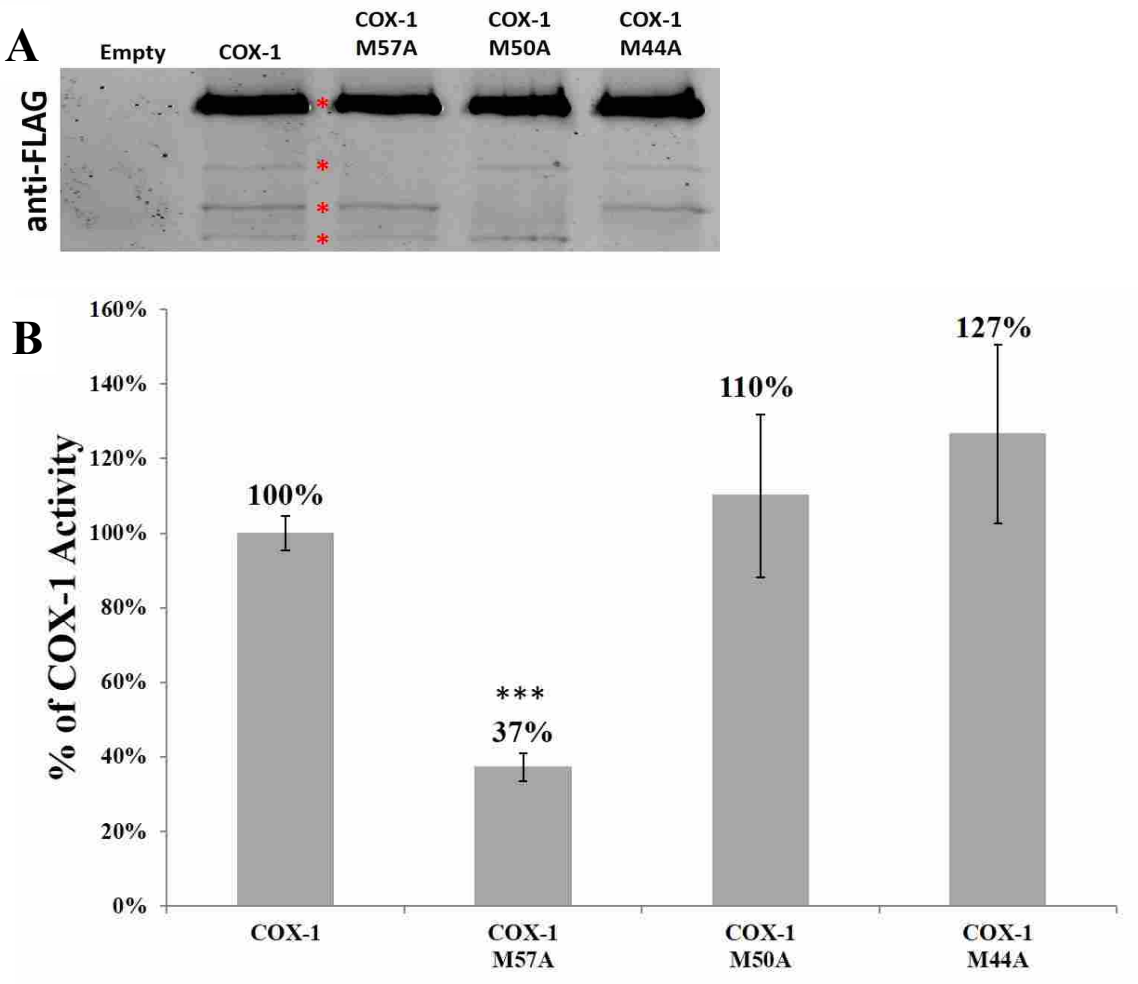

Figure 29: Initiating Met of rc57 is important for COX-1 activity. We mutagenized the initiating Met of the rc57, rc50, and rc44 to an alanine and transfected these into CHO cells for 24 hours. Cells were then incubated with media containing 30 μM AA 30 minutes before harvesting the cells. PGE_2 synthesis into the media was corrected based upon the level of ectopic COX-1 expression. A) Western blot of FLAG-tagged COX-1and the rc57, rc50, and rc44 proteins where * indicates COX-1 translated proteins. B) Graphs are averages of 3 experiments each performed in triplicate. * p-value < 0.05; ** p-value < 0.01; *** is p-value<0.001.

TASSER identified as having highly similar structures to rcCOXs. Among these, rcCOXs showed similarity to members of the peroxidase-cyclooxygenase superfamily such as plant α-dioxygenases, goat lactoperoxidase, and human myeloperoxidase. C-scores, which measure the quality of the predicted model, can range from -5 to 2, and the rc57, rc50, and rc44 models were 1.85, 1.63, and 1.61 respectively. The RMSD scores, which measures the average distance between 2 atoms, were good for the predicted models of the rc57, rc50, and rc44 which were 3.4+/-2.4 Å, 3.7+/-2.5 Å, and 3.4+/-2.4 Å respectively.

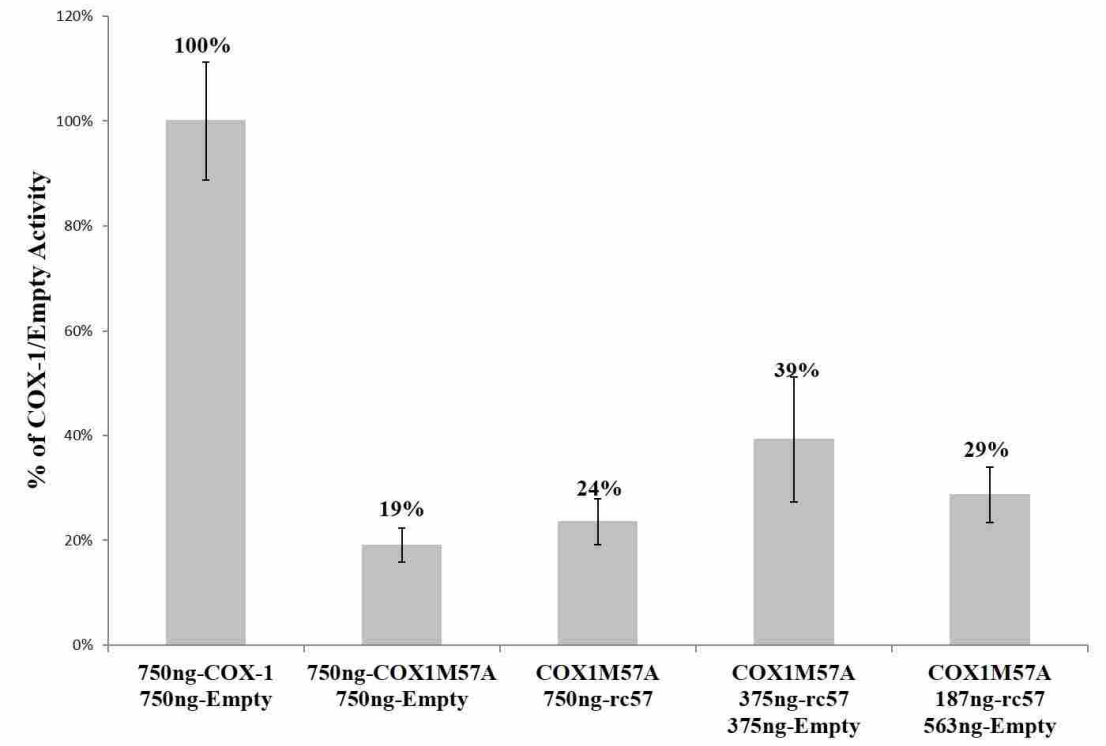

Figure 30: Co-expressing rc57 with M57A-COX-1 does not rescue loss activity. We titrated the rc57 transcript with M57A-COX-1 to test if COX activity was restored by rc57 protein. Graph is an average and SEM of 3 experiments each done in triplicate. T tests were done by comparing the titrations of rc57 and COX1M57A against COX1M57A/Empty.

Similar to most non-animal CLPs including the Ata-Dioxs, rcCOXs do not contain a dimerization domain and are not glycosylated. Like these proteins, however, the predicted structures for both rc57 and rc50 have globular peroxidase sites formed by alpha helices (numbering from N-terminus) four, twelve, and seventeen. The peroxidase site for rc44 is overall well conserved even though it is missing alpha helix 4 (Figure 31). Recoded 44 still

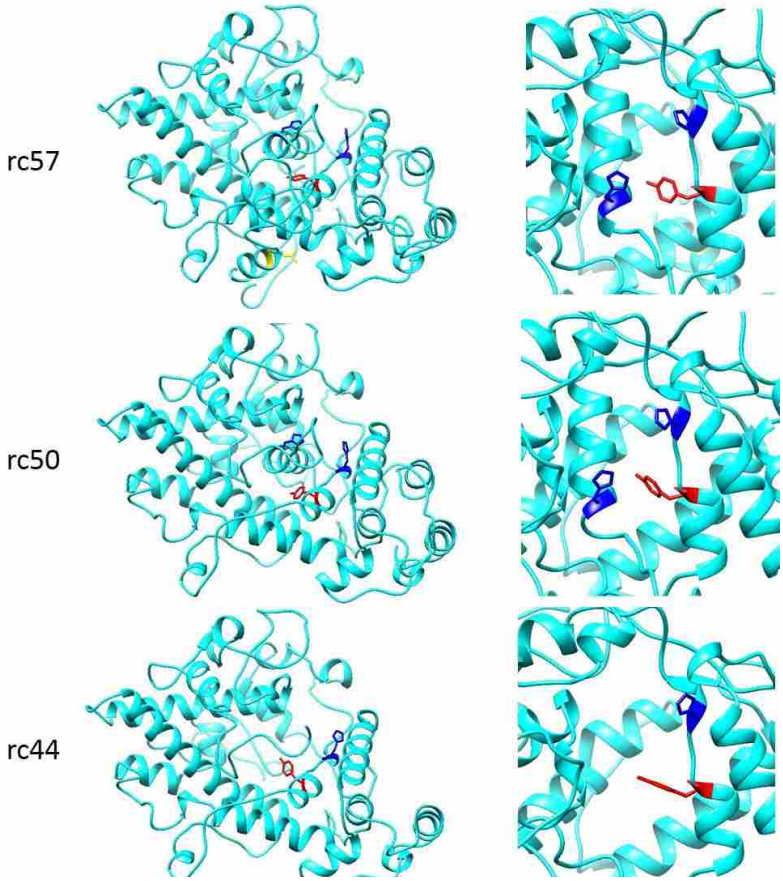

Figure 31: I-TASSER predicted structure of rc57, rc50, and rc44. Image of I-TASSER predicted structures of rc57, rc50 and rc44. On the left column is the side view of the rcCOXs and the right column is the top view of the rcCOXs specifically looking into the peroxidase site. The dark blue His residues are the His388 and His207 that are important for heme binding and the red Tyr is Tyr385, important for oxygenase activity. Images generated using UCSF Chimera package that was developed by the Resource for Biocomputing, Visualization, and informatics at the University of California, San Fanscisco (supported by NIGMS P41-GM103311).[1]

contains H388, the predicted proximal ligand to heme, but not His207, a potential distal ligand to heme. It also has an appropriately oriented Tyr385.

For rc57 and rc50, potential heme binding residues His207 and His388 are situated within a cleft that would coordinate the iron atom of heme. In contrast, rc44 lacks His207. Each rcCOX contains a predicted active tyrosyl residue (Tyr385) situated on the opposite side of the heme plane located at the base of the peroxidase site cleft (similarly found in COX-1 and COX-2), which would be indicative of an ability to oxygenate lipids. Unlike rc50 and rc44, rc57 also contains the Arg120 residue important for coordinating the carboxyl group of fatty acids, which directs the hydrophobic portion of the acyl-chain into the oxygenase site of COX. Together these data suggested that rcCOXs may possess peroxidase activity and potential oxylipin generating activity. Also, differences in each proteins' active site (e.g. retention of Arg120 in rc57, which is absent in rc50 and rc44) raises the potential for synthesis of differing products.

Site-directed mutagenesis of catalytic residues of rcCOXs influence localization

From our I-TASSER data we hypothesized the rcCOX effect on LLPS formation is by a heme mediated peroxidase or oxygenase activity. To test this, we first mutagenized important catalytic residues Tyr385, His388, and His207 to a Phe,[42] Gln, and Gln[43] respectively. We also made a construct wherein we mutated both His388 and His207 to Gln. We next co-transfected these constructs with cNuc and visualized LLPS formation using confocal microscopy. In these experiments we also used probes against Myc-tagged cNuc, FLAG-tagged rcCOX, and LC3-II and examined the localization pattern of the rcCOX constructs described above for possible

rc57									
Templates used by I-TASSER					Proteins with similar structure				
Rank	PDB Hit	Protein	Z score		Rank	PDB Hit	Protein	TM-score	RMSD
1	1cqeB	COX1	3.12		1	1prhA2	COX1	0.965	0.7
2	1cqeB	COX1	3.28		2	1cqeB	COX1	0.962	0.47
3	1cqeB	COX1	6.02		3	3nt1A2	COX2	0.953	0.9
4	1cqeB	COX1	5.49		4	4hhrA	αDIOX	0.824	2.92
5	1cqeB	COX1	3.41		5	2ehaB	LPO	0.823	3.46
6	2ay1A	COX1	3.24		6	4kvjA	αDIOX	0.82	2.96
7	1eqgA	COX1	8.99		7	1fe2A3	COX1	0.738	0.56
8	3nt1A	COX2	5.83		8	1mhlC	MPO	0.659	3.45
9	1eqgA	COX1	5.2		9	3k07A	CusA	0.363	7.19
10	3n8zA	COX1	6.33		10	3kk6A2	COX1	0.225	0.83

rc50									
Templates used by I-TASSER					Proteins with similar structure				
Rank	PDB Hit	Protein	Z score		Rank	PDB Hit	Protein	TM-score	RMSD
1	1cqeB	COX1	2.72		1	1prhA2	COX1	0.962	0.68
2	1cqeB	COX1	2.83		2	1cqeB	COX1	0.959	0.36
3	1cqeB	COX1	5.31		3	1pxxD	COX2	0.95	0.83
4	1cqeB	COX1	4.82		4	2ehaB	LPO	0.864	3.28
5	1cqeB	COX1	3.04		5	4hhrA	αDIOX	0.85	2.61
6	2ay1A	COX1	3.12		6	4kvjA	αDIOX	0.844	2.57
7	1cvuA	COX2	8.74		7	1mhlC	MPO	0.767	3.49
8	3nt1A	COX2	5.67		8	1fe2A3	COX1	0.71	0.48
9	1cvuA	COX2	4.83		9	3ne5A	CusBA	0.379	6.52
10	3n8zA	COX1	6.11		10	3kk6A2	COX1	0.251	0.75

rc44									
Templates used by I-TASSER					Proteins with similar structure				
Rank	PDB Hit	Protein	Z score		Rank	PDB Hit	Protein	TM-score	RMSD
1	1cqeB	COX1	2.85		1	1prhA2	COX1	0.955	0.85
2	1cqeB	COX1	2.3		2	1cqeB	COX1	0.952	0.57
3	1cqeB	COX1	4.49		3	1pxxD	COX2	0.941	0.91
4	1mh1C	MPO	4.18		4	2gjmA	LPO	0.863	3.03
5	1cqeB	COX1	2.6		5	1mhlC	MPO	0.862	2.97
6	2ay1A	COX1	2.88		6	4hhrA	αDIOX	0.843	2.31
7	1eqgA	COX1	8.25		7	4kvjA2	αDIOX	0.836	2.33
8	3nt1A	COX2	5.48		8	1fe2A3	COX1	0.668	0.57
9	1eqgA	COX1	4.34		9	4djiA	GadC	0.407	5.54
10	3n8zA	COX1	5.89		10	3kk6A2	COX1	0.285	0.75

Table 1 on previous page: Table of both PDB templates for rcCOX construction and PDB templates with similar structure. Tables of PDB templates used for rcCOX construction are in the right column and show I-TASSER utilized mainly COX PDB templates for tertiary structure prediction due to amino acid sequence similarity. The left column shows PDB structures similar to rcCOXs.

disruption of cNuc and rcCOX co-localization. The H388Q-rc57, H388Q-rc50, and H388Q-rc44 constructs continued to co-localize with cNuc at LC3-II-positive punctate structures (autophagosomes) at the periphery of the cell (Figure 32A). Also, the H207Q-rc57 and H207Q-rc50 constructs continued to co-localize with cNuc around LLPSs similar to wild type rcCOX/cNuc transiently transfected cells (Figure 32B). However, constructs H388/207Q-rc57 and H388/207Q-rc50 blocked rcCOX co-localization with cNuc; rcCOXs were instead localized in large patches around the nucleus. Cytosolic Nuc remained at the periphery of the cell and associated with autophagosomes (Figure 33A-B).

Most striking were the effects of Y385F-rc57 or Y385F-rc50 mutants co-transfected with cNuc, which showed no co-localization with cNuc. Here, however, Y385F-rc57 and Y385F-rc50 produced prominent membrane structures situated near the nucleus that were LC3-II negative. Mutation of the Tyr did not affect cNuc targeting to autophagosomes at the periphery of the cell. Mutation of the Tyr in rc44 (Y385F-rc44) also had an effect on its subcellular distribution, causing it to localize to autophagosomes in addition to having a diffuse cytosolic expression. Nuclear localization of rc44, seen in some cells, was unaffected by Tyr mutations (Figure 33B).

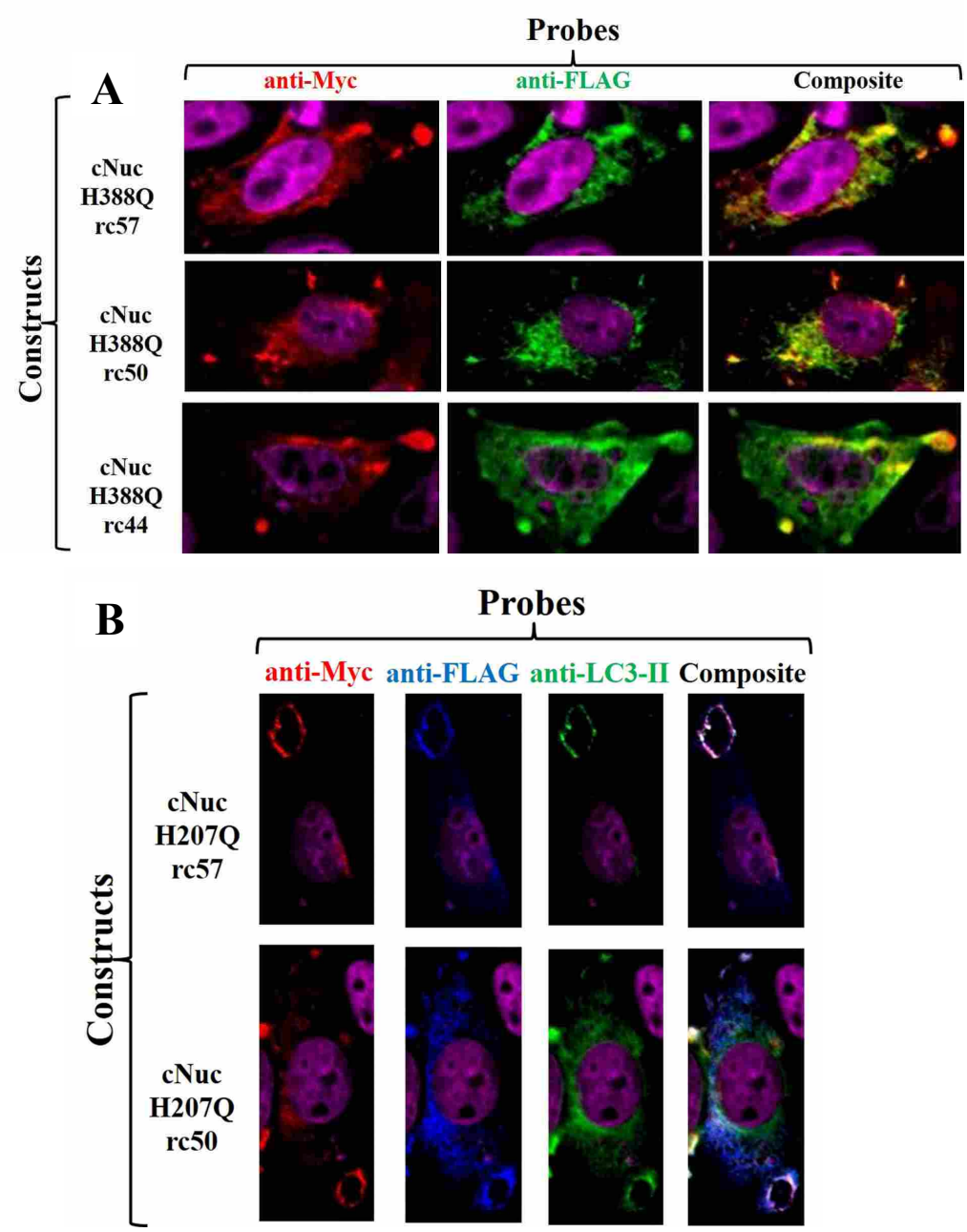

Figure 32: H388Q- and H207Q-rcCOXs continue co-localizing with cNuc. CHO cells were co-transfected with FLAG-tagged A) H388Q-rcCOX or B) H207Q-rcCOX and Myc-tagged cNuc and probed with anti-Myc, anti-FLAG, and anti-LC3-II antibodies and visualized using confocal microscope. Purple: Nucleus (DAPI); Red: cNuc; Blue: rcCOX; Green: LC3-II; Yellow: cNuc and rcCOX co-localization and White: LC3-II, cNuc, and rcCOX co-localization.

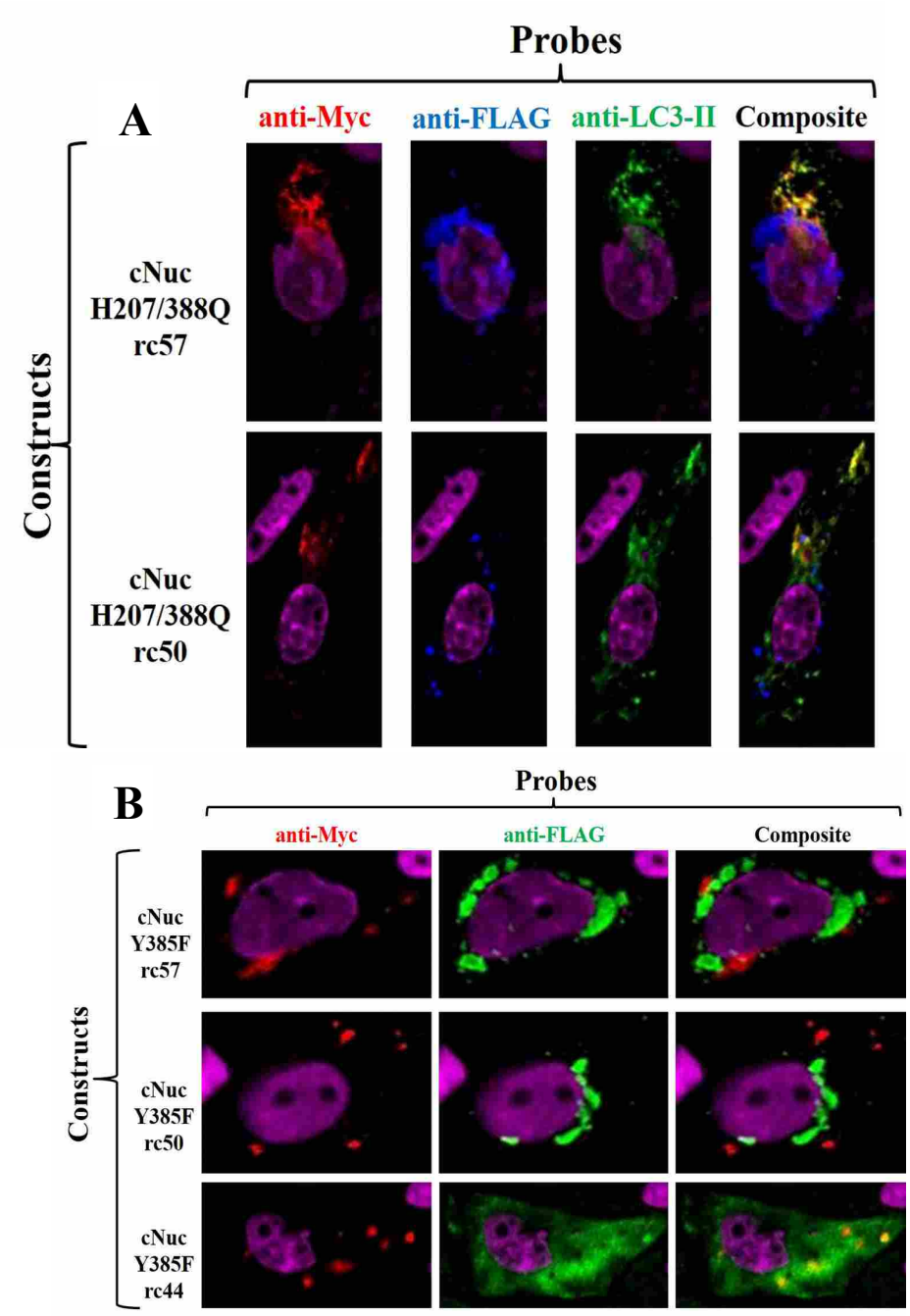

Figure 33: H388/207Q-rcCOX and Y385F-rcCOX constructs cease co-localizing with cNuc. Confocal images of CHO cells transfected with cNuc and either H388/207Q-rcCOX or Y385F-rcCOX and probed with antibodies against Myc tag, FLAG tag, and/or LC3-II A) Images of H388/207Q-rcCOX and cNuc. Purple: Nucleus (DAPI); Red: cNuc; Blue: rcCOX; Green: LC3-II; and Yellow: cNuc and LC3 co-localization. B) Images of cNuc transfected with Y385F-rcCOXs. Purple: Nucleus (DAPI); Red: cNuc and Green: rcCOX.

Site-directed mutagenesis of important catalytic COX residues influence LLPS formation.

We found cNuc induced LLPS formation in 30% of transfected cells while co-transfection with rcCOXs doubles (~60%) the percentage of transfected cells containing LLPSs. LLPSs are not found in non-transfected cells or cells transfected with empty vector. Mutation of His388 as well as the predicted catalytic Tyr385 caused LLPS production to drop precipitously, while the double mutation (His207, His388) gave an intermediate effect, and His207, alone, had no effect. Because Tyr385, and His388 are essential for oxygenase activity, whereas His207 is optional (particularly in CLPs), these results suggest rcCOXs possess catalytic activity to form LLPSs (Figure 34).

Analysis of rcCOX oxygenase activity through cPLA$_2$ inhibition

Cytosolic PLA$_2$ (cPLA$_2$) is an enzyme that cleaves arachidonic acid from membranes to initiate lipid oxygenase mediated pathways such as those producing prostaglandin and certain leukotrienes. Recently, Qi et. al. showed autophagy was induced in murine macrophage cell line RAW264.7 by overexpression of cPLA$_2$.[44] The authors concluded that interferon-γ-induced xenophagy involves activation of cPLA$_2$ and liberation of unsaturated fatty acids. From this report and our results showing that mutagenizing active residues of rcCOX decreases LLPS, we hypothesized that arachidonic acid-derived oxylipins drive LLPS formation. We tested this idea by incubating 100 nM of cPLA$_2$ specific inhibitor, N-{(2S,4R)-4-(Biphenyl-2-ylmethyl-isobutyl-amino)-1-[2-(2,4-difluorobenzoyl)-benzoyl]-pyrrolidin-2-ylmethyl}-3-[4-(2,4-dioxothiazolidin-*5-ylidenemethyl)-phenyl]acrylamide (Calbiochem) with CHO cells transiently transfected with* either rc57/cNuc or cNuc/Empty for 22 hours. We then counted LLPSs via confocal microscopy and compared these numbers with non-treated samples. We found both the rc57/cNuc and cNuc alone transfected samples only had 10-15% of transfected cells containing a LLPS (Figure 35), a

substantial decrease in LLPS formation compared to non-treated cells (p-values = 0.0002 and 0.02 respectively). These results indicate cPLA$_2$-generated arachidonic acid is vital for formation of LLPSs.

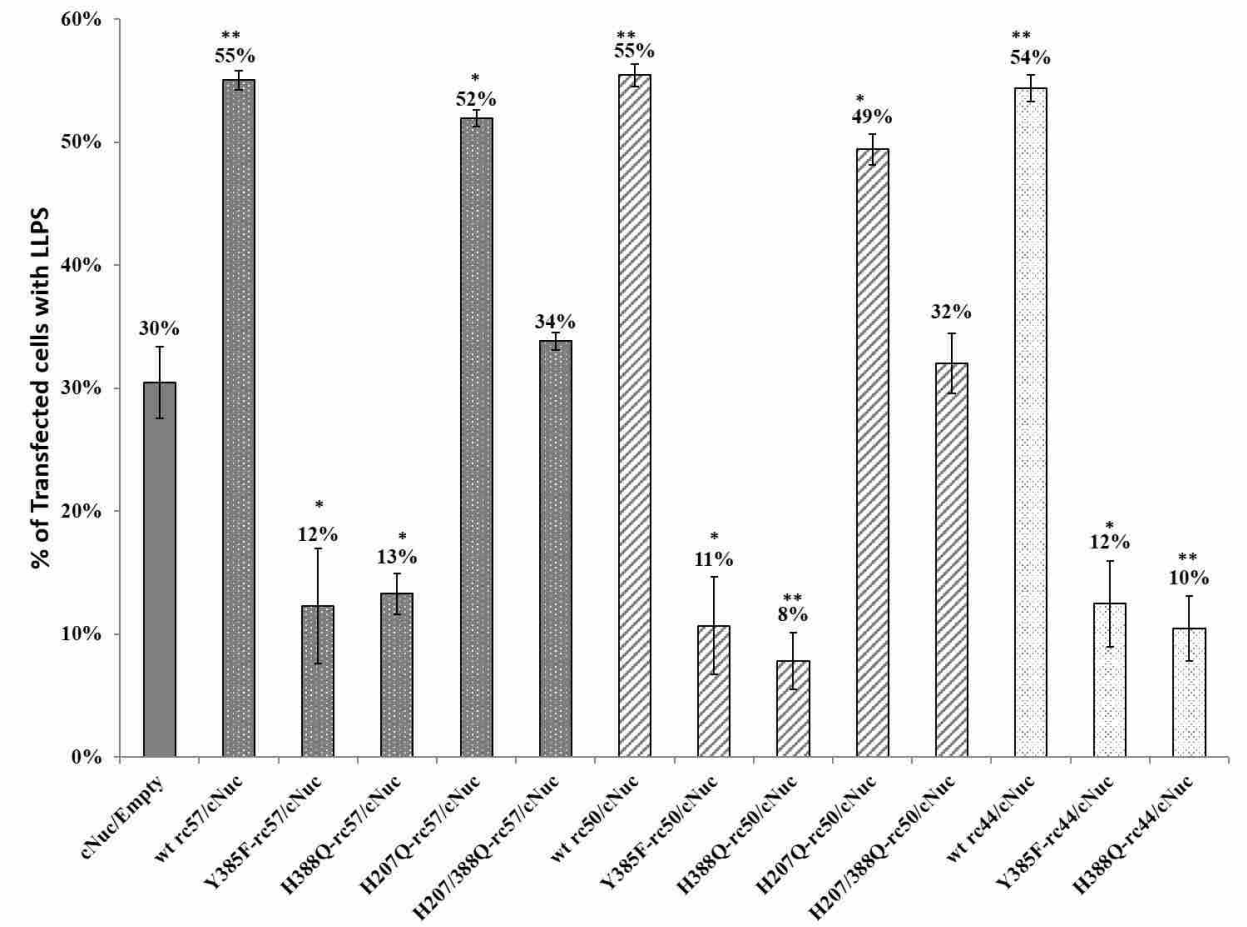

Figure 34: Mutation of catalytic residues of rcCOX affects LLPS formation. CHO cells were transfected with Myc-tagged cNuc and either empty vector or FLAG-tagged rcCOX construct, probed with anti-Myc, anti-FLAG and anti-LC3-II antibodies and LLPSs counted with a confocal microscope. Graph is the average of two to three experiments where over 150 transfected cells were counted each experiment. * p-value<0.05 and ** is p-value<0.01 and is compared to cNuc/Empty samples.

Sample	p-value
wt rc57/cNuc	0.009998
Y385F-rc57/cNuc	0.038835
H388Q-rc57/cNuc	0.012447
H207Q-rc57/cNuc	0.014169
H207/388Q-rc57/cNuc	0.369635
wt rc50/cNuc	0.008424
Y385F-rc50/cNuc	0.018844
H388Q-rc50/cNuc	0.004339
H207Q-rc50/cNuc	0.012263
H207/388Q-rc50/cNuc	0.706801
wt rc44/cNuc	0.007914
Y385F-rc44/cNuc	0.017473
H388Q-rc44/cNuc	0.007207

Table 2: List of p-values comparing LLPS formation between cNuc and cNuc and mutated rcCOX constructs**.** The left column lists the sample name while the right column lists p-values comparing cNuc against cNuc/rcCOX constructs' LLPS formation.

Lipid specific oxygenase inhibitors against LOX and other drugs affect LLPS formation

Cytosolic PLA_2 inhibition of LLPS production in cNuc transfected cells indicated that there is an endogenous enzyme which utilizes a $cPLA_2$ product as a substrate. It has also been reported that a COX product, prostaglandin D_2 (PGD_2), and LOX products, leukotriene E_4 (LTE_4) and leukotriene D_4 (LTD_4), induce autophagy,[44] therefore, we tested whether the endogenous enzyme may either be a LOX or COX enzyme.

We tested this by incubating the inhibitors indomethacin (COX-1 and COX-2), acetaminophen (COX-3), PD146176 (LOX15), and the LOX5 specific inhibitor cinnamyl-3, 4-dihydroxy-α-cyanocinnimate (CDC) and counted the number of transfected cells with a LLPS. The results are shown in Figure 36. We did not see any difference between 5 nM indomethacin-treated cells and non-treated cells with either cNuc or rc57/cNuc transfected cells (data not shown). However, acetaminophen, LOX5, and LOX15 inhibitors each inhibited rc57/cNuc transfected cells in forming LLPS (p-values=0.0008, 0.001, and 1.62E-05 respectively, Figure 36). Acetaminophen and LOX5 inhibitor showed selectivity in their inhibition in that they did not affect the percentage of cNuc transfected cells with a LLPS while LOX15 inhibitor did (p-

values=0.8, 0.94, and 0.02 respectively, Figure 37). These data indicate that a CHO endogenous enzyme provides lipids to cNuc-induced LLPSs in a LOX15 dependent fashion. In contrast, the c57/cNuc system that provides lipids for LLPSs is selectively sensitive to acetaminophen, LOX5 and is also dependent on LOX15.

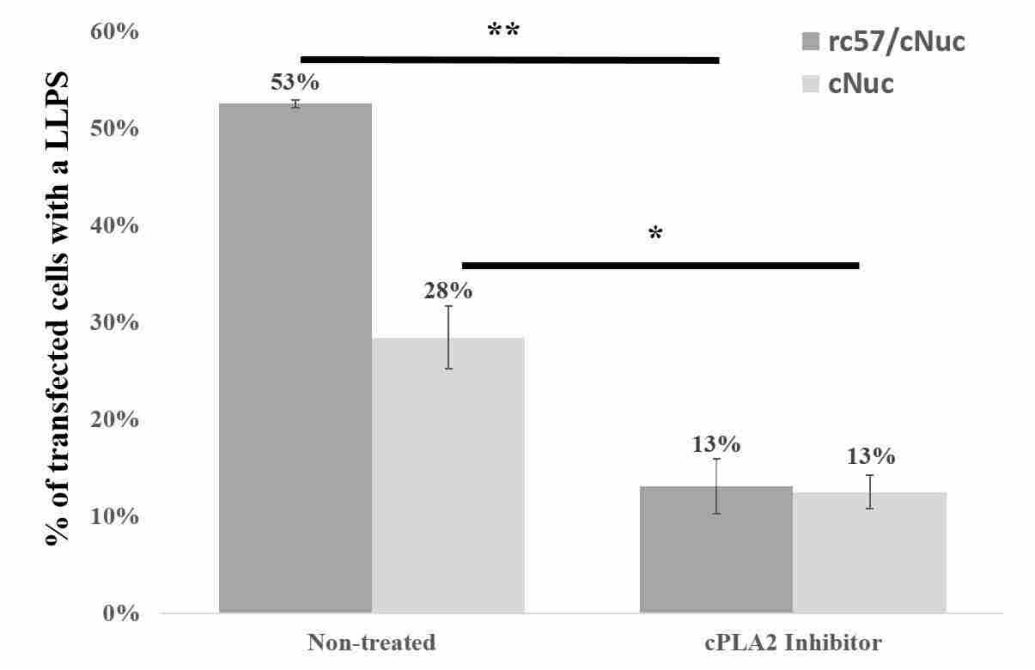

Figure 35: cPLA$_2$ inhibitor blocks LLPS formation. We transfected CHO cells with either rc57/cNuc or cNuc/Empty and incubated these cells for 22 hours with 100 nM cPLA$_2$ specific inhibitor. We then fixed the cells and prepared them for viewing via confocal microscopy. We counted the number of transfected cells that formed a LLPS. These results are averages and SEMs of 3 experiments where we counted between 100-150 cells per experiment. Two-tailed T tests was performed between non-treated samples and cPLA$_2$ treated samples. * p-value<0.05 and ** p-value<0.01.

Discussion

The initiating Mets of rc57, rc50 and rc44 are highly evolutionarily conserved in the COX-1 gene in multiple species, with the highest conservation of the Met codon that initiates translation of rc57. The initiating Met of rc57 is found within the cyclooxygenase active site

where COX-1's substrate, AA, binds and is then oxygenated by Tyr385.[2] The initiating Met of the rc50 and rc44 are solvent accessible residues on the surface of the globular catalytic domain of COX-1 away from the cyclooxygenase active site. We find for the first time through activity assays of COX-1 constructs in which we mutagenize the rc57, rc50, and rc44 initiating Met that the initiating Met of rc57 plays a role in prostaglandin synthesis. The initiating Met of rc50 and rc44 do not, hence, their evolutionary conservation may be due their translation of recoded proteins that functions in cellular processes. Further work is needed to determine the role the initiating Met of the rc57 plays in prostaglandin synthesis.

Heretofore, we have demonstrated that rcCOXs, under the influence of cNuc, help effect the creation of LLPSs. Yet the mechanism by which they exerted this unusual intracellular membrane remodeling was unknown. The biological importance of these structures has only recently emerged with regard to non-canonical autophagy in cells infected with pathogens such as coxsackievirus and *T. Salmonella*.

Our studies are the first finding that oxylipin generating activity promotes LLPS generation. We show through mutagenesis that LLPS formation is dependent on the COX gene oxygenase catalytic residues Tyr385 and His388 while His207 (the distal ligand to heme) plays an insignificant role. Tyr385 is invariably necessary in oxygenating lipids at carbon-carbon double bonds within cyclooxygenase and CLP active sites and is also essential in LLPS creation by rcCOX. The His388 is predicted to coordinate with the iron atom of heme, which is important for both priming Tyr385 and reducing oxygenated lipids to form the final product. However, even in COX-1 itself, His207 is less important to heme coordination than His388,[43] the proximal ligand histidine, and in rcCOXs it appears to be unimportant. Together these data

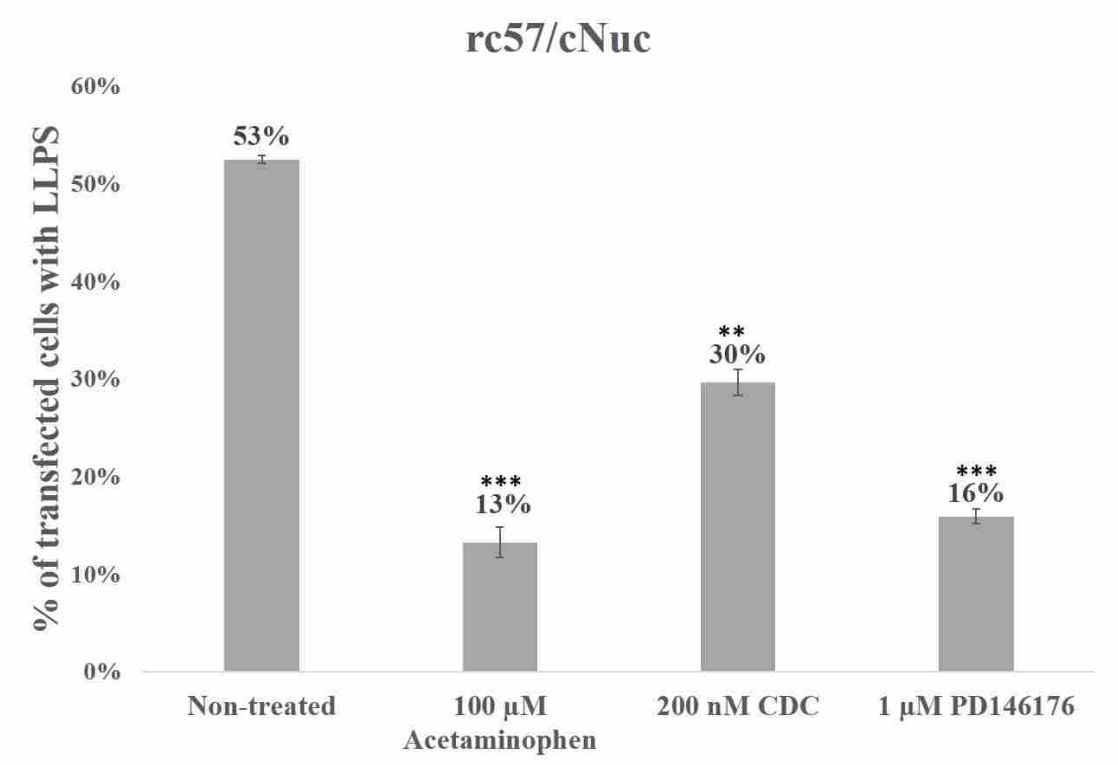

Figure 36: Recoded 57/cNuc-induced LLPSs are sensitive to acetaminophen, LOX5, and LOX15 inhibitors. We transfected CHO cells with Myc-tagged cNuc and FLAG-tagged rc57 transcripts and incubated various drugs with the cells for 22 hours. We then fixed the cells and prepared them for visualization using a confocal microscope by probing them with anti-Myc, anti-FLAG, and anti-LC3-II. The graph represents averages and SEM of 3 experiments where we counted between 80-140 cells per experiment. Two-tailed T tests were performed comparing non-treated samples against treated samples. * p-value<0.05; ** p-value<0.01; *** p-value<0.001.

indicate that the peroxidase sites of rcCOXs are different from COX-1 where His207 plays a greater role.

That a heme-mediated, tyrosyl radical-dependent catalytic activity of rcCOXs is important for LLPS formation in rcCOX/cNuc co-transfected cells is further buttressed by inhibition of LLPS formation by inhibitors of lipid oxygenation. The results from these inhibitors, in addition to supporting the redox-mediated catalytic activity of rcCOXs and the

mutagenesis studies, suggest, that rcCOXs are part of a protein complex. Thus, inhibiting rcCOXs, either by selective mutations or drug inhibition creates a dominant negative effect. Figure 38 provides a model that is consistent with our data.

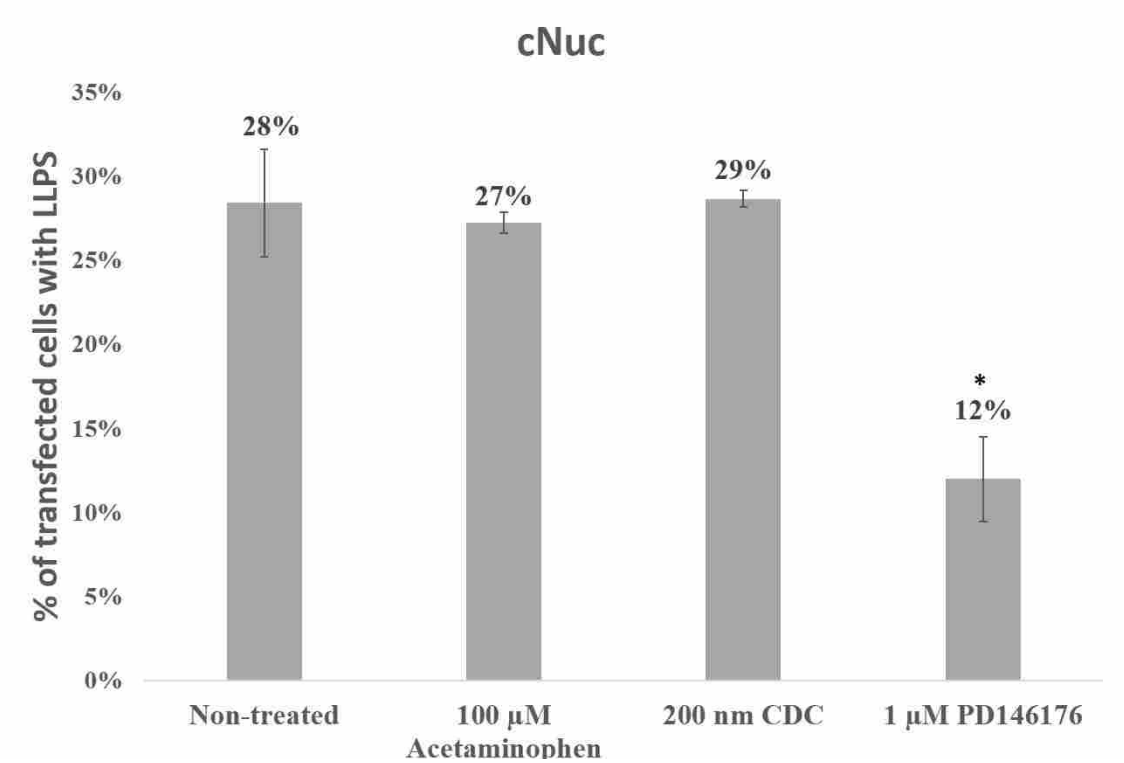

Figure 37: Only the LOX15 inhibitor PD146176 inhibited cNuc-induced LLPSs. We transfected CHO cells with Myc-tagged cNuc transcript and Empty vector and incubated various drugs with the cells for 22 hours. We then fixed the cells and prepared them for visualization using a confocal microscope by probing them with anti-Myc and anti-LC3-II. The graph represents averages and SEM of two to three experiments where we counted between 80-140 cells per experiment. * p-value<0.05.

For example, we find that two selective redox inhibitors, acetaminophen and CDC, target rcCOX/cNuc-induced LLPS formation but not cNuc-induced LLPS formation. As selective anti-oxidants, acetaminophen and CDC likely inhibit rcCOX targets by reducing heme iron, blocking the oxygenase ability to prime the Tyr important for oxygenizing substrate. This inhibition is by

selective redox targeting, not general ROSs scavenging, because the concentrations of acetaminophen and CDC (micromolar and nanomolar)[53] used are far below the concentrations by which they act as general antioxidants (millimolar and high micromolar concentrations).[52]

Both these inhibitors reduce rc57-created LLPS formation levels, but in the case of acetaminophen, LLPS levels were reduced to below that observed in cNuc-transfected cells where only the putative endogenous enzyme(s) are operative. Acetaminophen, therefore, has an effect similar to Tyr385 or His388 mutants in which they exert a dominant negative effect. Together these data are consistent with the notion that overexpression of rc57 causes it to supplant an endogenous enzyme from interacting in an LLPS effector complex, and that inhibition of rcCOXs – either by mutation or by drug inhibition – thus causes the observed dominant negative effect. ATG9a, from our experiments reported in Chapters 2 and 3 is a candidate as a member of this LLPS effector complex.

The mechanisms by which inhibitors of LLPS formation act upon their targets are important in interpreting our data. Inhibitors of COX and LOX that act either as competitor or redox inhibitors of these enzymes' active sites often do so by mimicking arachidonic acid. When these inhibit rcCOX they reinforce the concept that the substrate for rcCOX is likely derived from free arachidonic acid or is arachidonic acid itself. Even though they are frequently aromatic in structure, they mimic the resonance of a contorted arachidonic acid in the oxygenase sites of these enzymes. Inhibition by the LOX5 redox-acting inhibitor, CDC, could be interpreted as either the peroxidase or oxygenase site of rc57 is sufficiently similar to LOX5 that this arachidonic acid mimic is bound and quenches the heme or Tyr radical. This concept is buttressed by the finding that $cPLA_2$ inhibition blocks LLPS formation.

Inhibition by the LOX15 specific inhibitor PD146176 provided unexpected insights into the nature on the oxylipin-generating system involved in LLPS formation. This compound is a potent, non-competitive, non-redox affecting, highly selective inhibitor of LOX15.[51] Both rc57 and the putative endogenous enzyme were inhibited by this selective inhibitor. While it is theoretically possible that both rc57 and the endogenous enzyme are directly inhibited by the compound, it is unlikely. Although LOX15 is expressed at modest levels in CHO cells[50] and therefore could be our postulated endogenous enzyme in the LLPS effector complex, such a hypothesis would require rc57 to have the structural features of LOX15 that allow selective, non-competitive binding of the drug resulting in inhibition. More attractive is that both rc57 and the endogenous enzyme(s) both rely upon LOX15 for some part of their function. For example, they may both rely on a LOX15 product, such as 15HPETE to prime their catalytic activities (Figure 38).

Finally, inhibition of $cPLA_2$, which provides COX arachidonic acid substrate, shows rcCOX's catalytic activity and specifically metabolism of arachidonic acid is important for LLPS formation and that free fatty acids are likely involved in LLPS formation. We also found that inhibition of $cPLA_2$ blocked LLPS formation in cNuc transfected cells suggesting that the putative endogenous enzyme(s) likely utilizes $cPLA_2$ product, since $cPLA_2$ is selective for the SN2 position of phospholipids and acts selectively to liberate this fatty acid.[54] Free arachidonic acid is, therefore, a critical player in LLPS formation.

Our studies are consistent with the fact that LOX products such as leukotriene also induce autophagy.[45] Because LOX15 is important for LLPS formation in both cNuc and rc57/cNuc transfected cells, we propose it will have specific importance in autophagy and particularly non-canonical autophagy such as observed in these studies where significant membrane remodeling

occurs. LOX15's connection to membrane remodeling has been established in a host of cellular pathways including autophagy.[46,47]

Despite the above observations showing oxygenase activity of rcCOXs to be critical to LLPS formation, it is paradoxical that mutation of Tyr385 or His388 of rcCOXs, both necessary

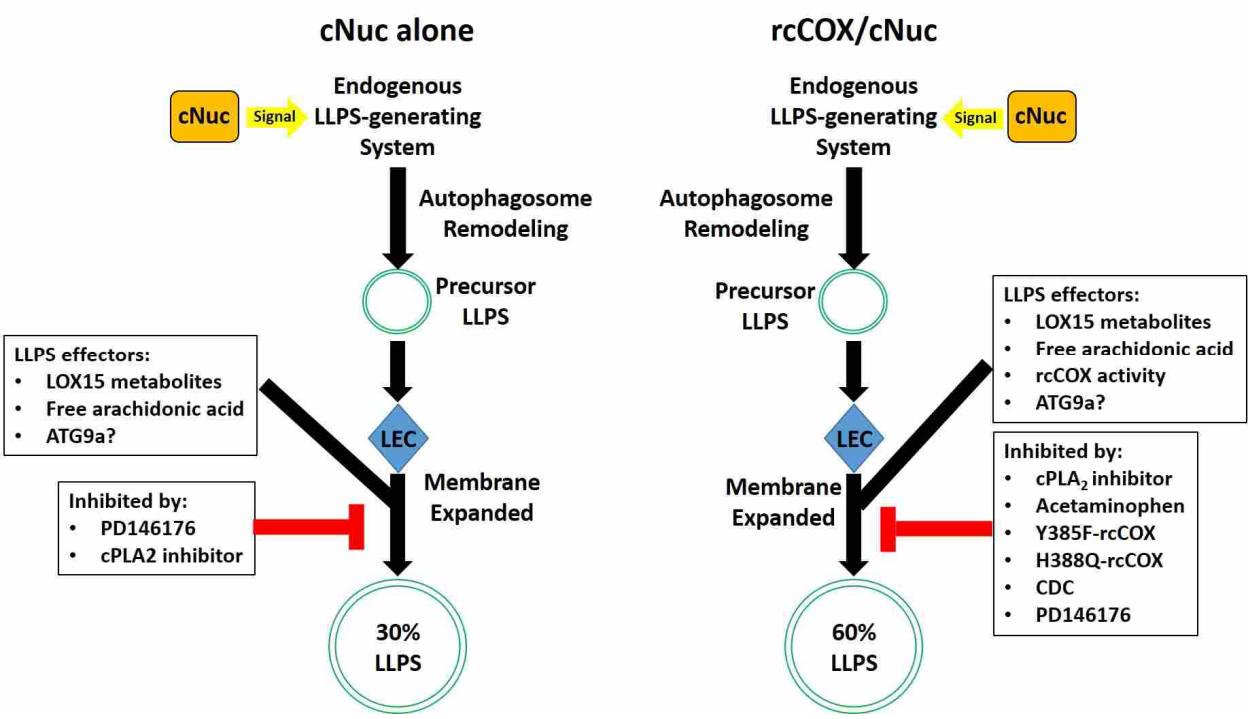

Figure 38: Model of LLPS formation in CHO cells. From our experiments, we propose LLPS formation is through a 2 step system similarly seen in autophagosome development. First, cNuc signaling activates an endogenous LLPS-generating system whereby autophagosomal membrane is remodeled to form a precursor LLPS. The LLPS effectors act at a LLPS effector complex (LEC) site whereupon the precursor LLPS is expanded to form a normal LLPS.

for lipid oxygenase activity, caused incomplete inhibition of LLPS formation in rcCOX/cNuc transfected cells. Residual LLPSs could occur because rcCOX incompletely competed with the putative endogenous enzyme for binding to the LLPS effector complex, thus leaving some endogenous activity associated with it. However, careful examination of the morphology of the LLPSs created in the presence of these mutations showed that they were all small and

dysmorphic. That is, the size of LLPSs in almost all cells transfected with either cNuc or cNuc with rcCOX were large (5-10 μm) and their morphology was distinctly circular. In contrast, the residual LLPSs in the Tyr385 or His388 mutant transfections were significantly smaller and were ringlets, partial ringlets or small patches of LC3-positive membrane that were larger than typical autophagosomes.

We questioned whether these structures were due to an incomplete dominant negative effect by rcCOX mutants, versus another model in which two separate cNuc-activated, LLPS – generating pathways exist – one that is similar to rc57 in nature, and in which mutants of rcCOX act in a dominant negative way, and another enzyme system responsible for the small structures. To address this, we analyzed the effects of other mutations and treatments on LLPS size.

Acetaminophen, LOX5, $cPLA_2$, and LOX15 inhibitors completely blocked (>99%) the formation of LLPSs in rcCOX/Nuc transfectants, leaving only smaller, dysmorphic LLPSs. However, this phenomenon was also seen in cells transfected with cNuc alone treated with $cPLA_2$ or LOX15 inhibitors (Figure 36-37). If blockade by these inhibitors of their respective enzymes is complete, which at the concentrations used should be the case, residual dysmorphic LLPSs in cNuc transfected cells do not require $cPLA_2$ or LOX15, unlike rcCOX. This leads us to favor that these dysmorphic LLPSs form through a separate enzyme system that does not compete with rcCOX overexpression. This separate system, from our data, is cPLA2 and LOX15 independent.

We have speculated that this system may initiate the formation of small, incomplete LLPSs that are precursors to fully formed LLPSs. The large structures would be promoted by rcCOX or similar endogenous enzyme activity – both dependent on $cPLA_2$ and LOX15 activity –

- to elongate or expand the small structures. Such a two-step process, initiation and elongation, occurs in autophagosome formation as described in Chapter 1, above.

Thus, in the two-enzyme model, our Tyr385 or His388 mutants, in addition to acetaminophen, LOX15, LOX5 and $cPLA_2$ inhibition, block the "expansion" phase of LLPS formation, indicating that rcCOX is a potent competitor of the putative endogenous LOX15, $cPLA_2$-dependent, LLPS "expansion" enzyme seen in cells transfected with cNuc alone.

However, if this is true, a contradictory observation is why cells transfected with the Tyr385 or His388 mutants of rcCOX and cNuc do not exhibit 60% of cells possessing dysmorphic LLPSs, when rcCOX/cNuc-transfected cells exhibit that percentage of normal LLPSs. We conclude that this discrepancy may be due to our inability to distinguish all incipient LLPSs. For example, those that were not distinctly larger than autophagosomes, would not have been detected in our assay.

Analysis of LLPS size also explained the enigmatic finding that mutation of His388 strongly suppressed LLPS formation while mutation of His388 along with His207 caused an increase (rather than a further decrease) in LLPS formation. Subsequent examination of LLPS size showed that the double mutant did not produce dysmorphic LLPSs as observed with the Tyr385 or His388 mutants but instead formed normal LLPS structures at a frequency similar to cNuc-transfected cells. In other words, the double mutant does not exert a dominant negative effect. We hypothesize that its inability to do so results from a structural change evoked by the double mutation that disallowed the resulting protein to competitively bind the LLPS effector complex.

The above studies show that rcCOXs have function. They interact with ATG9a in non-canonical autophagy. With recoded cNuc they drive the formation of novel membrane

structures, LLPS, which depend on oxygenase catalytic residues of rcCOXs for their formation. These studies establish COX-3 as a paradigm for a multiply recoded mRNA.

References

1. Petterson, E. F.; T.D., G.; C.C., H.; G.S., C.; D.M., G.; E.C., M.; T.E., F., UCSF Chimera--a visualization system for exploratory research and analysis. *J. Comput. Chem.* **2004,** *25* (13), 1605-1612.

2. Simmons, D. L.; Botting, R. M.; Hla, T., Cyclooxygenase isozymes: the biology of prostaglandin synthesis and inhibition. *Pharmacol Rev* **2004,** *56* (3), 387-437.

3. Zamocky, M.; Jakopitsch, C.; Furtmüller, P. G.; Dunand, C.; Obinger, C., The peroxidase-cyclooxygenase superfamily: Reconstructed evolution of critical enzymes of the innate immune system. *Proteins* **2008,** *72* (2), 589-605.

4. le Roes-Hill, M.; Khan, N.; Burton, S. G., Actinobacterial peroxidases: an unexplored resource for biocatalysis. *Appl Biochem Biotechnol* **2011,** *164* (5), 681-713.

5. Park, S.; Ely, R. L., Whole-genome transcriptional and physiological responses of Nitrosomonas europaea to cyanide: identification of cyanide stress response genes. *Biotechnol Bioeng* **2009,** *102* (6), 1645-53.

6. Sanz, A.; Moreno, J. I.; Castresana, C., PIOX, a new pathogen-induced oxygenase with homology to animal cyclooxygenase. *Plant Cell* **1998,** *10* (9), 1523-37.

7. Goulah, C. C.; Zhu, G.; Koszelak-Rosenblum, M.; Malkowski, M. G., The crystal structure of α-Dioxygenase provides insight into diversity in the cyclooxygenase-peroxidase superfamily. *Biochemistry* **2013,** *52* (8), 1364-72.

8. Liu, W.; Wang, L. H.; Fabian, P.; Hayashi, Y.; McGinley, C. M.; van der Donk, W. A.; Kulmacz, R. J., Arabidopsis thaliana fatty acid alpha-dioxygenase-1: evaluation of substrates, inhibitors and amino-terminal function. *Plant Physiol Biochem* **2006,** *44* (5-6), 284-93.

9. Hörnsten, L.; Su, C.; Osbourn, A. E.; Garosi, P.; Hellman, U.; Wernstedt, C.; Oliw, E. H., Cloning of linoleate diol synthase reveals homology with prostaglandin H synthases. *J Biol Chem* **1999,** *274* (40), 28219-24.

10. Garscha, U.; Oliw, E. H., Critical amino acids for the 8(R)-dioxygenase activity of linoleate diol synthase. A comparison with cyclooxygenases. *FEBS Lett* **2008,** *582* (23-24), 3547-51.

11. Su, C.; Sahlin, M.; Oliw, E. H., A protein radical and ferryl intermediates are generated by linoleate diol synthase, a ferric hemeprotein with dioxygenase and hydroperoxide isomerase activities. *J Biol Chem* **1998,** *273* (33), 20744-51.

12. Garscha, U.; Jernerén, F.; Chung, D.; Keller, N. P.; Hamberg, M.; Oliw, E. H., Identification of dioxygenases required for Aspergillus development. Studies of products, stereochemistry, and the reaction mechanism. *J Biol Chem* **2007,** *282* (48), 34707-18.

13. Dagenais, T. R.; Chung, D.; Giles, S. S.; Hull, C. M.; Andes, D.; Keller, N. P., Defects in conidiophore development and conidium-macrophage interactions in a dioxygenase mutant of Aspergillus fumigatus. *Infect Immun* **2008,** *76* (7), 3214-20.

14. Xie, W. L.; Chipman, J. G.; Robertson, D. L.; Erikson, R. L.; Simmons, D. L., Expression of a mitogen-responsive gene encoding prostaglandin synthase is regulated by mRNA splicing. *Proc Natl Acad Sci U S A* **1991,** *88* (7), 2692-6.

15. Needleman, P.; Moncada, S.; Bunting, S.; Vane, J. R.; Hamberg, M.; Samuelsson, B., Identification of an enzyme in platelet microsomes which generates thromboxane A2 from prostaglandin endoperoxides. *Nature* **1976,** *261* (5561), 558-60.

16. Engelmann, B.; Massberg, S., Thrombosis as an intravascular effector of innate immunity. *Nat Rev Immunol* **2013,** *13* (1), 34-45.

17. Gately, S., The contributions of cyclooxygenase-2 to tumor angiogenesis. *Cancer Metastasis Rev* **2000,** *19* (1-2), 19-27.

18. Davis, B. J.; Lennard, D. E.; Lee, C. A.; Tiano, H. F.; Morham, S. G.; Wetsel, W. C.; Langenbach, R., Anovulation in cyclooxygenase-2-deficient mice is restored by prostaglandin E2 and interleukin-1beta. *Endocrinology* **1999,** *140* (6), 2685-95.

19. Schwartz, J. I.; Chan, C. C.; Mukhopadhyay, S.; McBride, K. J.; Jones, T. M.; Adcock, S.; Moritz, C.; Hedges, J.; Grasing, K.; Dobratz, D.; Cohen, R. A.; Davidson, M. H.; Bachmann, K. A.; Gertz, B. J., Cyclooxygenase-2 inhibition by rofecoxib reverses naturally occurring fever in humans. *Clin Pharmacol Ther* **1999,** *65* (6), 653-60.

20. Seibert, K.; Zhang, Y.; Leahy, K.; Hauser, S.; Masferrer, J.; Perkins, W.; Lee, L.; Isakson, P., Pharmacological and biochemical demonstration of the role of cyclooxygenase 2 in inflammation and pain. *Proc Natl Acad Sci U S A* **1994,** *91* (25), 12013-7.

21. Myers, L. K.; Kang, A. H.; Postlethwaite, A. E.; Rosloniec, E. F.; Morham, S. G.; Shlopov, B. V.; Goorha, S.; Ballou, L. R., The genetic ablation of cyclooxygenase 2 prevents the development of autoimmune arthritis. *Arthritis Rheum* **2000,** *43* (12), 2687-93.

22. Hida, T.; Yatabe, Y.; Achiwa, H.; Muramatsu, H.; Kozaki, K.; Nakamura, S.; Ogawa, M.; Mitsudomi, T.; Sugiura, T.; Takahashi, T., Increased expression of cyclooxygenase 2 occurs

frequently in human lung cancers, specifically in adenocarcinomas. *Cancer Res* **1998,** *58* (17), 3761-4.

23. Gupta, R. A.; DuBois, R. N.; Wallace, M. C., New avenues for the prevention of colorectal cancer: targeting cyclo-oxygenase-2 activity. *Best Pract Res Clin Gastroenterol* **2002,** *16* (6), 945-56.

24. Zimmerman, D. C.; Vick, B. A., Lipoxygenase in Chlorella pyrenoidosa. *Lipids* **1973,** *8* (5), 264-6.

25. Brash, A. R., Lipoxygenases: occurrence, functions, catalysis, and acquisition of substrate. *J Biol Chem* **1999,** *274* (34), 23679-82.

26. Krieg, P.; Kinzig, A.; Heidt, M.; Marks, F.; Fürstenberger, G., cDNA cloning of a 8-lipoxygenase and a novel epidermis-type lipoxygenase from phorbol ester-treated mouse skin. *Biochim Biophys Acta* **1998,** *1391* (1), 7-12.

27. Boeglin, W. E.; Kim, R. B.; Brash, A. R., A 12R-lipoxygenase in human skin: mechanistic evidence, molecular cloning, and expression. *Proc Natl Acad Sci U S A* **1998,** *95* (12), 6744-9.

28. Ivanov, I.; Heydeck, D.; Hofheinz, K.; Roffeis, J.; O'Donnell, V. B.; Kuhn, H.; Walther, M., Molecular enzymology of lipoxygenases. *Arch Biochem Biophys* **2010,** *503* (2), 161-74.

29. Hada, T.; Ueda, N.; Takahashi, Y.; Yamamoto, S., Catalytic properties of human platelet 12-lipoxygenase as compared with the enzymes of other origins. *Biochim Biophys Acta* **1991,** *1083* (1), 89-93.

30. Hada, T.; Hagiya, H.; Suzuki, H.; Arakawa, T.; Nakamura, M.; Matsuda, S.; Yoshimoto, T.; Yamamoto, S.; Azekawa, T.; Morita, Y., Arachidonate 12-lipoxygenase of rat pineal glands:

catalytic properties and primary structure deduced from its cDNA. *Biochim Biophys Acta* **1994,** *1211* (2), 221-8.

31. Drazen, J. M., Leukotrienes in asthma. *Adv Exp Med Biol* **2003,** *525*, 1-5.

32. Rapoport, S. M.; Schewe, T., The maturational breakdown of mitochondria in reticulocytes. *Biochim Biophys Acta* **1986,** *864* (3-4), 471-95.

33. Feinmark, S. J.; Cornicelli, J. A., Is there a role for 15-lipoxygenase in atherogenesis? *Biochem Pharmacol* **1997,** *54* (9), 953-9.

34. Funk, C. D., The molecular biology of mammalian lipoxygenases and the quest for eicosanoid functions using lipoxygenase-deficient mice. *Biochim Biophys Acta* **1996,** *1304* (1), 65-84.

35. Samuelsson, B., Some recent advances in leukotriene research. *Adv Exp Med Biol* **1997,** *433*, 1-7.

36. Serhan, C. N., Lipoxins and novel aspirin-triggered 15-epi-lipoxins (ATL): a jungle of cell-cell interactions or a therapeutic opportunity? *Prostaglandins* **1997,** *53* (2), 107-37.

37. Tang, D. G.; Honn, K. V., 12-Lipoxygenase, 12(S)-HETE, and cancer metastasis. *Ann N Y Acad Sci* **1994,** *744*, 199-215.

38. Hunter, J. C. Multiple Recoding Mechanisms Produce Cyclooxygenase and Cyclooxygenase-Related Proteins from Frameshift-Containing COX-3/COX-1b Transcripts in Rat and Human. Brigham Young University, Brigham Young University, 2012.

39. Zhang, Y., I-TASSER server for protein 3D structure prediction. *BMC Bioinformatics* **2008,** *9*, 40.

40. Roy, A.; Kucukural, A.; Zhang, Y., I-TASSER: a unified platform for automated protein structure and function prediction. *Nat Protoc* **2010,** *5* (4), 725-38.

41. Roy, A.; Yang, J.; Zhang, Y., COFACTOR: an accurate comparative algorithm for structure-based protein function annotation. *Nucleic Acids Res* **2012,** *40* (Web Server issue), W471-7.

42. Shimokawa, T.; Kulmacz, R. J.; DeWitt, D. L.; Smith, W. L., Tyrosine 385 of prostaglandin endoperoxide synthase is required for cyclooxygenase catalysis. *J Biol Chem* **1990,** *265* (33), 20073-6.

43. Shimokawa, T.; Smith, W. L., Essential histidines of prostaglandin endoperoxide synthase. His-309 is involved in heme binding. *J Biol Chem* **1991,** *266* (10), 6168-73.

44. Qi, H. Y.; Daniels, M. P.; Liu, Y.; Chen, L. Y.; Alsaaty, S.; Levine, S. J.; Shelhamer, J. H., A cytosolic phospholipase A2-initiated lipid mediator pathway induces autophagy in macrophages. *J Immunol* **2011,** *187* (10), 5286-92.

45. Morgan, A. H.; Hammond, V. J.; Sakoh-Nakatogawa, M.; Ohsumi, Y.; Thomas, C. P.; Blanchet, F.; Piguet, V.; Kiselyov, K.; O'Donnell, V. B., A novel role for 12/15-lipoxygenase in regulating autophagy. *Redox Biol* **2015,** *4*, 40-7.

46. van Leyen, K.; Duvoisin, R. M.; Engelhardt, H.; Wiedmann, M., A function for lipoxygenase in programmed organelle degradation. *Nature* **1998,** *395* (6700), 392-5.

47. Grüllich, C.; Duvoisin, R. M.; Wiedmann, M.; van Leyen, K., Inhibition of 15-lipoxygenase leads to delayed organelle degradation in the reticulocyte. *FEBS Lett* **2001,** *489* (1), 51-4.

48. Yan, Z. and Hansson, G. K., Innate immunity, macrophage activation, and atherosclerosis. *Immuno. Rev.* **2007,** *219* (1), 187-203.

49. Kinder, M.; Wei, C.; Shelat, S. G.; Kundu, M.; Zhao, L.; Blair, I. A.; and Puré, E., Hematopoietic stem cell function requires 12/15-lipoxygenase-dependent fatty acid metabolism. *Blood.* **2010,** *155* (24), 5012-22.

50. Succol, F. and Praticò, D., A role for 12/15 lipoxygenase in the amyloid β precursor protein metabolism. *J. Neurochem.* **2007,** *103*, 308-87.

51. Sendobry, S. M.; Cornicelli, J. A.; Welch, K.; Bocan, T.; Tait, B.; Trivedi, B. K.; Colbry, N.; Dyer, R. D.; Feinmark, S. J.; and Daugherty, A., Attenuation of diet-induced atherosclerosis in rabbits with highly selective 15-lipoxygenase inhibitor lacking significant antioxidant properties. *Br. J. Pharmacol.* **1997,** *120* (7), 1199-206.

52. Borges, R. S. et. al., A structure and antioxidant activity study of paracetamol and salicylic acid. *Pharmacol. Pharm.* **2014,** *5,* 1185-91.

53. Lee, S.; Park, Y.; Kim, J.; Han, S., A fluorescence-based assay for measuring the redox potential of 5-lipoxygenase inhibitors. *PLOS One,* **2004,** *9* (2), e87708.

54. Burke, J. E. and Dennis, E. A. Phospholipase A2 structure/function, mechanism, and signaling. *J. Llipid Res.* **2009,** *50,* S237-42.

Appendix A: Table of Primers

Gene	Rat COX1			
Primer	**Directio**	**Sequence (5' to 3')**	**Tm**	**Description**
30	For	CATCCGAGAAGTACTCGCGCGCCTGGTACTCACGG	5	57 ATG to GCG
30	Rev	CCGTGAGTACCAGGCGCGCGAGTACTTCTCGGATG	5	57 ATG to GCG
30	For	AAAGACTGTCCCACACCCGCGGGAACCAAAGGGAAG	5	50 ATG to GCG
30	Rev	CTTCTTCCCTTTGGTTCCCGCGGGTGTGGGACAGTCTTT	5	50 ATG to GCG
306	For	TTCTTCAAGACCTCTGGAAAGGCGGGTCCTGGCTTTA CCAAGGC C	5	44 ATG to GCG
306	Rev	GGCCTTGGTAAAGCCAGGACCCGCCTTTCCAGAGGTC TTGAAG	5	44 ATG to GCG
DLS1	For	ATGCCAGAACCAGGGTGT	5	Sequencing
DLS1	Rev	ACACCCTGGTTCTGGCAT	5	Sequencing
DLS1	For	AGTACCACCTGCGGCT	5	Sequencing
DLS1	For	GAGTTGGAGGAGCTATATGGTG	5	Sequencing
DLS1	For	CGTGTACGGTGGGAGGTCTA	5	Seq pcDNA 3.1
48	For	CACCTCTATCACTGGCAACCGCTCATGCCTGATTCCTT	6	Mutates His 388 to Gln
48	Rev	AGTGATAGAGGTGGTTGAATTCCAAGGCGAT	6	Mutates His 388 to Gln
DLS	For	ATTCAACCACCTCTTTCACT	5	Mutate Tyr to Phe
DLS	Rev	AGGTGGTTGAATTCCAAGGC	5	Mutate Tyr to Phe
2014	For	GCACAACACTTCACCCAACAGTTCTTCAAGACCTCTG	5	Mutate Dist His COX-1
2014	Rev	GGTGAAGTGTTGTGCAAAGA	5	Mutate Dist His COX-1
2014	For	CATCATCATCATGAAGATCAGGTGGATCCTCGTCTTAT TGATG GGAAATAGGGGCTCTTCTGGAGGGA	5	Place HPC4 tag
2014	Rev	ATGATGATGATGATGATGCC	5	Place HPC4 tag
Gene	**ATG9a**			
Primer	**Directio**	**Sequence (5' to 3')**	**Tm**	**Description**
2014	For	TGAGCTACCCCCTCAGGT	5	Sequencing
2014	Rev	AGGCCTCTAGGCGCTG	5	Sequencing
2014	For	AGGGGAGGAGGACCTGTT	5	Sequencing
2014	Rev	AAGGTAGTGAAGGCAACCACA	5	Sequencing
2014	For	CTACTGGGAGATCCACTCCT	5	Sequencing
2014	For	ATCCTCGCTCACATCCACTA	5	Sequencing
2014	For	AAGGACAGCTGCAGAGCC	5	Sequencing
2014	For	CATCTTCTGCCTGCGCCCATAGAGAGGAATTTGGGGC	5	Truncate C-terminus
2014	Rev	CGCAGGCAGAAGATGAGGAT	5	Truncate C-terminus
Gene	**Mouse NUCB1**			
Primer	**Directio**	**Sequence (5' to 3')**	**Tm**	**Description**
2014	For	GGGGGGGGGGGGGGGGATATCGGGATGGCCTCCTCCG	5	PCR RFP from RFP-
2014	Rev	GGGGGGGGGGGGGGGGATATCCTAGCCGAATTCGCCG	5	PCR RFP from RFP-
2014	Rev	TTCTAAATGCTGGGAATCCA	5	Remove Myc add RFP
2014	For	TCCCAGCATTTAGAAGGCGCCTCCTCCGAGGACG	5	Remove Myc add RFP
	For	GGGGGGGCTAGCCTTTGCAGGGCTGGCAA	5	Clone from pGEX
	Rev	GGGGGGCCTAGGGCTGCATGTGTCAGAGGTTTT	5	Clone from pGEX
	Rev	CCCCCCCCCTAGGCTAGGTTAGAATTCCAGGTCTTCC TCACTGA	5	Clone from pGEX add

45	For	GTG GAATTGCCCTTGTGCCCGTGGACCG	5	Removes SP Nuc
	For	GTGGAATTGCCCTTATGGTGCCCGTGGACCG	5	Removes SP adds ATG
45	Rev	AAGGGCAATTCCACCACACT	5	Removes Signal Peptide
47	For	TACCACCTCTACTG**AAA**CTGTCTGCTGTGCTGGCAGTG	6	M19L
47	Rev	CAGTAGAGGTGGTAGGAGAAGAAAAGGG	6	M19L
	For	AAGGGCAATTCCACCACACT	5	M1 removed
	Rev	CCTACCTCGGTGCCCCGCGGGGCCCCTTT	5	M1 removed
38	For	ATGCCTACCTCGGTGCC	5	Sequence
38	Rev	CCAGCACAGCAGACAGCA	5	Sequence
38	For	AAAGTCAATGTTCCTGGCAG	5	Sequence
39	For	AGCAGGTGACCAGAAAGAT	5	Sequence

Appendix B: Antibodies used for this research

Antibodies Used for Confocal Imaging

Monoclonal Anti-LC3B antibody produced in mouse	SAB4200361-200UL Sigma-
UH1 LAMP-1 CHO 1.0mL SUPERNATANT mouse	UH-1
Anti-Cathepsin D antibody [EPR3057Y] (ab75852) Rabbit monoclonal	ab75852 ABCAM
Anti-Myc tag antibody (ab172) Chicken polyclonal	ab172 ABCAM
Anti-Mannosidase II antibody [53FC3] - Golgi Marker (ab24565) mouse	ab24565 ABCAM
Anti-TGN46 [2F7.1] antibody (ab2809) mouse monoclonal	ab2809 ABCAM
Anti- ACBD3 Antibody (2G2) mouse monoclonal	MCA3923Z, AbD Serotec
OctA-Probe Antibody (D-8): sc-807 rabbit polyclonal	sc-807, Santa Cruz
Monoclonal mouse ANTI-FLAG® M2 antibody produced in mouse clone M2, purified immunoglobulin, buffered aqueous solution	F3165, Sigma-Aldrich
GAPDH Antibody (6C5) sc-32233 Mouse monoclonal	sc-32233, Santa Cruz

Secondary Antibodies purchased from Molecular Probes

Alexa Fluor® 633 Goat Anti-Chicken IgG (H+L)	A-21103
Alexa Fluor® 546 Goat Anti-Rabbit IgG (H+L), highly cross-adsorbed	A-
Alexa Fluor® 488 Goat Anti-Mouse IgG (H+L) Antibody, highly cross-adsorbed	A-11029
DAPI	D1306

Antibodies used for Western Blotting

Anti-FLAG	sc-807 Santa Cruz
Anti-Myc	ab9106 ABCAM
Anti-Hemagglutinin	sc-7392 Santa Cruz
Anti-GST	ab6613 ABCAM
Anti-p62	610832 BD Transduction
Anti-Actin	ab3280 ABCAM

Secondary Antibodies purchased from Li-COR Biosciences

IRDye® 800CW Goat anti-rabbit IgG	926-32211
IRDye® 680CW Goat anti-mouse IgG	926-68070

Appendix C

Title:

Frameshift Containing COX-3/COX-1b Transcripts are Extensively Recoded to Produce ER-Associated Cyclooxygenases and Cyclooxygenase-Related Proteins Targeted to the Cytosolic Surface of the Golgi-Apparatus and Autophagosome.

Authors and Affiliations:

John C. Hunter[a,b], Jonathan J. Lee[a], Steven D. Scoville[a,c], Gideon N. Logan[a], Daniel R. Roberts[a], NV. Chandrasekharan[a,d], Matthew Lelegren[a], Bryan A. Ballif[e], Daniel L. Simmons[a]

[a]Department of Chemistry and Biochemistry, Brigham Young University, Provo, Utah 84601, [e]Department of Biology, The University of Vermont, Burlington, Vermont 05401

Contact:

Dan_Simmons@byu.edu

Additional Footnotes:

[b]Present address: Departments of Biochemistry and Radiation Oncology, The University of Texas Southwestern Medical Center at Dallas, Dallas, Texas 75390, [c]Present address: The Ohio State University College of Medicine, Columbus, Ohio, 43210, [d]Present address: Department of Chemistry, University of Colombo, Sri Lanka,

Running Head:

Abstract:

Significant progress has been made in expanding our understanding of eukaryotic translation mechanisms over recent decades. Advances in next-generation sequencing and ribosomal profiling methods have brought into focus the fact that the proteome is likely orders of magnitude larger than previously thought. Much of this expansion could occur through recoding processes, which result in translation of multiple variations of a protein from a single messenger RNA. Here we show that COX-3/COX-1b, an intron-1 retaining alternative splice variant of COX-1, is extensively recoded through multiple recoding mechanisms including alternative translation initiation and ribosomal frame-shifting. Expression of COX-3 cDNA in multiple cell lines results in translation of at least seven different COX-3 proteins, two of which are active prostaglandin synthases and are inhibited by non-steroidal anti-inflammatory drugs (NSAIDs). The other, non-prostaglandin generating recoded COX-3 proteins localize to the cytosolic surfaces of distinct domains of the golgi apparatus as well as adjacent autophagosomes, suggesting roles in golgi-mediated vesicle formation, trafficking and autophagy. Proteins of the same size and non-glycosylated character are detected by Western blot in rats in a tissue specific fashion. Potential roles for these COX-3 proteins in physiological and pathophysiological processes are broadly discussed. To our knowledge this represents the first example of a multiply recoded eukaryotic mRNA where each recoding event has been thoroughly studied and confirmed biochemically. The COX-3/COX-1b mRNA may serve as a paradigm for multiple recoding of other eukaryotic mRNAs, including those with interrupted reading frames that currently appear to be nonfunctional.

Introduction

Cyclooxygenase (COX) is a signaling enzyme that catalyzes the first step of prostaglandins synthesis and is involved in a wide range of processes including inflammation, nociception, thermoregulation, parturition, thrombosis, and cancer [1-6]. In 2002, our laboratory discovered a COX-1 alternative splice variant, COX-3 or COX-1b, in canine brain tissue [7]. This variant retains intron-1 (90bp long) in its fully processed transcript, inserting 30 amino acids into the N-terminal signal peptide region of the protein. Expression of this canine variant in Sf9 cells produced an active prostaglandin synthase enzyme that retains a signal peptide and has modified enzymatic activity compared to COX-1.

Northern blot analysis of multiple human tissues found significant levels of COX-3 mRNA in humans with highest expression in cerebral cortex, heart, and skeletal muscle [7]. However, intron-1 is 94 and 98 base pairs long in human and rodents respectively, and introduces a translational reading frame-shift beginning at exon-2. Uncorrected, the scanning model of translation predicts the synthesis of a small (~8kD) COX-3 polypeptide with little similarity to COX-1.

Some studies by others supported this hypothesis and proposed that COX-3 mRNA in these species does not encode cyclooxygenase-like proteins. However, because they did not clone and express the entire COX-3 mRNA these reports did not adequately investigate whether high molecular weight proteins are expressed from the COX-3 transcript. In some cases authors used clones that only contained a truncated portion of the putative coding region preventing a thorough analysis of the translational products [8,9]. Other studies have indicated that at least one high molecular weight

protein is synthesized from the human COX-3 mRNA through RNA editing, which corrects the frame-shift [10]. We, however, have been unable to detect edited COX-3 transcripts to verify these findings.

As knowledge of the mechanisms behind eukaryotic translation initiation has expanded over the past decade, a number of exceptions to the standard scanning model of translation have been documented [11-17]. While many of the first documented examples of recoding were originally discovered in the context of viral RNA translation, a growing number of reports suggest that recoding processes such as ribosomal frameshifting and alternative translation initiation site selection including the use of upstream and downstream initiation sites, are widely used in the translation of cellular messages as well[18-20]. We, therefore, hypothesized that similar recoding mechanisms could function to rectify the frame-shift in COX-3 and produce full-length cyclooxygenase-like proteins *in vivo* [7].

Here we demonstrate that at least three different recoding mechanisms are used to produce a minimum of 7 higher molecular weight proteins from the COX-3 mRNA. Two of these proteins, each around 72kD in size, are similar to COX-1 and are active cyclooxygenase enzymes. Confocal microscopy of the other COX-3 forms demonstrate that these proteins specifically localize to both the cytosol and the cystolic face of golgi-associated vesicles, suggesting potential new roles of COX-gene products in intracellular vesicle trafficking. At a high level, we suggest that the COX-3 mRNA may constitute a validated and reliable model system for future research towards elucidating the molecular mechanisms driving eukaryotic recoding processes.

Results

Detection of high molecular weight COX-3 proteins

In order to ascertain whether the COX-3 message is translated to form a COX-like protein, we cloned full-length rat COX-3 cDNA, including 5' and 3' untranslated regions into a mammalian expression plasmid. To prevent the intron from being spliced out upon ectopic expression we mutated the intron-1 splice acceptor site from AGGA to AAGA. RT-PCR analysis confirmed that intron-1 was retained unprocessed in the expressed mRNA transcript (Fig. S2). To facilitate detection of any high molecular weight COX-3 proteins encoded by the COX-3 cDNA we inserted green-fluorescent protein (GFP) into the C-terminal region of the protein in the COX-1 reading frame (Fig. S1-S2). Upon expression of GFP-COX-3 in CHO cells and subsequent analysis by fluorescence microscopy, we detected a high percentage of GFP positive cells, confirming that one or more mechanisms result in translation of COX-3 from its long open reading frame (Fig. 1A).

Immunoblot analysis of CHO cells transfected with a C-terminal Flag-tagged rat COX-3 construct (without GFP) detected a series of five COX-3 proteins of approximately 72, 68, 57, 50 and 44kD in size (Fig. 1B). Analysis of the relative band intensities of each of the rat COX-3 forms from anti-Flag Western blots demonstrated that the COX-3 forms are expressed at roughly one tenth the level of COX-1 in transiently transfected cells. Specifically, the 72, 68, 57, 50, and 44kD forms were expressed at 7, 12, 7, 10, and 6% of the level of COX-1 protein respectively.

Both COX-1 and COX-2 are glycosylated with N-linked, high-mannose oligosaccharides [6]. To determine whether any COX-3 protein(s) were glycosylated, we

treated the COX-3 proteins with endoglycosidase F (N-glycanase) and observed an increase in the electrophoretic mobility of the 72kD COX-3 protein, confirming that it is glycosylated in a manner similar to COX-1 (Fig. 1C). However, N-glycanase treatment had no effect on the 68, 57, 50 and 44kD COX-3 proteins, indicating that they are not glycosylated, are not processed through the ER-Golgi and, therefore, are not degradation products of the larger 72kD COX-3 form, but distinct translation products.

We next generated stable transfectants of the Flag-tagged COX-3 construct in order to determine whether high-level expression of COX-3 mRNA in transient transfection was artifactually causing expression of these five COX-3 proteins, driven by potentially high plasmid copy numbers in individual cells. While all of the colonies stably expressing COX-1 produced only a 72kD protein and Tunicamycin-sensitive degradation products, two clonally isolated stable COX-3 colonies showed differential expression of the COX-3 proteins. Both COX-3 colonies expressed the non-glycosylated 57, 50, and 44kD proteins, while only one colony showed expression of full-length, glycosylated 72kD COX-3 protein indicating that not all cells contain the ability to translate this COX-3 protein (Fig. 1E). We also note that none of these colonies expressed the 68kD protein, again indicating that cell-specific factors, signals, or mechanisms are required for expression of some COX-3 encoded proteins. To determine whether any of the COX-3 proteins are active peroxide synthases, we assayed these colonies for PGE_2 production and observed a statistically significant increase in prostaglandins from the colony expressing 72kD COX-3 (Fig. 1F).

Transient expression of a human COX-3 clone in multiple cell lines showed expression of multiple high molecular weight proteins similar to those seen for rat COX-

3 (Fig. S1B). Seven proteins are produced in A549 cells with molecular weights of approximately 72, 62, 57, 50, 49, and 44kD. However, HeLa and 293 cells only express the non-glycosylated lower molecular weight forms, again indicating that expression of some COX-3 proteins rely on processes expressed in a cell-type dependent manner. As a test for over-expression artifacts in these cells, we generated A549 cells stably expressing a human COX-3 construct and verified expression of the same proteins by anti-Flag Western blot (Fig. 1D).

Identification of putative COX-3 proteins in vivo

To study the *in vivo* expression of human COX-3, we screened 8 human cell lines for COX-3 expression by RT-PCR and by Western blot. As shown in figure 2, COX-3 mRNA is expressed widely in the majority of the cell types, with highest expression in K562 cells and MEG-01 cells. Immunoblot analysis with an anti-COX-1/COX-3 non-specific antibody detected immunoreactive proteins of approximately 72, 68, and 57kD in size in many of these cell lines (Fig. 2B). Expression levels of the 72kD protein correlated generally well with the level of COX-1 mRNA while expression of the 68kd and 57kD proteins correlated generally well with COX-3 mRNA expression.

To confirm that these proteins were derived from COX mRNA, we treated MEG-01 cells with siRNAs targeting exons 10 and 11 of the COX-1 and COX-3 mRNAs. RT-PCR analysis demonstrated that the siRNAs knockdown both COX-1 mRNA and COX-3 mRNA at about 90% efficiency. Immunoblotting of these cells 48 hours after transfection demonstrated a statistically significant ~50% decrease in the 72kD, 68kD, and 57kD proteins indicating these are derived from either the COX-1 or COX-3 transcripts (Fig. 3). We attempted to generate COX-3 specific siRNAs to definitively determine whether

the 68 and 57kD forms were derived from the COX-1 or COX-3 message, however due to the limited number of siRNA recognition sites in the short, 94bp, intron-1 we were unable to achieve a meaningful knockdown of the COX-3 mRNA.

To further study the expression of these proteins *in vivo*, we used a COX-3 induction model developed by Nurmi et. al. [21] and treated Caco-2 cells with 100mM NaCl (hypertonic) for 22 hours to induce both COX-3 and COX-1 (Fig. 4). RT-PCR analysis of these cells qualitatively demonstrated a significant increase in COX-1 mRNA and a more modest increase in COX-3 mRNA expression. Western blots analysis of these same cells detected a concomitant 11-fold increase in a 72kD protein, as well as a ~3 fold increase in 68kD, and 57kD proteins, corresponding in size with full-length COX-1 and two of the COX-3 derived proteins respectively. The relative fold induction in the 72kD protein compared with 68 and 57kD proteins correlates generally well with the relative increase in the expression level of COX-1 and COX-3 mRNA respectively and together with the fact that cells stably expressing COX-1 mRNA make only the full-length 72kD COX-1 protein indicates that the 68, 57, 50, and 44kD proteins are derived predominantly from the COX-3 or intron-1 containing mRNA. However, the data is not conclusive and we can not exclude the possibility that under certain conditions these lower molecular weight proteins can be translated from the COX-1 mRNA as well.

We next sought to determine whether we could detect translation of any putative COX-3 proteins *in vivo* in whole tissue samples. Polysome profiling of rat spleen tissue demonstrated that some COX-3 mRNA co-sediments with heavy polysomes, suggesting that at least a portion of the COX-3 message is actively translated in a similar manner as COX-1 and glyceraldehyde dehydrogenase (GAPDH) mRNAs, each

of which have long, actively translated open-reading frames (Fig. S3A-B). COX-3 mRNA was additionally detected co-sedimenting with monosomes and short reading frame mRNAs including fatty-acid binding protein-7(FABP), phospho-neuro protein-14 (PNP-14), and histone protein 2a (H2A). Western blot analysis of various rat tissues detected modest levels of 50kD and 44kD COX reactive proteins in multiple tissues with the highest levels seen in platelet, pancreas, testes and heart (Fig. S3C). These were shown to be N-glycanase insensitive, a signature of 50kD and 44kD COX-3 encoded proteins, but not of degradation products of COX-1.

Non-glycosylated COX-3 proteins are translated through internal initiation

We used site-directed mutagenesis to probe the mechanism(s) resulting in expression of high molecular weight COX-3 encoded proteins. Our initial hypothesis was that alternative translational initiation sites downstream of the consensus AUG start codon may be used to produce the shorter 57, 50, 47(human), and 44kD forms of COX-3 based on the identification of four highly conserved in-frame AUG codons at positions 441, 591, 693(human), and 750bp downstream from the consensus AUG codon (Fig. 5). Mutation of these AUG codons to non-initiating GCG (ala) codons in both the human and rat constructs prevented translation of each COX-3 protein respectively, confirming that these forms are translated through internal translation initiation (Fig. 6 A-B). The 57kD form of human COX-3 appears as a doublet on Western blot, and our analysis demonstrates that there are in fact two AUG codons in the human COX-3 sequence. Mutation of AUG-435, reduced expression of the 57kD protein by ~80%, while mutation of the second AUG-441 reduced expression by ~20%. Mutation of both codons

completely eliminated expression of this doublet indicating that either site can be used, but that AUG-435 is preferentially used for initiation.

CHO cells transiently transfected with rat COX-3 express a 68kD form, which is not expressed from the human cDNA. Based on the electrophoretic migration we hypothesized that this protein was also translated through initiation at a downstream initiation site. However, the cDNA does not contain any in frame-AUG codons in the region predicted to contain the start codon based on the apparent molecular weight. Therefore, to identify the region of translation initiation we introduced stop codons at various positions in the rat COX-3 cDNA. We reasoned that stop codons downstream of the translation initiation site would lead to premature truncation of the nascent peptide and a corresponding loss of the 68kD band on the Western blot. Conversely, stop codons placed upstream of the internal initiation site should have no effect on expression of the 68kD form. We observed that stop codons placed at nucleotides 231, 240 and 252 completely eliminated expression of the 68kD protein. However, stop codons introduced upstream of this at position 216 had no significant effect on expression indicating that translation initiates at some point between codons 216 and 231 (Fig. 6C). Because this region does not contain any in-frame cognate AUG initiation codons, we hypothesized that translation initiation must be occurring at a non-standard codon in this region. To identify the codon(s) required for translation initiation we used site-directed mutagenesis to sequentially change each codon between 204 and 237 to AAA codons. Mutation of codons 210, 213, 216, 219, 222, and 228 eliminated expression, or in the case of codon 228 significantly decreased expression of the 68kD protein, while the other mutations had no significant effect on the translation. Together

this data indicates that translation initiation of the 68kD form of rat COX-3 is dependent upon a long 21-nucleotide element (Fig. 6D).

We recognized the possibility that translation of these lower molecular weight forms could be the result of translation of truncated COX-3 mRNAs produced through cryptic promoter sites or broken mRNAs missing the 5' upstream region. However, 5'RACE analysis of the COX-3 mRNA following transient transfection in CHO cells found only full-length COX-3 transcripts, confirming that these lower molecular weight proteins are translated from the full-length COX-3 mRNA (Fig. S2D).

These recoding processes, therefore, produce a series of COX-3 proteins each missing progressively larger portions of the N-terminus. Because the N-terminus encodes the signal peptide, dimerization, and the membrane binding domains the resulting proteins may be expected to have significantly different properties from full-length COX-1 (Fig. 7).

Translation of full-length, glycosylated 72kD COX-3 proteins

Based on the apparent molecular weight of the 72kD COX-3 form(s), we hypothesized that the protein may be translated through initiation at the consensus AUG-1 initiation codon, the same codon that is utilized for translation of COX-1. Due to retention of intron-1 in the COX-3 message this codon is out of frame with the downstream COX-3 coding sequence and the C-terminal Flag-tag. Therefore, translation initiation at this codon would require a ribosomal frame-shift later in the transcript to rectify the reading frame. To test this we mutated AUG-1 to a non-initiating CCC and determined the effect on translation by anti-Flag Western blot. Mutation of this codon resulted in a ~50% decrease in the expression level of the 72kD COX-3 protein,

indicating that there may be at least two different translation mechanisms producing 72kD COX-3 proteins, one of which relies on this AUG-1 codon (Fig. 8D).

We next introduced TAA (stop) codons at different locations downstream of this AUG codon. Stop codons at positions 13 and 19 in the same reading frame as the initiating AUG-1 (+1 relative to the downstream coding sequence) eliminated expression of ~50% of the protein whereas stop codons further downstream in this same +1 reading frame, at 34 and 46, had no effect on translation levels. Concordantly, TAA stop codons introduced in the +0 reading frame at positions 18 and 27 had no effect on expression, but stop codons further downstream at positions 36 and 48 in the +0 reading frame eliminated ~50% of the expression of the 72kD COX-3 protein (Fig 7A,B). These results are consistent with one 72kD protein being translated by ribosomes which initiate at AUG-1 in the +1 reading frame, and continue to translate in the +1 reading frame until some point between nucleotides 27 and 34. At this point (a sequence of CCCCCACG) the ribosome appears to perform a -1 or +2 frame-shift, placing it into the correct, +0 reading frame allowing it to translate the rest of the COX coding sequence and C-terminal Flag-tag.

Expression of the remaining 50% of the 72kD protein was eliminated by introduction of TAA stop codons into the +0 reading frame at position 63, 72, and 84 (Fig. 8A) consistent with the presence of a second 72kD COX-3 protein which initiates at a site between nucleotides 48 and 63. Point mutation of each codon between these two nucleotides demonstrated that mutation of only one, TGC-57 to AAA or TGG, consistently and significantly lead to a ~50% decrease in the expression of the 72kD

band, indicating that the second 72kD COX-3 protein is translated by initiation at this in-frame cysteine codon (Fig. 8C).

Together this data suggests a model whereby two distinct 72kD COX-3 proteins are expressed. The first relies on initiation at the consensus AUG-1 in the mRNA sequence and a concomitant -1 or +2 ribosomal frame-shift at position between nucleotides 27-34 to correct the reading frame. Expression of the second relies on an in-frame TGC codon located within intron-1, which our data suggests is utilized as the translation initiation codon. As confirmation of this model we generated a double mutant, AUG-1 to GCG to prevent expression of the frame-shifted form, and TGC-57 to AAA to prevent expression of the cysteine-initiated form. These two mutations eliminated expression of essentially all of the 72kD protein (Fig. 8D).

Following the nomenclature suggested by the human genome variation society, we propose these two recoded COX-3 proteins be named COX-3 p.del19(cys) for the TGC (cys) initiated 72kD form and COX-3 p.tyr11fs for the frame-shifted 72kD COX-3 form. Consequently, following this convention, the 57, 50, 47, and 44kD COX-3 proteins derived through alternative initiation would be named COX-3 p.del142, p.del192, p.del226, and p.del245 respectively to signify the number of amino-acid residues missing from the N-terminus relative to the putative full-length COX-3 protein. However, for simplicity in this manuscript we will refer to them as recoded or rc-72kD(cys) and rc-72kD(fs), rc-57kD, rc-50kD, rc-47kD, and rc-44kD COX-3 in this manuscript. Likewise and acknowledging our inability to define the initiation site of the 68kD COX-3 protein we will to refer to it as rc-68kD COX-3.

Analysis of COX-3 translation products by Mass Spectrometry

Toward confirmation of our general mechanism, Flag- and 6Xhis-tagged COX-3 protein was doubly-purified from transiently transfected CHO cells by anti-Flag immunoprecipitation followed by Flag peptide elution and subsequent purification over an immobilized metal affinity column. The purified COX-3 protein was subjected to SDS-PAGE and in-gel tryptic digestion. To the extracted peptides were added 5 synthetic tryptic COX-3 peptides harboring stable isotopes of carbon and nitrogen to distinguish them from the tryptic peptides of COX-3 derived from the CHO cells. The peptide mixtures were subjected to liquid chromatography tandem mass spectrometry (LC-MS/MS) in a linear ion trap-orbitrap hybrid mass spectrometer. Importantly, the synthetic peptides co-elute and show nearly identical MS/MS spectra with the cellular-derived tryptic peptides. The synthetic peptides were chosen as they would directly test for the presence of 5 different peptides from the +0 and +1 reading frames of COX-3 (Fig. S4). Following LC-MS/MS, two of the five tryptic peptides from the purified cellular COX-3 were not identified. These two peptides resided at the N-termini of either of the two glycosylated forms of COX-3. Their absence was later shown to be due to the fact that like COX-1, the N-terminal region of both of these forms encodes a signal-peptide that is cleaved from the fully processed protein (Fig. S6).

We did however, detect two peptides from the +1 reading frame as well as a third peptide from the +0 reading frame (Fig. S4), consistent with expression of a third Tunicamycin insensitive COX-3 protein, which is translated in the +1 reading frame, before a -1 or +2 ribosomal frame-shift at some point in the last 19 codons of the +1 open reading frame (Fig. S4). We note that treatment with N-glycanase consistently caused a mobility shift for about 90% of the 72kD protein(s), the remaining 10% of N-

glycanase resistant, non-glycosylated 72kD COX-3 protein is likely this third 72kD COX-3 protein which does not contain a signal peptide because the frameshift occurs downstream of this domain.

Pharmacological analysis of COX-3 proteins

As stated earlier, cells stably expressing the authentic COX-3 cDNA exhibited an increase in PGE_2 synthesis indicating that at least one COX-3 form is an enzymatically active prostaglandin synthase. Given the similarities between the two 72kD glycosylated forms of COX-3 with COX-1, we hypothesized that these may be the active forms. To test this we prepared clones designed to efficiently express either the rat rc-72kD frame-shifted or cys-initiated forms. For the frame-shifted form we artificially corrected the reading-frame by inserting an additional cytosine at the identified frame-shift site, position 27 (CCC to CCCC). For the cysteine-initiated form we replaced the initiating TGC codon at position 57 with an AUG codon. We additionally mutated the upstream AUG-1 codon to a GCG to prevent expression of the other forms. Both of these clones efficiently expressed a 72kD glycosylated protein of the same apparent molecular weight as that produced by the authentic COX-3 clone. Cells transiently expressing each of these 72kD COX-3 proteins showed a high level of cyclooxygenase activity with a similar specific activity as COX-1 (Fig. S5A). Indomethacin and the COX-1 specific inhibitor SC-560 inhibited both 72kD COX-3 forms with IC_{50} values around 0.1 to 1.0 μM, near that seen for COX-1. The analgesic/antipyretic drug acetaminophen weakly stimulated the activity of both COX-3 forms with an EC_{50} near that of COX-1 (Fig. S5B-D).

Recoded forms of COX-3 localize to distinct organelles

Confocal micrographs of cells transfected with constructs expressing rc-68kD COX-3 demonstrated that it localizes to the endoplasmic reticulum like COX-1 and both rc-72kD COX-3 proteins (Fig. S7). In contrast, rc-44kD COX-3 exhibited a diffuse cytosolic and intranuclear localization while rc-57kD and rc-50kD COX-3 proteins displayed both a cytosolic and punctate localization within the cells with some cells exhibiting predominantly a diffuse staining consistent with cytosolic localization while in other cells the protein localized to discrete puncta, near or around the nucleus (Figs. 9A and S7). To determine precise localization, we co-stained the cells with cis-golgi, intermediate golgi, or trans-golgi apparati markers and assessed the level of colocalization. Rc-57kD COX-3 colocalized strongly with intermediate and trans-golgi (Pearson's coefficient: 0.695 and 0.559 respectively), but not with cis-golgi (Pearson's coefficient: 0.059). Additional puncta were found adjacent to these golgi, suggesting they may be vesicles derived from golgi. In contrast, rc-50kD COX-3 co-localized with cis and intermediate golgi (Pearsons' coefficient: 0.58 and 0.863 respectively) and less so with trans-golgi (Pearsons' coefficient: 0.127). However, not all of the punctate structures observed for rc-57 and rc-50 colocalized with golgi. In a subset of cells we observed that both proteins localized to microtubule-associated protein 1A/1B-light chain 3 (LC3-II) containing autophagosomes (Fig 9A).

Given that rc-57 and rc-50kD COX-3 appear to localize to both the cytosolic fraction as well as the golgi and autophagosomes we wondered whether the proteins associate with the cytosolic or luminal face of the membrane. We therefore

permeabilized the plasma membrane with digitonin prior to imaging the cells. As a control we verified that digitonin treatment eliminated GAPDH, a cytosolic enzyme, staining while intraluminal golgi proteins (TGN46 & mannosidase-II) and autophagosome proteins (LC3-II) were unaffected. Digitonin eliminated the cytosolic, golgi, and autophagosome localized forms of 57, 50, and 44 kD COX-3 indicating that they are located on the cytosolic surface of golgi and autophagosomes (Fig. 9B). We note that, while the majority of rc-57 and rc-50kD COX-3 fluorescence disappeared upon digitonin treatment, some punctate signal remained. By in large, this residual staining was not localized to golgi or autophagosomes, suggesting additional vesicles where rc-57 and rc-50kD binding differs from these structures.

Discussion

In total our data indicate that COX-3 mRNA is translated through multiple recoding mechanisms to produce at least five cyclooxygenase-related proteins whose individual expression depends upon specific tissue and cellular conditions. This is consistent with prior reports of other eukaryotic mRNAs which give rise to multiple versions of a protein by alternative translation initiation (reviewed by *[22]*). Ingolia, et al. [18,19] recently demonstrated, using ribosomal profiling, that 65% of all transcripts in mouse embryonic stem cells contain more than one translational initiation site that is used at a relatively high level. Notably, 16% of messages contain four or more start sites producing either N-terminal extended or N-terminal truncated proteins [19].

In support of our findings, Lee et. al. recently reported the independent identification of additional translation initiation sites for a large number of mRNAs,

including COX-1/COX-3, in mouse embryonic fibroblast cells using a modified ribosome profiling method. An analysis of their data shows that while the overall signal for COX-1/COX-3 mRNA is low, they are able to identify four previously unreported downstream translation initiation sites for COX-1 (or COX-3) in addition to the annotated AUG-1 codon [20] confirming that the mRNA is heavily recoded. One of the initiation sites they identified in these mouse cells (155bp) is very close to the position of the initiation site we identified for rc-68kD COX-3.

The precise mechanism by which internal translation start sites are selected, in light of the scanning model, is not currently well understood, but likely involves one of two processes. The first, leaky scanning, requires the ribosome to scan from the 5' cap site and skip over the first AUG codon to instead initiate at a down-stream AUG codon [17,23]. Often this occurs when the nucleotides surrounding the first AUG codon (known as the Kozak consensus sequence) are sub-optimal. The second mechanism relies on cap-independent translation. In this process the ribosome is recruited directly to internal portions of the mRNA, usually through the action of structurally complex RNA motifs known as internal ribosomal entry sites (IRES) or related RNA sequences known as cap-independent translation enhancer sequences (CITEs)[24]. Both contain high-affinity binding sites for either the ribosome itself or eukaryotic initiation factors which lead to internal translation initiation [25]. It is worth noting here that human COX-1 mRNA contains an out-of frame upstream AUG codon; and therefore, classical COX-1 protein itself is likely translated through a process of leaky scanning.

Our data indicate efficient translation of rc-68kD COX-3 depends on a ~22 nucleotide-long region near the initiation site perhaps suggesting that it is translated

through a cap-independent mechanism. Whether a similar large region is necessary for translation of rc-57, 50, 47, or 44kD COX-3 has not been directly assessed, and the mechanism of initiation site selection for these forms will require further research. However, if the lower molecular weight forms of COX-3 are produced through cap-independent initiation mechanisms, this may suggest the expressed proteins play a role in processes such as viral infection response, hypoxia, cancer, and other conditions in which cap-dependent translation is shut down and cap-independent translation predominates [26-28].

One of the COX-3 proteins we identified appears to initiate on a non-consensus cys (TGC) codon. Although often associated with prokaryotes, eukaryotic translation initiation can occur at non-AUG codons, and reportedly accounts for as much as 55% of all initiation events [19,22]. Near-cognate codons are often used, but translation can initiate at other codons as well. Recently, Anaganti et. al. reported the cloning of a short CAPC (a tumor suppressor and inhibitor of NF-κB signaling, also known as leucine rich repeat containing 26, LRRC26) variant from human cancer cell lines that lacked any AUG codons [29]. Upon expression it was determined, using mass spectrometry, that a 44 amino-acid polypeptide is efficiently expressed through translation initiation at a cysteine encoded by a TGC codon. Analysis of the mRNA sequence at the initiating TGC codon for this S-CPAC variant (GCC TGC CGT) shows some similarity with the start site identified in our study for the 72kD TGC-initiated COX-3 form (GCC TGC AGG) perhaps indicating a role for surrounding nucleotides in initiation at TGC or other non-cognate codons.

Sequence alignment between COX-1 and COX-2 suggest the possibility of recoding of the COX-2 mRNA as well. The details of the mechanisms by which translation, splicing and recoding of COX-3 are coordinated are being further investigated, however, we have previously shown for COX-2 that the retention of a portion of intron-1 is exquisitely regulated in response to mitogenic stimulation [30]. The final translational product of the intron-1 retained COX-2 mRNA has never been determined due to the presence of multiple stop codons within the intron, but in light of our results showing extensive recoding of intron-1 retained COX-1 (COX-3 mRNA) we propose that a careful analysis of this alternatively spliced COX-2 mRNA will demonstrate similar recoding mechanisms result in translation of COX related proteins from this mRNA as well.

Role of COX-3 proteins

The functions of the lower molecular weight COX-3 encoded proteins are intriguing because rc-57, 50, 47, and 44kD COX-3 are missing signal peptides, preventing translocation of these proteins to the ER lumen for glycosylation. Glycosylation has previously been shown to be necessary for folding of the COX enzyme to its catalytically active form; however, if the carbohydrate residues are removed post-translationally the enzyme retains peroxidase activity [31]. Due to the fact that the entire peroxidase active site region is still present in these truncated proteins it is possible that even without glycosylation these proteins may fold into active peroxidase enzymes. Notably rc-68kD COX-3 lacks only the first ~11 amino acids compared with fully processed COX-1, and retains the entire dimerization, membrane

binding, peroxidase and cyclooxygenase active site domains and localizes to the endoplasmic reticulum.

The fact that rc-68kD COX-3 specifically localizes to the ER whereas rc-57kD and rc-50kD COX-3 localize to separate domains of the golgi body and adjacent vesicular structures, and rc-44kD COX-3 is cytosolic/intranuclear suggests specific and distinct roles for each protein. These functions are clearly different from that of either COX-1 or COX-2, which generate prostaglandin H2 from their locations in the lumen of the nuclear envelope/ER and which only transiently passage through the lumen of the golgi apparatus. The exquisite location of these recoded COX proteins is exemplified by the fact that rc-57kD COX-3 localizes primarily to medial/trans-golgi and associated structures, whereas rc-50kD COX-3 associates with cis/medial golgi and associated structures. Furthermore, these COX-3 recoded proteins, as shown by their lack of N-glycosylation and their digitonin-mediated release, are on the cytosolic surface of their respective membranes (or are potentially associated with chromatin, nucleoplasm, or cytosol in the case of rc44KD). In each instance, however, the recoded COX-3 proteins retain sequence that enable them to bind heme and catalyze redox reactions via a reactive tyrosyl radical, which is conserved in each of the recoded proteins.

Further investigation will be required to demonstrate enzymatic activities, binding partners or other biochemical functions of recoded COX-3 proteins specific to their unusual cytosolic subcellular locations. Such roles do not involve classical prostaglandin synthesis typically associated with proteins from cyclooxygenase genes, but may involve or result in other oxylipin products. Furthermore, the finding of rc-57kD and rc-50kD colocalizing with LC3-II on autophagosomes clearly suggests a role of

these proteins in autophagy, a process critical to innate immunity [32-34]. This finding is fully consistent with the well-known function of cyclooxygenases as pivotal controllers of the innate immune response in eukaryotes – but suggests new previously unknown roles in this process.

The fact that COX-3 mRNA is expressed at significantly high levels in a tissue and cell-specific fashion further suggest a role in physiology. We initially found COX-3 mRNA expressed in specific regions of brain and heart [7]. Kis et. al. further looked at expression of COX-3 mRNA in various brain cell populations by RT-PCR and determined that COX-3 mRNA in the brain is strongly expressed in endothelial cells, but at much lower levels in neurons, astrocytes, pericytes and choroidal epithelial cells [35]. This is corroborated by Northern blot studies demonstrating the highest levels of COX-3 mRNA expression in highly vascularized tissues including heart, skeletal muscle, placenta, liver, spleen and stomach [10]. Taken together these data suggest that COX-3 may play a role in vascular function, perhaps in processes including vasodilatation, clotting, or remodeling, or in immune surveillance.

With regard to acetaminophen, we determined that unlike canine COX-3, which is selectively inhibited by acetaminophen, the 72kD forms of COX-3 were both stimulated in the presence of micromolar concentrations of acetaminophen in our assay. Stable expression of COX-3 demonstrated that the 72kD forms of COX-3 require cell-specific conditions to be efficiently expressed. It is likely that in our over-expressed COX-3 assay we are not fully mimicking the cellular conditions required for acetaminophen inhibition, which is highly dependent upon intracellular oxidant tone. Alternatively, this could also represent an authentic difference between canine and

rodent COX-3 enzymes. Further research will be needed to fully elucidate the contribution of COX-3 to acetaminophen-induced analgesia and antipyresis.

Cyclooxygenases function at the heart of critical physiological processes including nociception, pyresis, thrombosis, inflammation, regulation of vascular tone, ovulation, implantation, angiogenesis, parturition and pathophysiological processes such as neoplasia and inflammatory diseases. These results lay groundwork for additional studies that will further explain how the cyclooxygenase enzyme system regulates aspects of these dynamic processes.

Experimental Procedures

Detailed experimental methods are available in supplemental material.

Cell Culture and protein expression

Low passage number cells were grown under standard culture conditions outlined in supplemental methods. For salt treatment, Caco-2 cells were incubated in media supplemented with or without 100mM NaCl for 22 hours at 37 °C.

Transient transfection of COX-3 was performed using lipofectamine reagent (Invitrogen) following the recommended procedure. Stable transfectants were selected from standard growth medium containing 750 μg/mL Geneticin (Gibco). Single cells were isolated and screened for COX expression by immunoblot using an anti-Flag and an anti-COX-1 antibody. Protein expression was quantified by Western blot analysis using densitometry. N-glycanase treatment was performed using enzyme purchased from Prozyme following the recommended protocol.

Anti-Flag immunoprecipitation was performed using an anti-Flag resin (Sigma) and his-tagged proteins were purified over a cobalt resin column (Thermo Scientific) following standard protocols. 5' and 3' RACE analysis on transiently transfected CHO cells was performed using GeneRacer kit (Invitrogen) following the recommended procedures.

Cyclooxygenase activity assays

CHO cells transfected with COX-1, COX-3, or empty vector constructs were treated with exogenous arachidonic acid (5 μM) for 15 minutes at 37 °C and the media was subsequently assayed for PGE_2 levels via dextran coated charcoal based competitive radioimmunoassay (RIA) using an anti-PGE_2 antibody (Sigma-Aldrich) and

tritiated PGE_2 (Perkin Elmer) following the antibody manufacturer's recommended protocol. For inhibition studies, cells were pretreated with drug for 30 minutes at 37 °C. Whole cell lysates of COX-3 stable transfectants were analyzed in the same manner, except that cells were first lysed into PBS containing protease inhibitors.

siRNA knock-down of COX-3 expression

Anti-COX-1/COX-3 siRNAs (Dharmacon, 100 nanomoles/150,000 cells) were transfected into MEG-01 and K562 cells using Lipofectamine RNAiMAX reagent (Invitrogen) using the recommended transfection protocol. After 72 hours cells were harvested and analyzed by RT-PCR and immunoblot. As a negative control, cells were transfected with 100 nanomoles of Dharmacon's non-targeting siRNA #2.

Rat tissue screen

All animal studies were reviewed and approved by the institutional animal care and use committee at Brigham Young University. Organs and tissues were obtained from a male long evans rat. Polysome profiling was performed following the protocol of Zhu et. al.[36]. For Western blot, tissues were homogenized into PBS with protease inhibitor cocktail (Roche). Protein was electrophoresed, transferred to a nitrocellulose membrane, and probed using either an anti-COX-1 antibody (Cayman) or purified non-immune rabbit IgG's at a 1:1000 dilution.

Site-directed mutagenesis

All mutagenesis was performed using the Geneart site-directed mutagenesis kit (Invitrogen). A forward primer was prepared which overlapped the mutation site and contained the desired mutation. A reverse primer was also prepared so that there were at least 12 nucleotides of overlap between the 5' end of the reverse primer and the 5'

end of the forward primer. PCR amplification was performed using platinum Pfx (Invitrogen). The reaction mixture was subjected to overnight DpnI digestion followed by i*n vitro* recombination to circularize the amplicon prior to transformation into DH5α cells.

Confocal Microscopy

Cells were seeded onto collagen coated glass cover slips and transfected with the indicated plasmid, fixed in a PBS solution with 4% paraformaldehyde, blocked with a solution of 1% goat serum in PBS with 0.1% Tween 20 (PBS-T), and stained with respective antibodies overnight before being mounted on a glass slide in ProLong® Gold antifade reagent (Molecular Probes). In the case of GFP fusion proteins, the blocking and antibody staining procedure was omitted. Cells were imaged using an Olympus FluoView FV 1000 confocal laser-scanning microscope and final images prepared using ImageJ software [37]. Pearson's Correlation Coefficients were calculated using FluoView Viewer software (Olympus).

Mass spectrometry

Flag- and His6-tagged COX-3 cDNA was transiently expressed in CHO cells and its encoded proteins were immunoprecipitated using an anti-Flag resin. This was followed by elution using the Flag peptide and a second round of affinity purification using cobalt resin chromatography. The purified proteins were subjected to SDS-PAGE using a 10% acrylamide gel and were stained with coomassie blue (Pierce). Proteins with an electrophorectic mobility between 50-80 kDa were subjected to in-gel tryptic digestion and peptide extraction as described previously [38]. To the dried, extracted peptides were added approximately 250 fmol each of five synthetic, stable isotope-containing tryptic peptides (Cell Signaling Technology). Liquid chromatography tandem mass

spectrometry using a linear ion trap-orbitrap (LTQ-Orbitrap, Thermo Electron) was set up and run as described previously [39], except that instead of a top ten data-dependent analysis cycle, one data-dependent MS/MS scan was followed by targeted MS/MS scans on the calculated average m/z values (+/- 1.6) of each of the doubly-charged precursors for the synthetic peptides and their cell-derived counterparts.

Author Contributions

JCH, JJL, SDS, GL, DRR, ML, BAB, and DLS designed and performed experiments. JCH, JJL, SDS, DRR, BAB, and DLS analyzed experimental results. NVC contributed reagents. JCH, JJL, and DLS wrote the manuscript.

Acknowledgements

We thank Jeffrey Knott and Jason Reynolds at Cell Signaling Technology for synthesizing the stable isotope-containing peptides. Mass spectrometry analyses were funded by the Vermont Genetics Network through NIH Grant 8P20GM103449 from the INBRE program of the NIGMS. Sean Phipps, Jeffery Chen, Austin Burge, and Victoria Chen provided invaluable assay development technical support in this work. The authors declare no conflicts of interest.

References

1. Vane JR (1971) Inhibition of prostaglandin synthesis as a mechanism of action for aspirin-like drugs. Nat New Biol 231: 232-235.
2. Roth J, Rummel C, Barth SW, Gerstberger R, Hubschle T (2006) Molecular aspects of fever and hyperthermia. Neurol Clin 24: 421-439, v.
3. Khan AH, Carson RJ, Nelson SM (2008) Prostaglandins in labor--a translational approach. Front Biosci 13: 5794-5809.
4. Moncada S, Vane JR (1979) The role of prostacyclin in vascular tissue. Fed Proc 38: 66-71.
5. Toomey DP, Murphy JF, Conlon KC (2009) COX-2, VEGF and tumour angiogenesis. Surgeon 7: 174-180.
6. Simmons DL, Botting RM, Hla T (2004) Cyclooxygenase isozymes: the biology of prostaglandin synthesis and inhibition. Pharmacol Rev 56: 387-437.
7. Chandrasekharan NV, Dai H, Roos KL, Evanson NK, Tomsik J, et al. (2002) COX-3, a cyclooxygenase-1 variant inhibited by acetaminophen and other analgesic/antipyretic drugs: cloning, structure, and expression. Proc Natl Acad Sci U S A 99: 13926-13931.
8. Snipes JA, Kis B, Shelness GS, Hewett JA, Busija DW (2005) Cloning and characterization of cyclooxygenase-1b (putative cyclooxygenase-3) in rat. J Pharmacol Exp Ther 313: 668-676.
9. Kis B, Snipes JA, Gaspar T, Lenzser G, Tulbert CD, et al. (2006) Cloning of cyclooxygenase-1b (putative COX-3) in mouse. Inflamm Res 55: 274-278.
10. Qin N, Zhang SP, Reitz TL, Mei JM, Flores CM (2005) Cloning, expression, and functional characterization of human cyclooxygenase-1 splicing variants: evidence for intron 1 retention. J Pharmacol Exp Ther 315: 1298-1305.
11. Atkins J, Gesteland, RF (2010) Recoding: Expansion of Decoding Rules Enriches Gene Expression: Springer.
12. Dinman JD (2012) Control of gene expression by translational recoding. Adv Protein Chem Struct Biol 86: 129-149.
13. Ivanov IP, Matsufuji S (2010) Autoregulatory Frameshifting in Antizyme Gene Expression Governs Polyamine Levels from Yeast to Mammals

Recoding: Expansion of Decoding Rules Enriches Gene Expression. In: Atkins JF, Gesteland RF, editors: Springer New York. pp. 281-300.

14. ichel AM, Roy Choudhury K, Firth AE, Ingolia NT, Atkins JF, et al. (2012) Observation of dually decoded regions of the human genome using ribosome profiling data. Genome Res.
15. Gerashchenko MV, Su D, Gladyshev VN (2010) CUG start codon generates thioredoxin/glutathione reductase isoforms in mouse testes. J Biol Chem 285: 4595-4602.
16. Kochetov AV (2008) Alternative translation start sites and hidden coding potential of eukaryotic mRNAs. Bioessays 30: 683-691.
17. Kozak M (2002) Pushing the limits of the scanning mechanism for initiation of translation. Gene 299: 1-34.

18. Ingolia NT, Ghaemmaghami S, Newman JR, Weissman JS (2009) Genome-wide analysis in vivo of translation with nucleotide resolution using ribosome profiling. Science 324: 218-223.
19. Ingolia NT, Lareau LF, Weissman JS (2011) Ribosome profiling of mouse embryonic stem cells reveals the complexity and dynamics of mammalian proteomes. Cell 147: 789-802.
20. Lee S, Liu B, Huang SX, Shen B, Qian SB (2012) Global mapping of translation initiation sites in mammalian cells at single-nucleotide resolution. Proc Natl Acad Sci U S A 109: E2424-2432.
21. Nurmi JT, Puolakkainen PA, Rautonen NE (2005) Intron 1 retaining cyclooxygenase 1 splice variant is induced by osmotic stress in human intestinal epithelial cells. Prostaglandins Leukot Essent Fatty Acids 73: 343-350.
22. Touriol C, Bornes S, Bonnal S, Audigier S, Prats H, et al. (2003) Generation of protein isoform diversity by alternative initiation of translation at non-AUG codons. Biol Cell 95: 169-178.
23. azykin GA, Kochetov AV (2011) Alternative translation start sites are conserved in eukaryotic genomes. Nucleic Acids Res 39: 567-577.
24. hatsky IN, Dmitriev SE, Terenin IM, Andreev DE (2010) Cap- and IRES-independent scanning mechanism of translation initiation as an alternative to the concept of cellular IRESs. Mol Cells 30: 285-293.
25. errick WC (2004) Cap-dependent and cap-independent translation in eukaryotic systems. Gene 332: 1-11.
26. Braunstein S, Karpisheva K, Pola C, Goldberg J, Hochman T, et al. (2007) A hypoxia-controlled cap-dependent to cap-independent translation switch in breast cancer. Mol Cell 28: 501-512.
27. ilvera D, Formenti SC, Schneider RJ (2010) Translational control in cancer. Nat Rev Cancer 10: 254-266.
28. Chiluiza D, Bargo S, Callahan R, Rhoads RE (2011) Expression of truncated eukaryotic initiation factor 3e (eIF3e) resulting from integration of mouse mammary tumor virus (MMTV) causes a shift from cap-dependent to cap-independent translation. J Biol Chem 286: 31288-31296.
29. Anaganti S, Hansen JK, Ha D, Hahn Y, Chertov O, et al. (2009) Non-AUG translational initiation of a short CAPC transcript generating protein isoform. Biochem Biophys Res Commun 380: 508-513.
30. Xie WL, Chipman JG, Robertson DL, Erikson RL, Simmons DL (1991) Expression of a mitogen-responsive gene encoding prostaglandin synthase is regulated by mRNA splicing. Proc Natl Acad Sci U S A 88: 2692-2696.
31. Otto JC, DeWitt DL, Smith WL (1993) N-glycosylation of prostaglandin endoperoxide synthases-1 and -2 and their orientations in the endoplasmic reticulum. J Biol Chem 268: 18234-18242.
32. Gomes LC, Dikic I (2014) Autophagy in antimicrobial immunity. Mol Cell 54: 224-233.
33. Joven J, Guirro M, Marine-Casado R, Rodriguez-Gallego E, Menendez JA (2014) Autophagy is an inflammation-related defensive mechanism against disease. Adv Exp Med Biol 824: 43-59.
34. uballa P, Nolte WM, Castoreno AB, Xavier RJ (2012) Autophagy and the immune system. Annu Rev Immunol 30: 611-646.

35. is B, Snipes JA, Isse T, Nagy K, Busija DW (2003) Putative cyclooxygenase-3 expression in rat brain cells. J Cereb Blood Flow Metab 23: 1287-1292.
36. Zhu J, Spencer ED, Kaspar RL (2003) Differential translation of TOP mRNAs in rapamycin-treated human B lymphocytes. Biochim Biophys Acta 1628: 50-55.
37. chneider CA, Rasband WS, Eliceiri KW (2012) NIH Image to ImageJ: 25 years of image analysis. Nat Methods 9: 671-675.

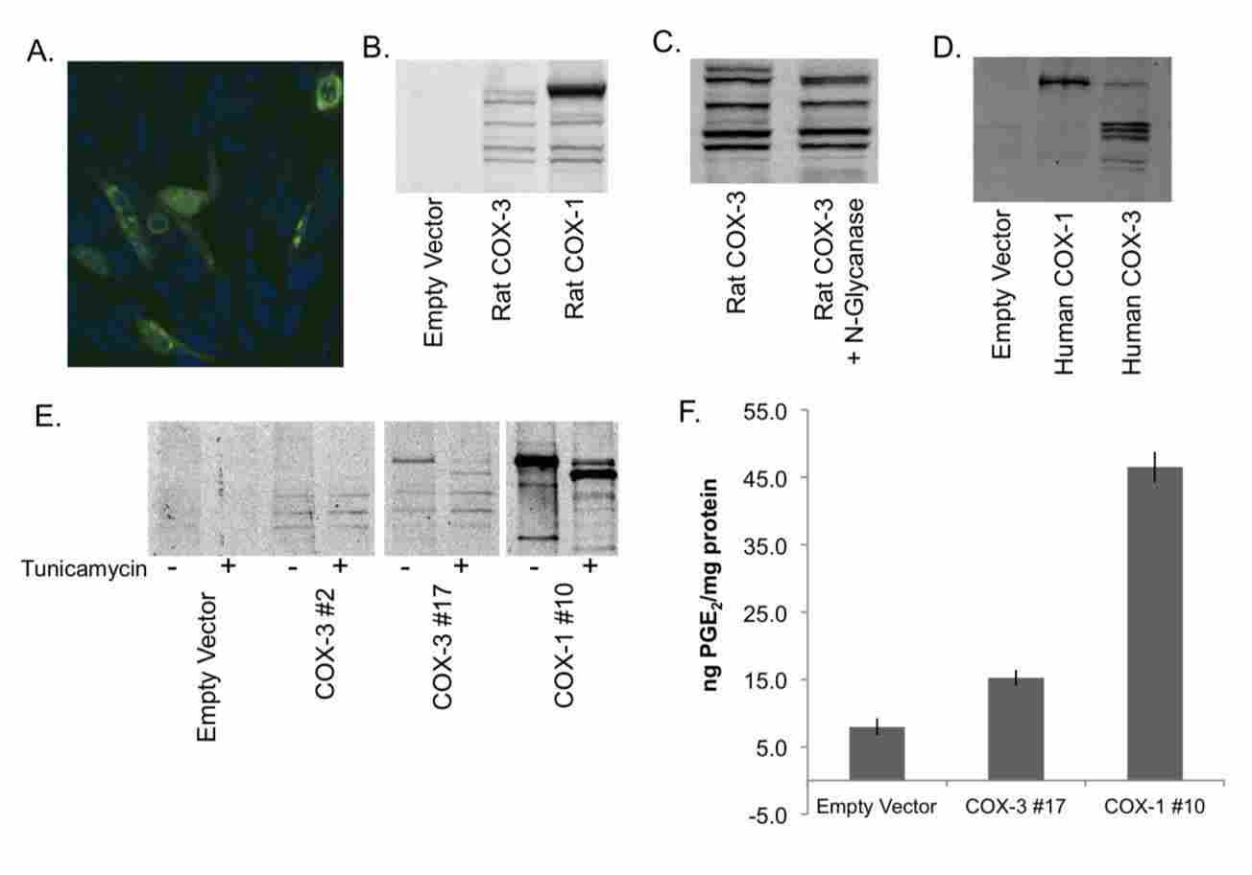

Figure 1: Expression of COX-3 cDNA.

A) CHO cells were transfected with GFP-COX-3 cDNA and co-stained with the nuclear stain TOPRO (blue). Cells were imaged using a laser scanning confocal microscope at 60X magnification. Image is representative of more than 3 experiments.

B) Anti-Flag immunoblot of CHO cells transiently expressing either a rat COX-3, COX-1 or empty pcDNA 3.1 expression clone. Five immunoreactive bands at 72, 68, 57, 50, and 44kD were detected in COX-3 transfected cells.

C) N-glycanase treatment of COX-3 proteins demonstrates that only one, the 72kD form, is N-glycosylated as indicated by an increase in the electrophoretic mobility. The four lower molecular weight COX-3 encoded proteins are not affected.

D) Human COX-3 and COX-1 cDNAs were stably expressed in A549 cells. Single colonies were isolated and analyzed for COX expression by anti-Flag immunoblot.
E) CHO cells were stably transfected with either empty pcDNA3.1 vector, rat COX-3 or rat COX-1. Single colonies were isolated and screened for COX expression by anti-Flag IP and immunoblot following treatment with Tunicamycin or DMSO. Colony #2 expresses only the 57kD, 50kD and 44kD COX-3 forms whereas colony #17 expresses predominantly the 72kD glycosylated COX-3 form in addition to the lower three forms. COX-1 positive colonies only expressed the 72kD full-length COX-1 form as well as lower molecular weight breakdown products as demonstrated by Tunicamycin treatment.
F) PGE_2 synthesis by stable transfectants. Colonies stably expressing an empty vector, rat COX-3 or rat COX-1 were tested for cyclooxygenase activity by anti-PGE_2 radioimmunoassay. COX-3 colony #17 and COX-1 colony #10 had a significant increase in cyclooxygenase activity over the background level detected in cells expressing empty vector control. Data is a meta-analysis of 3 separate experiments +/- SE.

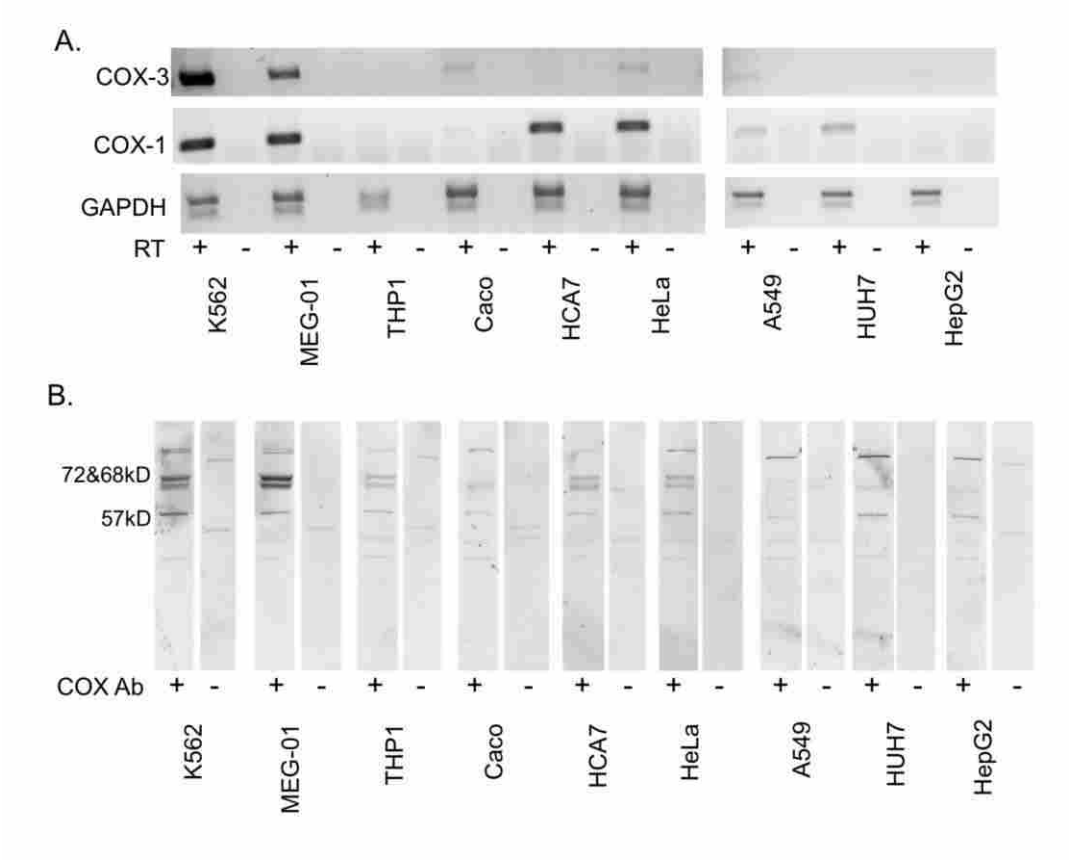

Figure 2: *In vivo* screen for COX-3 expression.

Human cells lines were screened for expression of COX-3 and COX-1 by reverse transcription-PCR (A) and immunoblot (B) with either an anti-COX-1/3 antibody or a non-immune rabbit antibody. Expression of 68kD and 57kD COX proteins generally correlates with expression of the COX-3 mRNA.

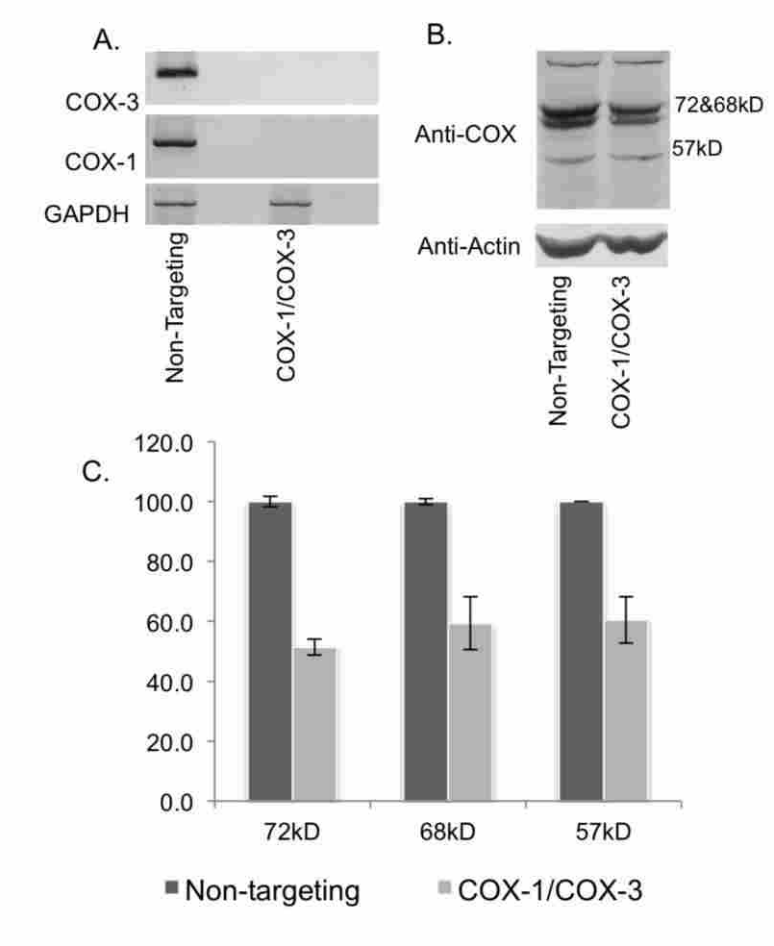

Figure 3: COX-1 siRNAs downregulate COX-1 and putative COX-3 proteins in MEG-01 cells.

MEG-01 cells were transfected with siRNA targeting both COX-1 & COX-3 mRNA (exons 10 and 11) or non-targeting control siRNA. COX-1 and COX-3 mRNA (A) and protein (B) was quantified by RT-PCR and anti-COX immunoblot.

C) The mean band intensity of the 72kD, 68kD, and 57kD Western blot bands from 3 separate experiments are plotted, normalized to cells treated with non-targeting siRNA and actin +/- SE. A significant decrease (P-value less than 0.05) was observed in the level of all three proteins indicating that they are encoded by the COX-1 and COX-3 transcripts.

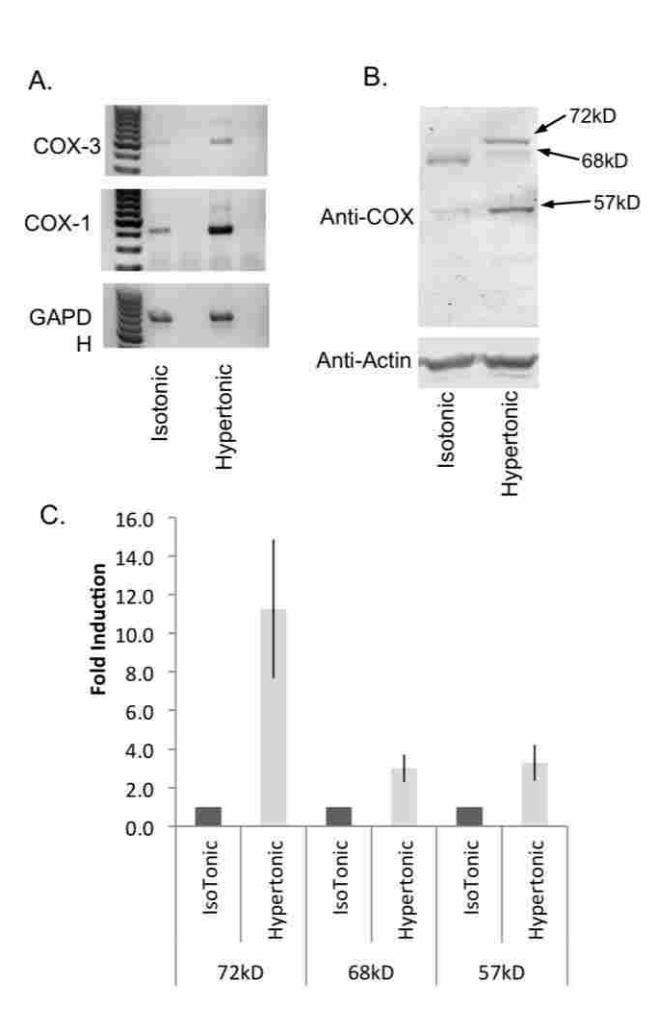

Figure 4: COX-3 induction in Caco-2 cells.

Caco-2 cells were treated for 22 hours in isotonic (Serum Free Media) or hypertonic (100mM NaCl) conditions or to induce COX-1 and COX-3 expression. An increase in the expression levels of COX-1 and COX-3 mRNA (A) and protein (B) was observed by RT-PCR and immunoblot respectively.

C) The intensity of the 72kD, 68kD, and 57kD proteins from 3 separate experiments were plotted and normalized to control cells and actin +/- SE. A significant (P-value less than 0.05) ~3 fold increase in the expression of the 68kD and 57kD proteins was

observed in response to hypertonic treatment. A larger 11.3 fold increase in the expression of a 72kD protein was also observed in these cells.

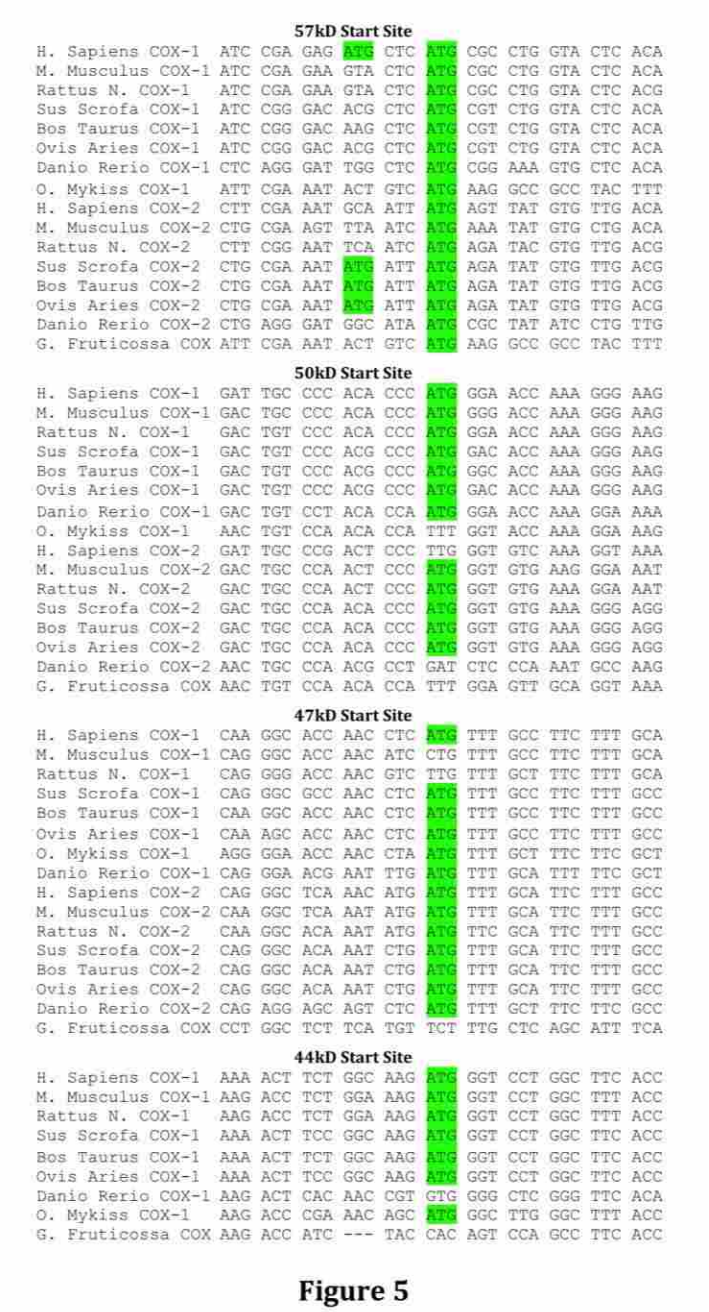

Figure 5

Figure 5: Conservation of downstream in-frame AUG codons.

Comparison of COX mRNA sequences from a selection of vertebrate species demonstrates that all four of the internal initiation sites used by COX-3 are highly conserved. The 57, 50 and 47kD initiation sites are also conserved in COX-2.

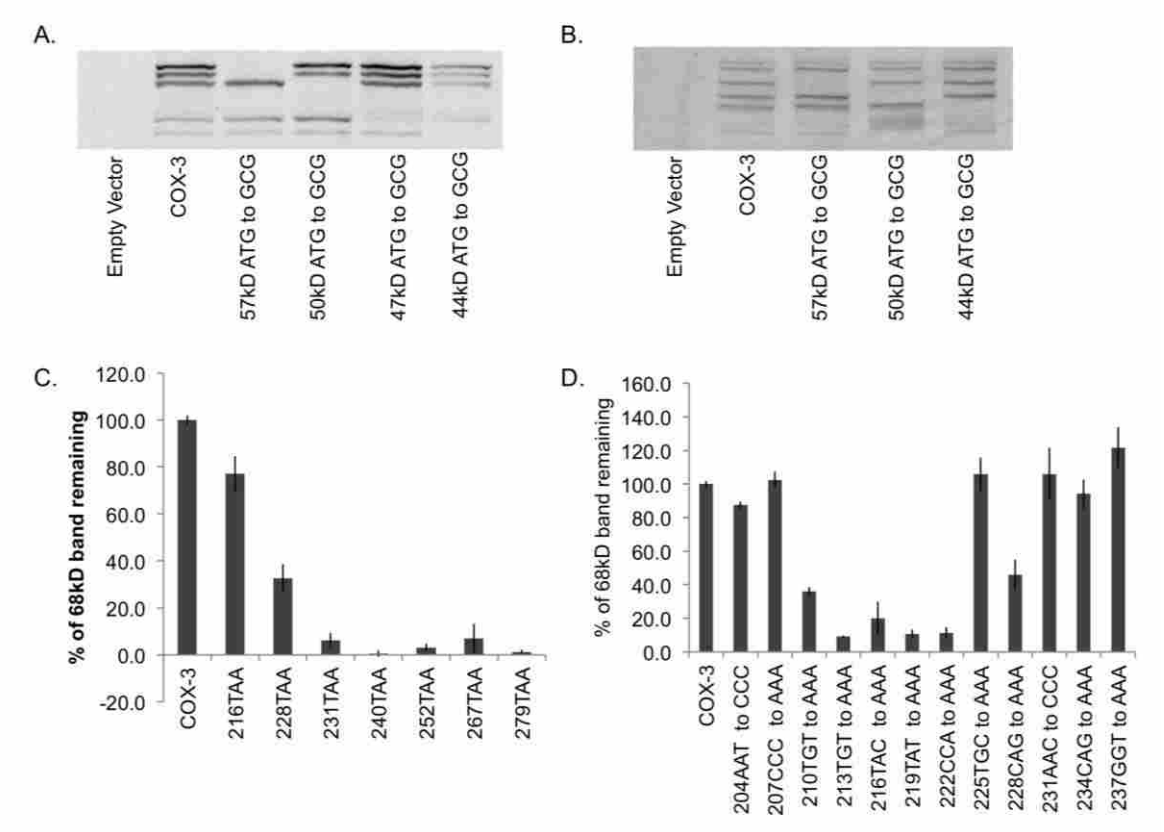

Figure 6: Site directed mutagenesis of non-glycosylated COX-3 forms.

Site-directed mutagenesis was used to mutate four in-frame AUG codons to GCG (ala) at positions 441bp, 591bp, and 693, and 750bp in the human (A) and rat (B) COX-3 cDNA. Mutated cDNAs were transiently expressed in CHO cells and protein expression analyzed by anti-Flag immunoblot. Mutation of each codon prevented translation of the 57kD, 50kD, 47kD, and 44kD COX-3 proteins respectively, indicating that these COX-3 proteins are translated through translation initiation at these downstream codons.

In order to understand the translation of the 68kD COX-3 protein, site-directed mutagenesis was used to introduce TAA stop codons into the +0 reading frame (C) or to mutate each codon from 204 to 237 (D). Mutated clones were transiently expressed in CHO cells and the level of 68kD COX-3 protein expression was determined by anti-Flag

immunoblot. Results indicate that translation initiation of the 68kD form is dependent on a 21nt region from 210 to 222, and codon 228.

Mean intensity data is from 3 separate experiments +/-SE, normalized to cells expressing the non-mutated COX-3 control and neomycin transferase to control for differences in transfection efficiency.

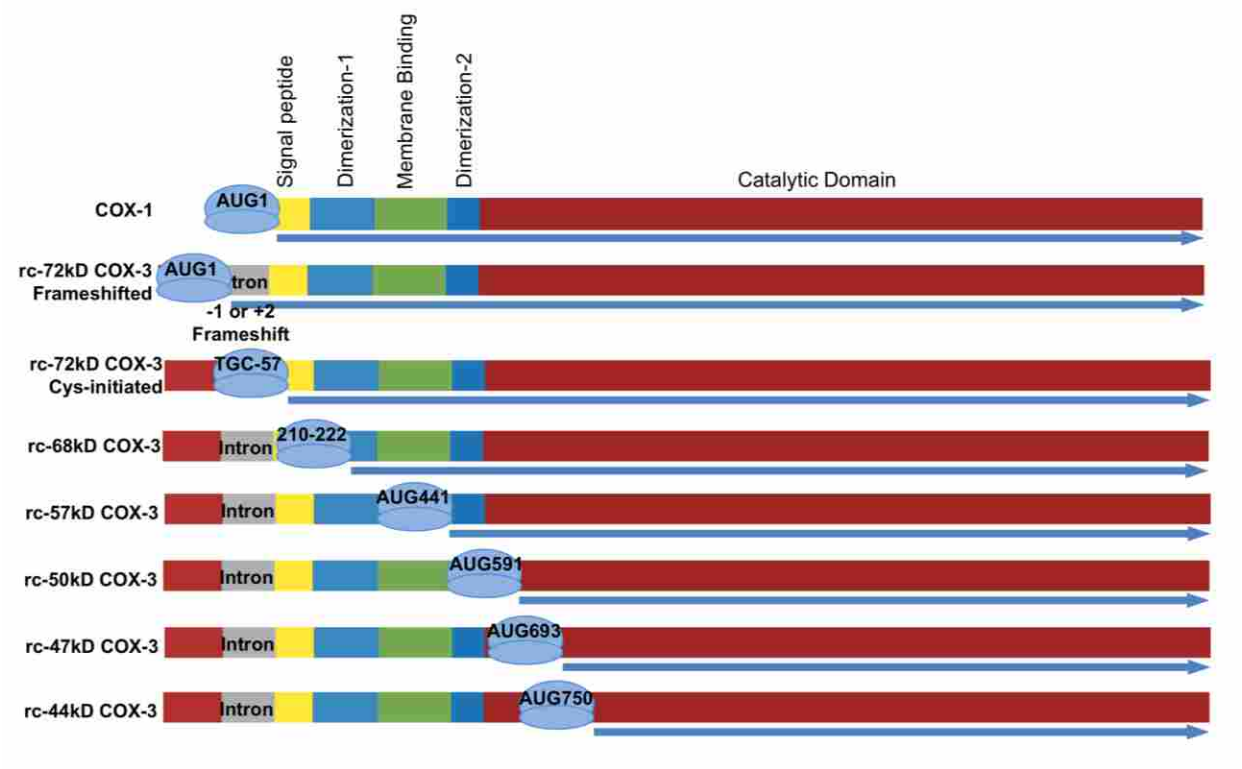

Figure 7. COX-3 mRNA is translated through multiple recoding mechanisms to produce a series of high molecular-weight proteins. Seven different translation initiation sites were identified resulting in expression of a series of N-terminally truncated cyclooxygenase-like proteins.

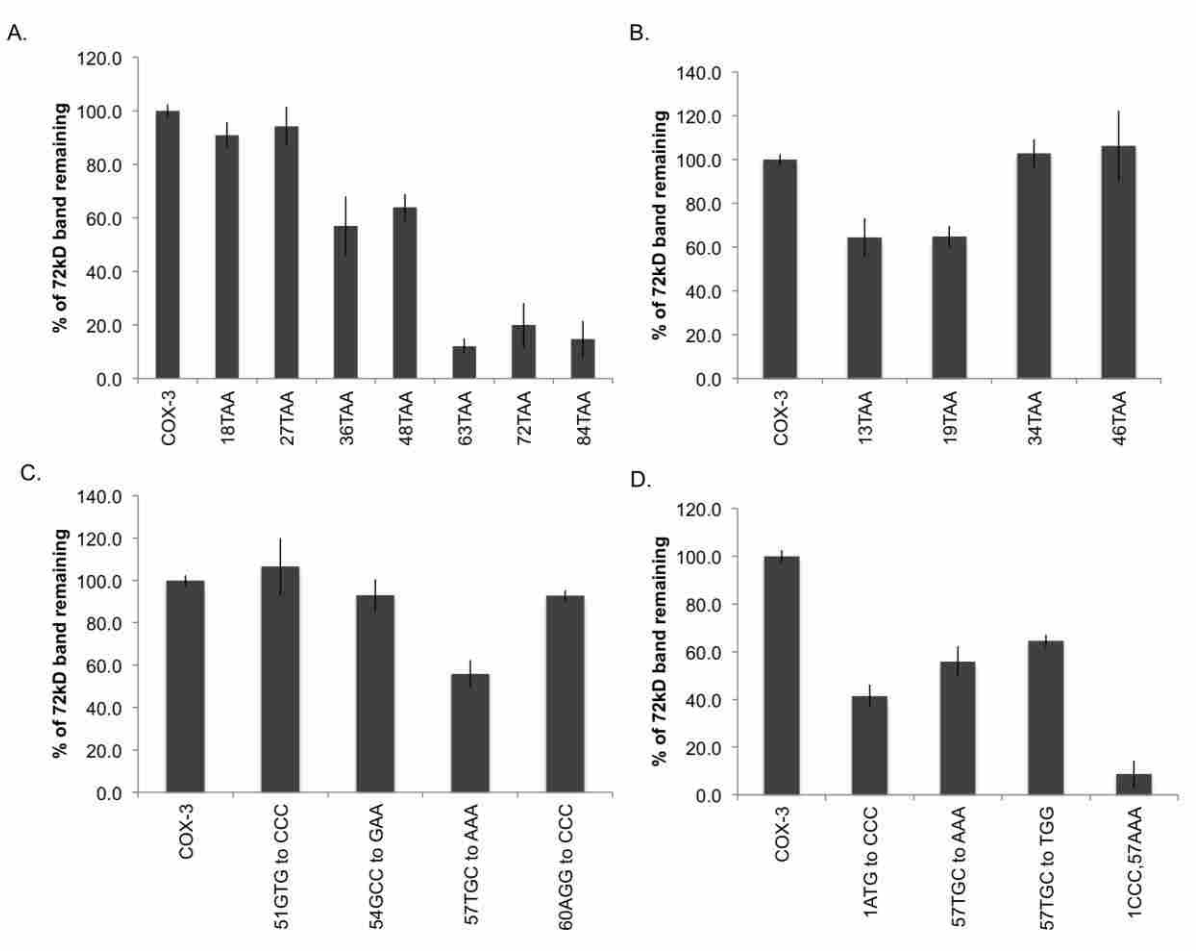

Figure 8: Site directed mutagenesis of 72kD COX-3 forms.

Site-directed mutagenesis was used to introduce TAA stop codons into the +0 (A) and +1 (B) reading frames of COX-3 at the indicated nucleotide positions (relative to the consensus start codon). Stop codon insertional results indicate the presence of two separate initiation sites. The first one in the +1 reading frame upstream of codon 34, and a second one in the +0 reading frame between codons 48 and 63. Translation of the first appears to progress in the +1 reading frame until a point between codons 19 and 34. In this region translation appears to shift to the +0 reading frame as indicated by the stop codon inserted at position 36.

C) Site-directed mutagenesis of each codon between 51 and 60 in the +0 reading frame indicates that codon 57TGC is required for efficient expression of the second 72kD COX-3 form, suggesting that this codon is used for translation initiation.

D) Point mutation of AUG-1 to CCC and TGC57 to AAA confirm that these are the translational start sites for each COX-3 form. Mutated clones were transiently expressed in CHO cells and the level of 72kD COX-3 protein expression determined by anti-Flag immunoblot. Mean band intensity is plotted relative to unmutated COX-3 control and normalized to neomycin transferase to control for differences in transfection efficiency. Data is the average of 3 or more experiments +/- SE.

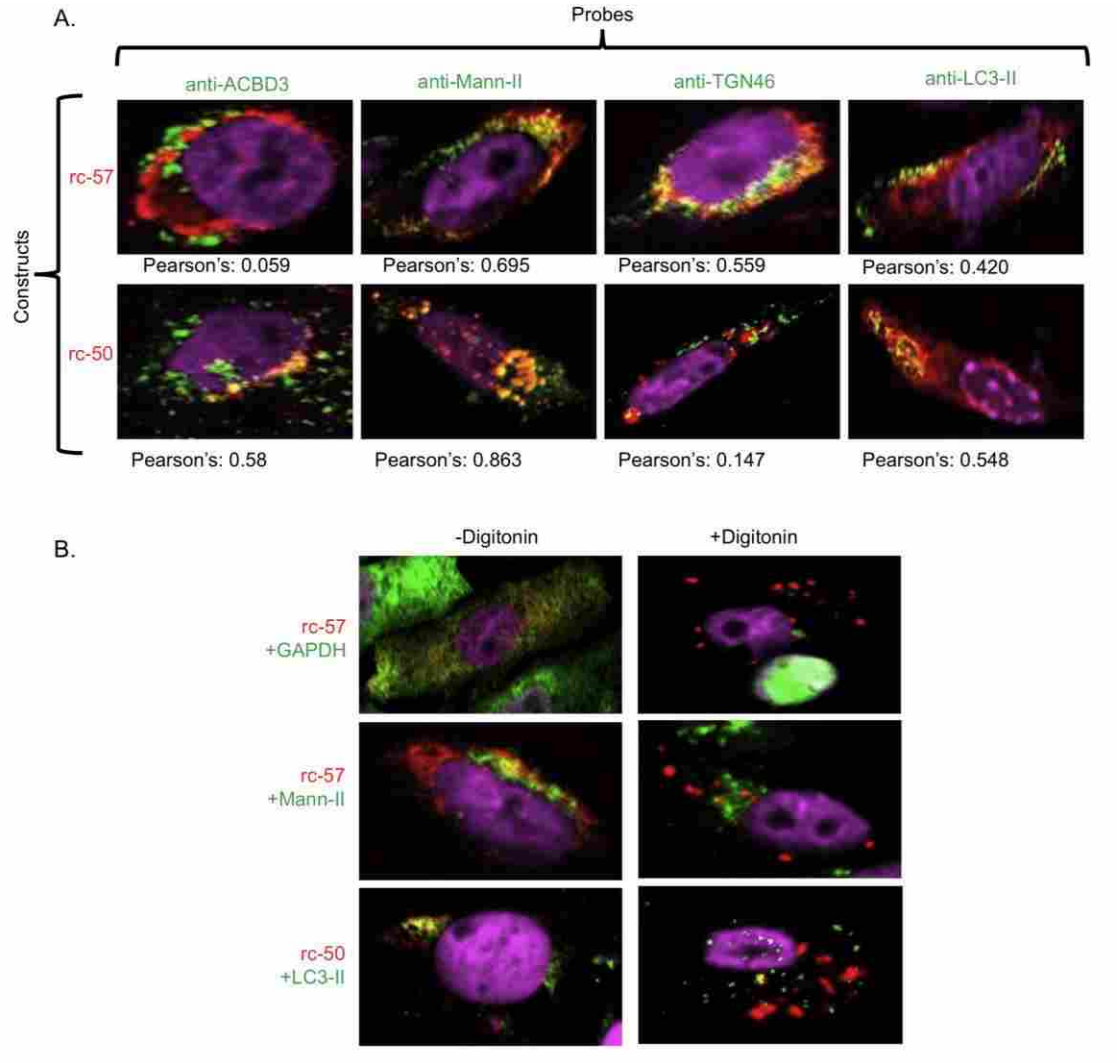

Figure 9: Confocal microscopy.

A) Rc-57kD and rc-50kD Flag-tagged constructs were each transfected into CHO cells and dually labeled using antibodies against Flag and either cis-golgi (ACBD), intermediate golgi (mannosidase), trans-golgi (TGN46) or autophagosomes (LC3-II) markers and visualized by confocal microscopy. COX-3 rc-57kD predominantly localizes to intermediate golgi, trans-golgi and autophagosomes with little localization to cis-golgi. In contrast, rc-50kD COX-3 is localized to cis-golgi, intermediate golgi, and autophagosomes.

B) CHO cells transfected with either rc-57 or rc-50 COX-3-Flag were permeabilized using digitonin and dually labeled with antibodies against Flag peptide (red) and either cytosolic marker GAPDH, golgi markers mannosidase-II, or autophagosome marker LC3-II (green). With digitonin treatment rc-57 and rc-50kD COX-3 staining is almost entirely lost confirming that rc-50kD and rc-57kD COX-3 reside on cytosolic surface of golgi and autophagosomes. Some residual staining for these COX-3 forms is found on punctate structures that do not co-localize with autophagosome or golgi.